DSPACE

https://dspace.org/

Optimal Design and Operation Control of Electrical Vehicle Battery Swapping Station incorporating Hybrid Renewable Energy and Grid Power Systems

Nyamayoka, Lumbumba Taty-Etienne

2025

University of the Witwatersrand, Johannesburg

https://hdl.handle.net/10539/47630

Nyamayoka, Lumbumba Taty-Etienne . (2025). Optimal Design and Operation Control of Electrical Vehicle Battery Swapping Station incorporating Hybrid Renewable Energy and Grid Power Systems [PhD thesis, University of the Witwatersrand, Johannesburg]. WIReDSpace. https://hdl.handle.net/10539/47630

Downloaded from a DSpace repository. https://dspace.org/



UNIVERSITY OF THE
WITWATERSRAND,
JOHANNESBURG

Optimal Design and Operation Control of Electrical Vehicle Battery Swapping Station incorporating Hybrid Renewable Energy and Grid Power Systems

by

Lumbumba Taty-Etienne Nyamayoka

A thesis submitted to the Faculty of Engineering and the Built Environment, University of the Witwatersrand, Johannesburg, in fulfillment of the requirements for the degree of Doctor of Philosophy

2025

Declaration

I, **Lumbumba Taty-Etienne Nyamayoka**, hereby declare that this thesis report is my own original work, submitted to the University of the Witwatersrand for the degree of Doctor of Philosophy. This work **has not** been submitted to any institute of learning for a degree.



Lumbumba Taty-Etienne Nyamayoka

Braamfontein, Johannesburg

June, 2025

Dedication

This thesis is lovingly dedicated to my precious firstborn daughter, **Mishondo Thaïs Nyamayoka**. You came into this world amid my PhD journey when my academic pursuits demanded much of my time and energy. Though I was present as you grew, there were moments when my studies took me away from fully embracing every milestone. However, this achievement is as much yours as it is mine. May it inspire you to embrace education, not just for the sake of knowledge but to become a thinker and an innovator in whatever path you choose.

To my beloved wife, **Eunicia Mpenga**, your unwavering love and support have been my most significant source of strength. Through every challenge, your words comforted me, your presence gave me warmth, and your resilience kept everything together. You endured my struggles as if they were your own and rejoiced in my successes as if they were yours. This accomplishment is as much yours as it is mine.

I also dedicate this work to my wonderful parents, **Mr. Raymond Lumbumba** and **Mrs. Hortance Nguama**. Your sacrifices, unconditional love, and relentless efforts laid the foundation for my educational journey. Every milestone I achieve is a testament to your dedication and belief in me.

To my dear siblings, **Axel Nguama**, **Joelle Kinda**, **Kito Kitila**, **Hurgue Mbilambangu**, **Ina Inabur**, **Gaston Makidi**, **Phillipe Manemo**, **Mira Mirang**, and **Jacquie Idjang**, you played a meaningful role in my life. Your unwavering support, encouragement, and faith in me have been invaluable in shaping the person I have become. This achievement reflects the love and strength of our family bond.

And to all those who dare to dream, persist, and overcome, may this work serve as a small testament to the power of dedication and perseverance.

Above all, I give my deepest gratitude to the Almighty God for His guidance, strength, and blessings throughout this journey.

Acknowledgements

This thesis marks the culmination of an incredible journey that would not have been possible without many individuals' support, guidance, and encouragement.

First and foremost, I would like to express my deepest gratitude to my supervisor, **Prof. David G. Dorrell**, and co-supervisor, **Dr. Lesedi Masisi**, for their unwavering support, invaluable insights, and constructive feedback throughout this research. Your mentorship and expertise have been instrumental in shaping the direction of this work and fostering my growth as a researcher.

I extend my sincere appreciation to **Prof. Shuo Wang** from the National Engineering Research Center of Electric Vehicles, Beijing Institute of Technology, China, for granting permission and access to crucial research data that contributed significantly to this study.

I am also profoundly grateful to the School of Electrical and Information Engineering at the University of the Witwatersrand, Johannesburg, for providing an environment that fostered learning, collaboration, and innovation. My heartfelt thanks go to my colleagues and friends, whose willingness to share knowledge and offer advice was invaluable. Your camaraderie made the long hours and late nights much more manageable.

I would also like to express my sincere gratitude to the management team and colleagues at Impaphala Project and Consulting (Pty) Ltd for their unwavering support, professionalism, and collaborative spirit, all of which were deeply appreciated throughout this academic journey.

Special thanks go to the funding bodies, notably the Postgraduate Merit Award (PMA), for their financial support, which made this research possible.

I want to extend my heartfelt appreciation to my family, especially my parents, for their unconditional love, understanding, and encouragement throughout this challenging journey. To my beloved wife, **Eunicia Mpenga**, your unwavering support, patience, and belief in me have been my most significant source of strength. You stood by me through every high and low, and I am eternally grateful for your love. To my daughter, **Mishondo Thaïs Nyamayoka**, and all my beloved siblings, your presence in my life has been a constant source of motivation and joy.

Lastly, I extend my gratitude to all the participants and contributors to this study. Your input and collaboration have enriched this research and enhanced its impact. This thesis is dedicated to all those who have believed in me and supported me on this journey.

Above all, I acknowledge the Almighty God for His guidance, protection, and strength throughout this phase.

To God be all the glory!

Abstract

Transportation is a major contributor to air pollution and one of the largest consumers of fossil fuels. As a sustainable alternative, electric vehicles have gained widespread adoption due to advances in technology, the expansion of public charging networks, and improvements in battery materials and charging infrastructure. However, limitations in the charger power capacity and battery characteristics of electric vehicles often result in longer charging times compared to refueling traditional vehicles, leading to range anxiety and hindering broader adoption. To address this challenge, battery swapping stations have emerged as an innovative solution, allowing drivers to exchange depleted batteries for fully charged ones, thus minimizing downtime and enhancing the feasibility of electric vehicles for modern transportation systems.

Recent research has explored the concept of battery swapping stations, presenting various optimization approaches and operational systems. Battery swapping station providers have successfully implemented swapping services at both private and commercial stations. This research study focuses on the optimal design approach and operation management strategy of battery swapping stations, with a particular emphasis on leveraging renewable energy sources, such as wind turbines and photovoltaic systems, as primary resources for charging the depleted electric vehicle battery. The aim is to develop solutions that minimize energy consumption and operational costs while enhancing charging performance by reducing the swapping service time.

For this purpose, first, an optimal design for a battery swapping station integrated with a grid-connected hybrid power supply system is developed and evaluated. The optimization problem is formulated to minimize the overall life cycle cost and reduce electricity costs purchased from the utility grid while maximizing its reliability. This model provides continuous, cost-effective power support and implements a scheduling strategy that consistently meets charging demand. Mixed integer linear programming is used to determine key decision variables, such as the power drawn from the utility grid and the number of wind turbines and solar photovoltaic panels. Simulation results demonstrate that the optimal configuration, including wind turbines and solar panels, yields significant energy cost savings over its lifecycle. In addition, an economic analysis is performed to assess the payback period, an essential metric for investors.

Secondly, an optimal operational control strategy is developed and evaluated for grid-connected wind-solar power generation with a storage system for the battery swapping station. The strategy minimizes the total operational costs associated with the cost of electrical energy purchased from the utility grid and the wear cost of the hybrid system due to the frequent charging and discharging of the battery energy storage system. At the same time, it maximizes the self-consumption of locally generated renewable energy. This optimization model ensures a cost-effective power supply that efficiently meets charging demands while selling excess energy back to the utility grid. The simulation results from four scenarios show that the model optimizes energy use, reduces costs, and increases hybrid power feedback to the utility grid. The main outcome is improved energy efficiency, cost savings, and additional revenue from surplus power sales.

The impact of this outcome is enhanced financial viability, demonstrated through an economic analysis that evaluates the investment feasibility and payback period of the proposed system.

Thirdly, a model predictive control approach is designed and evaluated to determine the optimal operational strategy for a battery swapping station integrated with a grid-connected wind-solar power generation system and a battery energy storage system. The primary objective is to minimize the operational costs of the proposed system. By implementing model predictive control (MPC), the system dynamically optimizes power flow in real-time to account for uncertainties and disturbances. A comparative analysis is conducted between open-loop control and MPC-based closed-loop control under various scenarios, with and without disturbances. The simulation results demonstrate that the closed-loop MPC approach consistently outperforms the open-loop model, exhibiting superior robustness and adaptability in handling uncertainties. By optimizing power flow in real-time, MPC ensures efficient power distribution, reduces reliance on the utility grid, and maximizes renewable energy utilization. Despite its computational complexity, model predictive control offers significant advantages in industrial applications, enhancing efficiency, reliability, and cost-effectiveness through real-time optimization.

The findings of this research underscore the effectiveness of integrating battery swapping stations with demand-side management strategies. This integration plays a crucial role in advancing sustainable urban transportation, enhancing the efficiency of electric vehicle infrastructure, and improving the reliability and stability of the utility grid.

Contents

List of Figures x

List of Tables xii

List of Abbreviations xiii

1 INTRODUCTION 1
- 1.1 Chapter overview . . . 1
- 1.2 Research background . . . 1
- 1.3 Research motivation and problem statement . . . 3
- 1.4 Research contribution and objectives . . . 4
- 1.5 Research approach . . . 5
- 1.6 Research outputs . . . 6
- 1.7 Thesis layouts . . . 7

2 THEORETICAL BACKGROUND 9
- 2.1 Chapter overview . . . 9
- 2.2 Overview of electric vehicle technologies . . . 9
- 2.3 Electric vehicles charging systems . . . 10
  - 2.3.1 Electric vehicles charging technology . . . 10
  - 2.3.2 Electric vehicle charging structure design . . . 11
- 2.4 Electric vehicle battery swapping station . . . 11
  - 2.4.1 Definition and concept . . . 11
  - 2.4.2 Electric vehicle charging and swapping configuration . . . 12
  - 2.4.3 Electric vehicle battery swapping approach perspective . . . 13
    - 2.4.3.1 Electric vehicle owner perspective . . . 13
    - 2.4.3.2 Station owner perspective . . . 14
    - 2.4.3.3 Power system perspective . . . 15
- 2.5 Hybrid renewable energy systems for battery swapping station . . . 15
- 2.6 Energy management in battery swapping stations . . . 17
- 2.7 Optimization and control strategies in electric vehicle battery swapping station . . . 17
- 2.8 Summary . . . 18

3 LITERATURE REVIEW 20
- 3.1 Chapter Overview . . . 20
- 3.2 Review on previous studies related to the battery swapping station . . . 20
  - 3.2.1 Development and implementation of BSSs . . . 20
  - 3.2.2 Optimization and energy management in BSSs . . . 21
  - 3.2.3 Identified research gaps . . . 22
- 3.3 Summary . . . 23

4 OPTIMAL DESIGN AND TECHNO-ECONOMIC FEASIBILITY OF GRID-CONNECTED WIND-SOLAR ENERGY SYSTEM FOR BATTERY SWAPPING STATION 25
4.1 Chapter overview . . . 25
4.2 Mathematical model formulation . . . 26
4.2.1 Schematic model layout . . . 26
4.2.2 Wind turbine system . . . 28
4.2.3 Solar photovoltaic system . . . 30
4.2.4 Inverter . . . 31
4.2.5 Utility grid power supply system . . . 32
4.2.6 Battery swapping station power demand . . . 33
4.2.7 Economic evaluation parameters of the proposed system . . . 34
4.2.8 Reliability consideration of the proposed system . . . 38
4.2.9 Objective function . . . 39
4.2.10 System Constraints . . . 40
4.2.11 Algorithm formulation . . . 41
4.3 Case study . . . 41
4.3.1 EV BSS power demand load profile . . . 42
4.3.2 Renewable energy power supply . . . 43
4.3.3 Time-of-use electricity tariff . . . 44
4.4 Results and discussion . . . 45
4.4.1 Optimal hybrid power system sizing and management strategy . . . 47
4.4.2 LCC analysis for the payback period . . . 50
4.5 Summary . . . 51

5 OPTIMAL OPERATION CONTROL OF GRID-CONNECTED WIND-SOLAR POWER GENERATION WITH STORAGE SYSTEM FOR BATTERY SWAPPING STATION 54
5.1 Chapter overview . . . 54
5.2 Operation modelling and problem formulation . . . 55
5.2.1 Schematic model layout . . . 55
5.2.2 Wind turbine system . . . 55
5.2.3 Solar PV system . . . 57
5.2.4 Battery energy storage system . . . 58
5.2.5 Utility Grid . . . 60
5.2.6 Battery swapping station power demand . . . 61
5.2.7 Objective function and constraints . . . 62
5.2.8 Constraints . . . 63
5.2.9 Algorithm formulation . . . 64
5.3 Case study . . . 65
5.3.1 EV BSS power demand load profile . . . 65
5.3.2 Renewable energy power supply . . . 65
5.3.3 Time-of-use electricity tariff . . . 66
5.4 Simulation results and discussion . . . 69
5.4.1 High demand electricity pricing season . . . 70
5.4.1.1 Scenario 1: Optimal operation strategy of the proposed system in high demand season for one day on the weekday (June to August). . . . 70
5.4.1.2 Scenario 2: Optimal operation strategy of the proposed system in high demand season for one day on the weekend (June to August). . . . 71
5.4.2 Low demand electricity pricing season . . . 72
5.4.2.1 Scenario 3: Optimal operation strategy of the proposed system in low demand season for one day on the weekday (September to May). . . . 72

5.4.2.2 Scenario 4: Optimal operation strategy of the proposed system in low demand season for one day on the weekend (September to May). 74
5.4.3 Baseline and optimal cost saving 77
5.4.4 Economic analysis for the payback period 78
5.5 Summary 81

6 MODEL PREDICTIVE CONTROL STRATEGY FOR GRID-CONNECTED WIND-SOLAR POWER GENERATION WITH STORAGE SYSTEMS FOR BATTERY SWAPPING STATION 82
6.1 Chapter overview 82
6.2 System modelling and Formulation 83
6.2.1 Schematic model layout 83
6.2.2 Wind turbine system 83
6.2.3 Solar PV system 85
6.2.4 Battery energy storage system 86
6.2.5 Utility Grid 88
6.2.6 Battery swapping station power demand 88
6.2.7 Open loop optimal control model 90
6.2.8 MPC optimization problem 91
6.2.8.1 Discrete linear MPC model 91
6.2.8.2 Objective function 93
6.2.9 MPC algorithm 94
6.3 Case study 95
6.3.1 EV BSS power demand load profile 95
6.3.2 Renewable energy power supply 95
6.3.3 Time-of-use electricity tariff 97
6.4 Simulation results and discussion 98
6.4.1 Open-loop control simulation results 98
6.4.2 Model predictive control simulation results in high demand season 99
6.4.3 Model predictive control simulation results in low demand season 101
6.5 Summary 103

7 CONCLUSIONS AND FUTURE WORKS 104
7.1 Conclusions 104
7.2 Recommendations for Future Work 106

Bibliography 107

List of Figures

2.1 EV drive system diagram. 10
2.2 Different types of EV charging technologies. 11

4.1 Schematic layout of the proposed system. 27
4.2 Wind generator power curve. 29
4.3 Charging patterns of electric vehicles battery swapping station. 42
4.4 Average hourly wind speed. 43
4.5 Monthly average wind speed. 43
4.6 Daily average shortwave solar power. 44
4.7 Monthly average shortwave solar energy. 44
4.8 Wind and photovoltaic power generated by the hybrid systems. 48
4.9 Load side power flows at EV-BSS. 49

5.1 Schematic layout of the proposed system. 56
5.2 Charging patterns of the electric vehicle battery swapping station on a weekday. 65
5.3 Charging patterns of the electric vehicle battery swapping station on a Weekend. 65
5.4 Average hourly wind speed HD. 66
5.5 Average hourly wind speed LD. 66
5.6 Daily average shortwave solar power HD. 67
5.7 Daily average shortwave solar power LD. 67
5.8 Monthly average wind speed. 67
5.9 Monthly average shortwave PV power 67
5.10 Charging demand side power flows. 71
5.11 BESS side power flows. 71
5.12 BESS SoC. 71
5.13 Hybrid power to the Grid. 71
5.14 Charging demand side power flows. 73
5.15 BESS side power flows. 73
5.16 BESS SoC. 73
5.17 Hybrid power to the Grid. 73
5.18 Charging demand side power flows. 75
5.19 BESS side power flows. 75
5.20 BESS SoC. 75
5.21 Hybrid power to the Grid. 75
5.22 Charging demand side power flows. 76
5.23 BESS side power flows. 76
5.24 BESS SoC. 76
5.25 Hybrid power to the Grid. 76

6.1 Schematic layout of the proposed system. 84
6.2 Charging patterns of the electric vehicle battery swapping station on a weekday. 95
6.3 Average hourly wind speed HD. 96

6.4 Average hourly wind speed LD. 96
6.5 Daily average shortwave solar power HD. 96
6.6 Daily average shortwave solar power LD. 96
6.7 Monthly average wind speed. 97
6.8 Monthly average shortwave PV power 97
6.9 Simulation result of open loop control. 99
6.10 Simulation result of BESS dynamic SoC. 99
6.11 Simulation result of open loop system. 100
6.12 Simulation result of BESS dynamic SoC 100
6.13 Simulation result of close loop system without disturbances. 100
6.14 Simulation result of BESS Dynamic SoC without disturbances. 100
6.15 Simulation result of close loop system with disturbances. 101
6.16 Simulation result of BESS Dynamic SoC with disturbances. 101
6.17 Simulation result of close loop system without disturbances. 102
6.18 Simulation result of BESS Dynamic SoC without disturbances. 102
6.19 Simulation result of close loop system with disturbances. 103
6.20 Simulation result of BESS Dynamic SoC with disturbances. 103

List of Tables

4.1 Simulation parameters used in this chapter. 46
4.2 Simulation results of the proposed system. 48
4.3 Daily optimal energy and annual cost savings of the proposed system. 48
4.4 Costs components of the proposed system. 51
4.5 Life cycle cost analysis and payback period of the proposed system 52

5.1 Simulation parameters used in this chapter. 69
5.2 Different case scenario with daily optimal energy and cost savings 77
5.3 Weekly and Annual cost savings. 78
5.4 Costs components of the proposed system. 79
5.5 Payback period of the proposed system 80

6.1 Daily energy consumption savings and hybrid feed-in. 103

List of Abbreviations

AC	**A**lternative **C**urrent
AI	**A**rtificial **I**ntelligence
B2G	**B**attery to **G**rid
B2B	**B**attery to **B**attery
BESS	**B**attery **E**nergy **S**ource **S**ystem
BEV	**B**attery **E**lectric **V**ehicle
BMS	**B**attery **M**anagement **S**ystem
BSS	**B**attery **S**wapping **S**tation
COP21	**C**onference **o**f the **P**arties (21^{st}*annual session*)
CS	**C**harging **S**tation
DC	**D**irect **C**urrent
DER	**D**istributed **E**nergy **R**esources
DG	**D**istributed **G**eneration
DoD	**D**epth-of- **D**ischarge
DSM	**D**emand **S**ide **M**anagement
EM	**E**lectric **M**otor
EMS	**E**nergy **M**anagement **S**ystem
ESS	**E**nergy **S**torage **S**ystem
EV	**E**lectric **V**sehicle
EV BSS	**E**lectric **V**ehicle **B**attery **S**wapping **S**tation
EVCS	**E**lectric **V**ehicle **C**harging **S**tation
FCEV	**F**uel **C**ell **E**lectric **V**ehicle
FCS	**F**ast **C**harging **S**tation
GA	**G**enetic **A**lgorithm
G2B	**G**rid to **B**attery
GHG	**G**reenhouse **G**az
HEV	**H**ybrid **E**lectric **V**ehicle
HRE	**H**ybrid **R**enewable **E**nergy
ICE	**I**nternal **C**ombustion **E**ngine
IEA	**I**nternational **E**nergy **A**gency

IoT	**I**nternet of **T**hings
IPCC	**I**ntergovernmental **P**anel on**C**limate **C**hange
LCC	**L**ife **C**ycle **C**ost
LP	**L**inear **P**rogramming
LPS	**L**oss **P**ower **S**upply
LPSP	**L**oss **P**ower **S**oad **P**robability
MILP	**M**ixed **I**nteger **L**inear **P**rogramming
MINLP	**M**ixed **I**nteger **N**on-**L**inear **P**rogramming
ML	**M**achine **L**earning
MPC	**M**odel **P**redictive **C**ontrol
PHEV	**P**lug-in **H**ybrid **E**lectric **V**ehicle
PV	**P**hoto**V**oltaic
PSO	**P**article **S**warm **O**ptimization
RE	**R**enewable **E**nergy
RESs	**R**enewable **E**nergy **S**ources
SA	**S**outh **A**frica
SAE	**S**ociety of **A**utomotive **E**ngineers
SCIP	**S**olving **C**onstraint **I**nterger **P**rogram
SoC	**S**tate of **C**harge
TOU	**T**ime-of-**U**se
UNFCCC	**U**nited **N**ationsr **F**ramework **C**onvention on **C**limate **C**hange
V2G	**V**ehicle to **G**rid
V2H	**V**ehicle to **H**ome
WC	**W**ireless **C**harging
WT	**W**ind **T**urbine

Chapter 1

INTRODUCTION

1.1 Chapter overview

In this chapter, Section 1.2 presents background information that underscores the need to design and optimize energy efficiency, economic viability, and operational performance of electric vehicle battery swapping stations. Section 1.3 outlines the motivation behind the study and articulates the problem statement. Section 1.4 highlights the contributions of the study and defines its objectives. Section 1.5 elaborates on the methodological approach employed in this study, while Section 1.6 lists the research output publications reported in this thesis. Finally, Section 1.7 provides an overview of the thesis layout.

1.2 Research background

Global warming remains one of the most critical issues of our time and significantly impacts human and natural systems worldwide. Climate change has heightened the urgency for coordinated global efforts to mitigate its effects. The 2015 Paris Agreement, adopted at the 21st Conference of the Parties (COP21) of the United Nations Framework Convention on Climate Change (UNFCCC), marked a milestone in this endeavour. It aims to limit the increase in global temperature well below 2 °C above preindustrial levels, with further efforts to limit it below 1.5 °C [1]. Achieving these goals requires substantial reductions in greenhouse gas (GHG) emissions, as emphasized by the Intergovernmental Panel on Climate Change (IPCC) and the International Energy Agency (IEA) [1–3]. These agencies estimate that the implementation of appropriate policies, technologies, and infrastructure could cut GHG emissions by 40–70% by 2050, promoting sustainable lifestyles and behaviours [4, 5].

The transportation sector is a significant contributor to global climate change, accounting for approximately 23% of energy-related carbon dioxide (CO_2) emissions, primarily due to the widespread use of

[1] https://unfccc.int/sites/default/files/english_paris_agreement.pdf

vehicles with an internal combustion engine (ICE) [6–8]. However, motorized transportation has become an integral part of the human experience. It is considered an essential part of personal mobility, providing delivery services, and facilitating the movement of goods daily. This sector is critical for economic growth [9–11]. Given the anticipated increase in demand for transportation services, industry stakeholders and policymakers need to address climate change and its detrimental effects on the environment while improving mobility in a way that aligns with the goals of the Paris Agreement. A dynamic shift to less pollution has been brought about by combining policy responses and technological advancement in the transportation sector. These include road, rail, high-speed ground transportation, maritime, and air transportation systems [12]. Due to economic, practical, and technological constraints, the ideal result of zero emissions in the transportation sector is still a long way off. Compared to traditional ICE for driving vehicles on the road, fuel cell and electric vehicle (EV) technologies have been slow to gain traction due to these limitations [13, 14]. In addition to strategies to completely replace ICEs with alternative technologies, EVs offer significant promise as less polluting. They are increasingly becoming attractive as a better solution for vehicles powered by ICEs [15–17].

EVs have emerged as a transformative solution, leveraging clean energy sources to significantly reduce CO_2 emissions compared to traditional ICE vehicles. The global EV market has grown exponentially in the past decade, and the International Energy Agency (IEA) projects that global EV sales could reach between 55 to 72 million units by 2025, accounting for 8% of total vehicle sales [18]. The adoption of EVs could reduce the dependency on fossil fuel and greenhouse gas (GHG) emissions, aligning with the goals of the Paris Agreement on climate change [19, 20]. However, with the widespread adoption of EVs, the growing demand for EV charging infrastructures is inevitable. As a result, EV marketing depends on the overall infrastructure of the charging system to promote EVs. Several factors still discourage potential users from acquiring EVs, including the high cost of replacing the EV battery, the limited driving mileage range, and the long waiting hours for charging the EV battery. Although the number of EV charging infrastructures is growing, charging times fluctuate but are generally too long. This situation requires fast charging processes, which negatively impacts the longevity of EV batteries. Implementing battery swapping stations (BSSs) is an efficient and cost-effective solution to these challenges by enabling drivers to quickly exchange depleted EV batteries for fully charged ones. BSSs are emerging as a promising solution for EV charging infrastructure. The depleted EV battery swap takes only a few minutes, and these stations allow drivers to replace their depleted EV battery with a fully charged one of the same type at various locations. As these EV batteries are depleted, they are charged according to the charging management protocol before being swapped with a new driver. This system addresses concerns regarding charging times and battery lifespan, making EVs more attractive to consumers. BSS can also optimize energy management by charging batteries during off-peak hours, leveraging renewable energy sources, and operating as flexible charging demands within the power utility grid. Despite these benefits, implementing BSS faces hurdles, including the need for battery standardization, substantial space requirements for battery storage, and high initial investment costs [21–25].

The integration of renewable energy sources (RES), such as solar and wind power, into the energy mix has become essential for reducing carbon emissions and achieving sustainability goals. Hybrid renewable energy

(HRE) systems, which combine multiple renewable sources, provide a reliable and environmentally friendly alternative to traditional grid power. Integrating BSS with HRE systems offers a unique opportunity to optimize their design and operation, reducing dependence on the power grid and ensuring a stable, sustainable power supply [20, 26]. However, the intermittent nature of renewable energy poses challenges to continuous power availability, which requires the complementary use of grid power for reliability. The effective integration of grid power with renewable energy is critical for the optimal operation of BSS. The inclusion of an additional energy storage system improves the flexibility of BSS to utilize renewable energy efficiently, allowing them to act as a demand-response resource that benefits both the environment and the power system [22, 27]. Despite these potential advantages, the integration of BSS with existing power grids and renewable energy systems faces challenges, including high capital costs, limited renewable resources, and the need for advanced management systems. Key issues include optimizing battery inventory, ensuring energy efficiency, minimizing costs, and maintaining service reliability. Addressing these challenges requires a comprehensive approach that considers technical, economic, and environmental factors.

This thesis introduces a pioneering multidirectional optimization approach to integrate renewable energy systems and grid power with BSS, considering infrastructure limitations and exploring practical solutions. Using MATLAB, the optimization focuses on designing a reliable and efficient BSS that maximizes profitability. From an EV driver's perspective, the BSS offers a convenient service similar to traditional fuel stations, providing on-demand fully charged EV batteries. From a power system perspective, the BSS acts as a flexible load that can adapt to Time-of-Use (TOU) electricity tariffs. It maximizes profitability by purchasing electricity during off-peak hours in Grid-to-EV Battery (G2B) mode, discharging EV batteries to the utility grid during peak hours in EV Battery-to-Grid (B2G) mode, and utilizing stored energy for Battery-to-EV Battery (B2B) charging. This multifaceted approach not only conserves resources and reduces costs but also brings us closer to achieving sustainable and efficient EV charging infrastructure. The work presented in this thesis effectively addresses the existing technical and operational challenges of integrating these technologies, maximizing their benefits and paving the way for a greener future.

1.3 Research motivation and problem statement

The global shift towards EVs is driven by the increasing need for sustainable and environmentally friendly transportation solutions. In addition to this, rising fuel prices and growing environmental concerns due to climate change and air pollution have raised concerns. As a result, several governments have encouraged automobile manufacturers to develop low-emission and ecologically friendly vehicles [28]. This context has led to the development of electric vehicles and their use to reduce reliance on fossil fuels, which has led to a decrease in greenhouse gas emissions and other pollutants [20]. However, the widespread adoption of EVs is hindered by several challenges, including high EV battery costs, varying charging times, and limited driving range. Firstly, EV batteries are among the most expensive components of an electric vehicle, attributable to their life expectancy and initial purchase cost. Secondly, charging times can vary significantly depending on the type of charging equipment and technology used. Thirdly, the chemistry or energy density of an EV battery greatly influences the vehicle's range per charge. Currently, lithium-ion

batteries are the most commonly used in EVs, providing a driving range of approximately 320 to 480 km per charge [29, 30]. However, EV drivers who need to commute long distances within a day may find the driving range too limited [31–33]. To address these challenges, BSSs have been proposed as a potential solution to the limitations of the current charging technologies and the driving range. BSSs offer a convenient and efficient way to recharge EV batteries by allowing EV drivers to quickly swap their depleted EV batteries for fully charged ones.

South Africa faces a significant challenge in meeting its power demands, with a high dependency on non-renewable energy sources. To address this issue, the integration of renewable energy sources into the power utility grid has become a necessity. BSSs, when powered by hybrid renewable energy and grid systems, can significantly reduce the transportation sector's carbon footprint and enhance utility grid resilience. However, the effective design and operation of these stations require addressing various technical, economic, and environmental challenges, including the intermittent nature of renewable energy sources, charging patterns of EV batteries, and grid stability. Despite the potential benefits, there is a lack of comprehensive approaches to the design and operation management of BSSs that incorporate hybrid renewable energy and grid power supply systems. This gap creates a significant barrier to the widespread adoption of EVs, as it results in an unreliable charging infrastructure. The intermittent nature of renewable energy sources, the varying charging patterns of EV batteries, and the need to maintain grid stability pose complex challenges that must be addressed. Therefore, this thesis aims to explore an optimal approach for the design and operation management of BSSs that integrate renewable energy and grid power supply systems. The study will investigate the technical, economic, and environmental aspects that affect the performance of BSSs and their integration with the power utility grid. Additionally, the thesis will develop a decision-making tool to guide the selection of optimal BSS designs and operation strategies, enhancing the sustainability and economic viability of the transportation sector in South Africa.

1.4 Research contribution and objectives

Participants in the energy ecosystem who use energy responsibly gain from it on both supply and demand sides. These advantages also have a favourable effect on how an energy system interacts with society since they promote economic efficiency and environmental preservation. In general, a few non-renewable and renewable technologies are used to generate power, and various operators of generation infrastructure can adopt the same strategy to increase the efficiency of power generation. On the demand side, however, there are a variety of power users with unique requirement profiles and differing degrees of habit flexibility. In order to pursue energy efficiency in each situation, different power consumers may have systems that are distinctive and consequently different from one another. In this research study, grid-connected hybrid power source systems is used to charge the EV battery then swap it when needed. The aim is to optimally design and evaluate the operation management strategy at the BSS that is capable of coordinating the power flows among the different energy sources associated with the hybrid system and satisfying the EV swapping demand for EV customers. DSM programs will be used to evaluate an integrated control strategy for energy efficiency in the operation of the BSS to reduce energy consumption, energy cost, and produce

a suitable load profile for a reliable and stable utility grid. The intended performance of the charging process in conjunction with energy efficiency measures will be shown, as well as the techniques required to overcome the technical and operational constraints of realising the interaction between renewable energy and the power grid. The following objectives will be addressed in order to achieve these outcomes:

- **To design and analyse an optimization model that will optimally size the EV BSS integrated with a grid-connected hybrid power supply system**. The optimization model aims to minimize the system's total life cycle cost and grid electricity expenses while ensuring reliability through optimal power flow control within a demand-side management framework. The optimization model ensures low-cost, continuous power for the BSS while meeting charging demand at any time of the day.
- **To design and develop an optimal control strategy that minimizes the BSS's operational cost while maximizing self-consumption of locally generated energy to meet the charging demand**. The operation cost of the BSS depends on the electricity cost consumption from the utility grid, the hybrid wear cost of the proposed system, the number of battery swapped from the stock, and the potential damage with different charging rates. Using this approach, the charging, discharging, and swapping of depleted EV batteries is modelled and optimised based on the arrival of EV customers as well as the fluctuating electricity tariffs on the utility grid.
- **To design and develop a model-predictive control (MPC) approach for optimizing the operation of a BSS integrated with a grid-connected hybrid power generation with storage system, by maximizing RE utilization**. The optimization problem aims to minimize the total operation costs of the proposed system while satisfying the charging demand and enhance the profitability of BSS. The MPC coordinates the power grid and its interaction with the RESs by purchasing and selling electricity while taking into account the intermittent nature of the wind and solar energy sources and variations in charging demand.

By achieving these objectives, the research will provide a comprehensive framework for the optimal design and operation of EV battery swapping stations, addressing economic, environmental, and operational challenges. This approach has the potential to significantly contribute to the development of sustainable and efficient EV infrastructure integrated with renewable energy sources.

1.5 Research approach

In order to address the outlined objectives, this research thesis adopts the following systematic approach:

- **Literature review**: A comprehensive survey of existing works in electrical vehicle battery swapping stations, renewable energy, and hybrid grid power supply systems has been conducted to investigate the current status, trends, and future perspectives. This helps to identify gaps in the current knowledge and provides a foundation for the research work.

- **Model development**: The mathematical models encompassing all components to simulate the design and operation of battery swapping stations integrated with grid-connected hybrid renewable energy power supply systems have been formulated. The formulated model should consider key parameters such as charging demand, battery energy storage capacity, renewable energy generation, and grid connectivity. An objective function has been further developed, and the relevant constraints and variables have been identified to establish the main structure for this research study. The computation optimization is solved using a linear programming approach in MATLAB software.

- **Case study analysis**: After obtaining the daily charging demand data of existing battery swapping stations, the necessary daily renewable resource data for a selected location and the technical and economic data for the hybrid system's components are given. Then, the hybrid system is optimally designed. The results from this design are then used as inputs for simulating the optimal operation control strategies for the battery swapping station. This simulation considers the trade-offs between energy cost, renewable energy generation, and battery energy storage life.

- **Optimization**: Using optimization techniques such as linear programming, mixed-integer programming, heuristics to determine the optimal design and operation strategies for the battery swapping station. This simulation considers the trade-offs between energy cost, renewable energy generation, and battery energy storage life.

- **Simulation results discussion and analysis**: Following the research objectives identified earlier, the simulation results have been thoroughly discussed and analyzed using real-world data from existing battery swapping stations. This includes evaluating the performance metrics, assessing the economic viability, and examining the environmental impact of the proposed system designs.

- **Validation and conclusion**: The validation process ensures the reliability and applicability of the proposed models. Based on the study's results, conclusions are drawn regarding the effectiveness of the optimization strategies and recommendations for further research to enhance the design and operation of battery swapping stations.

  This research approach combines theoretical and practical elements. It provides a robust framework for evaluating the optimal approach for battery swapping station design and operation energy management strategies incorporating renewable energy/grid hybrid power supply systems.

1.6 Research outputs

The study presented in this thesis has led to the following publications:

1. L. T.-E. Nyamayoka, L. Masisi, D. Dorrell, and S. Wang. "Techno-economic feasibility and optimal design approach of grid-connected hybrid power generation systems for electric vehicles battery swapping station." *Energies*, vol. 18, no. 5, 2025.

2. L. T.-E. Nyamayoka, L. M. Masisi, D. G. Dorrell. "Optimal power dispatch of solar PV-battery storage system for electric vehicle battery swapping stations under grid scheduled load-shedding." In 2025 33nd Southern African Universities Power Engineering Conference (SAUPEC), pp. 1–6. IEEE, 2025.
3. L. T.-E. Nyamayoka, L. M. Masisi, D. G. Dorrell, S. Wang. "Optimisation Design of On-Grid Hybrid Power Supply System for Electric Vehicle Battery Swapping Station." In 2023 IEEE International Future Energy Electronics Conference (IFEEC), pp. 296–299. IEEE, 2023.
4. L. T.-E. Nyamayoka, L. M. Masisi, D. G. Dorrell. "Optimization of solar-wind powered battery swapping station under Time-of-Use tariff: South African Context." In South African National Research Data Workshop 2023, CSIR, Pretoria, from 05 - 06 July 2023.
5. L. T.-E. Nyamayoka, L. Masisi, D. Dorrell, and S. Wang. "Optimal power flow management of electric vehicle battery swapping station with Grid-integrated hybrid renewable generation and battery storage system." (Under review)
6. L. T.-E. Nyamayoka, L. Masisi, D. Dorrell, and S. Wang. "Model predictive control for energy dispatch in grid-connected hybrid power systems for electric electric vehicle battery swapping station." (Under review)

1.7 Thesis layouts

This thesis is generally presented in two broad categories: the optimal design and the operational control management strategies of battery swapping stations integrated with hybrid renewable energy and grid power supply systems. The layout of this thesis is outlined as follows:

Chapter 1 is the introduction chapter of this thesis. This chapter provides relevant background information and the research motivation that describes the problem and the corresponding research gap. Moreover, the main contribution and objectives of this research, the research approach, research outputs and the thesis layout are also given in this chapter.

Chapter 2 provides a comprehensive theoretical background on the modeling and operational optimization of EV BSSs. It begins with an overview of EV technologies, followed by a discussion on charging systems and BSSs. The chapter then explores the integration of hybrid renewable energy systems (RESs) in BSSs, various energy management approaches, and the optimization and control strategies essential for enhancing system efficiency and performance.

Chapter 3 presents a literature review of previous studies on EV BSSs. It examines existing research on the energy consumption of EV BSSs, highlights the importance of optimal energy management and operational strategies, and concludes with key insights derived from the literature.

Chapter 4 explores the techno-economic feasibility and optimal design of grid-connected hybrid power generation systems for EV BSS. The mathematical model formulation of the proposed system is presented

to assess the viability of the hybrid system as an alternative energy source, with a particular focus on cost-effectiveness. An optimal control model is developed and solved using MILP to determine the optimal number of wind turbines (WT) and solar PV panels, as well as the power consumption from the utility grid through a case study. The proposed optimization framework and mathematical models are adaptable for application in various global contexts.

Chapter 5 presents an integrated optimization approach for operating a grid-connected wind-solar hybrid power system with a BESS for an EV BSS. It builds on the previous chapter's focus on minimizing electricity purchases from the utility grid and the hybrid system's wear cost caused by frequent BESS charging and discharging cycles while enhancing renewable energy utilization. The proposed model optimally balances power flows to improve system efficiency, reduce operational costs, and increase the reliability of energy supply for EV charging demands.

Chapter 6 presents a model predictive control approach for a grid-connected wind-solar photovoltaic generator with a battery energy storage system for an EV BSS under a time-of-use tariff. Building on the previous chapter, it extends the closed-loop control based on receding horizon control to determine the optimal operation strategy of the proposed system over a 24-hour period, considering external disturbances. Additionally, it compares the performance of open-loop and closed-loop models in mitigating uncertainties and fluctuations in charging demand and renewable energy generation within the 24-hour control horizon.

Chapter 7 summarizes the methods and findings presented in the previous chapters. It also outlines key recommendations and directions for future research.

Chapter 2

THEORETICAL BACKGROUND

2.1 Chapter overview

The rapid adoption of electric vehicles (EVs) as a sustainable alternative to vehicles with internal combustion engines has required advances in charging infrastructure. Among the various solutions, battery swapping stations (BSSs) have emerged as a viable alternative to conventional plug-in charging, addressing challenges such as long charging durations and grid stress while enabling seamless integration of renewable energy sources. This chapter presents the theoretical background essential for understanding the technological and operational aspects of BSSs. It explores the fundamental principles of EV charging technologies, the configuration and functionality of battery swapping stations, the integration of hybrid renewable energy systems, and the optimization and control strategies employed in these systems. By establishing this theoretical foundation, the chapter provides critical insights into the role of BSSs in enhancing the efficiency, reliability, and sustainability of EV infrastructure.

Section 2.2 describes the overview of EVs, while Section 2.3 presents studies related to EV charging systems. Section 2.4 presents the EV battery swapping station, while Section 2.5 explores the hybrid renewable energy system for the BSS. Section 2.6 presents energy management consumption in EV BSSs while Section 2.7 introduces the optimization and control method in EV BSS. Section 2.8 concludes the theoretical background.

2.2 Overview of electric vehicle technologies

An EV is described as a vehicle powered by an electric motor driven by electrical energy stored in batteries [34]. The drive system is straightforward: the EV batteries supply electric power to the controller, which regulates power delivery to the electric motor. The electric motor then converts electrical energy into mechanical energy, driving the gearbox, which in turn rotates the wheels. Figure 2.1 represents EV drive

system diagram. The EV battery, electric motor, and controller are all vital components of an EV. However, for this research study, a focus will be placed on the EV batteries.

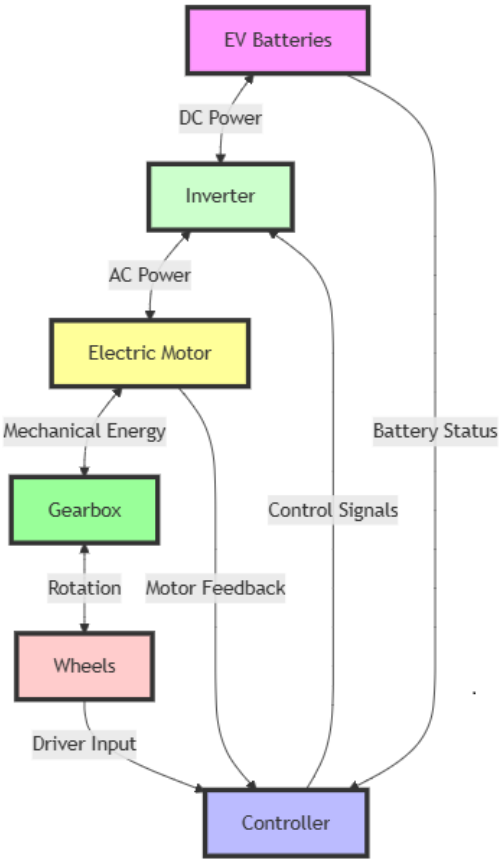


FIGURE 2.1: EV drive system diagram.

2.3 Electric vehicles charging systems

2.3.1 Electric vehicles charging technology

EVs require points of refuelling, i.e., charging stations. The purpose of a charging station is to deliver electrical energy from a source, typically the utility grid, to charge an EV battery. It consists of physical equipment, which enables the connection between the EV and the distribution grid. There are three main types of EV charging technology: conductive, wireless, and battery swapping. Figure 2.2 represents the different types of EV charging technologies. The simplest and most common charging technology is conductive charging. The power supply and EV battery make direct physical contact during conductive charging, but this is not the case with wireless charging. The EV battery can be charged without having any physical contact with the power supply or cable in wireless charging. In battery swapping, the discharged EV battery is exchanged with a fully charged EV battery within a few minutes. Through this technology, the charging station must keep a stock of batteries that can be exchanged with EV users. EV owners can then use EV batteries by leasing them from a service provider [35–37].

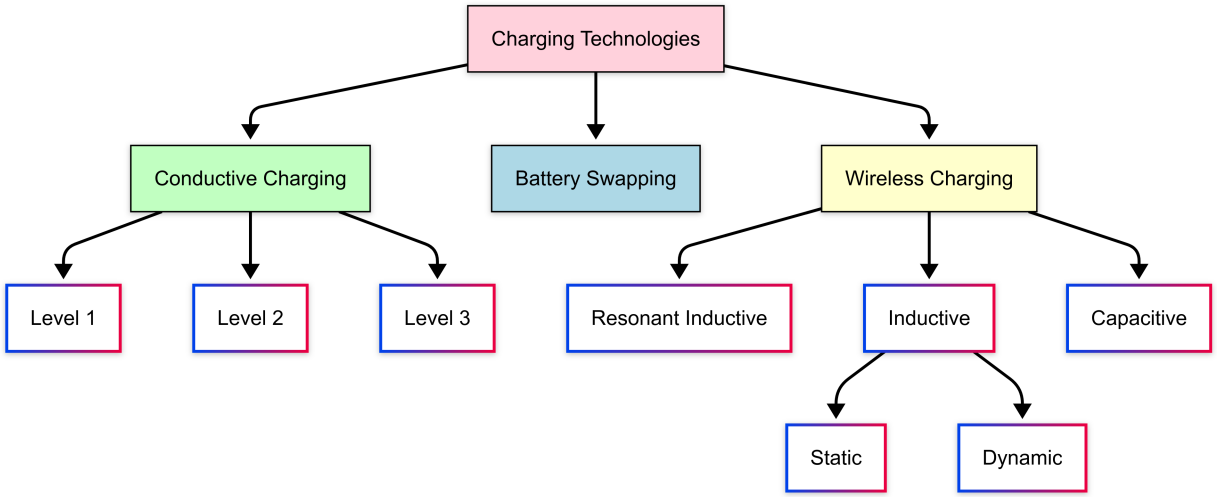


FIGURE 2.2: Different types of EV charging technologies.

Among the charging technologies presented, this thesis focuses on battery swapping stations (BSSs), which use renewable energy systems in conjunction with the utility grid to charge depleted EV batteries after being swapped or exchanged.

2.3.2 Electric vehicle charging structure design

In terms of EV charging architecture design, there are several types available, for instance, a station with a single power source, or a station with multiple hybrid power sources. EV charging stations that use hybrid power sources may offer benefits over those that use single power sources. Numerous concepts are offered to improve the usage of RE systems in conjunction with the utility grid to charge EVs. These include reducing the charging costs of EVs while simultaneously reducing the electricity bills from the utility grid through the power generated by RESs. Moreover, to meet charging demands, the charging process is sustained by power from the RESs in the event of a utility grid failure [38–40]. In order to store surplus RES, a battery energy storage system (BESS) needs be installed as an energy buffer. However, compared to a standalone renewable energy installation, the grid-connected station has higher penetration levels [41, 42].

2.4 Electric vehicle battery swapping station

This section examines the EV BSS in terms of its concept, configuration, and approach perspective.

2.4.1 Definition and concept

EV BSSs represent a significant advancement in electric mobility by offering a rapid and efficient alternative to traditional charging methods. In a battery swapping process, a depleted EV battery is quickly

replaced with a fully charged one, thereby reducing downtime. This approach is particularly beneficial for applications that require quick turnaround times, such as public transportation and commercial fleets. Moreover, integrating hybrid RESs with utility grid power further enhances the sustainability and operational efficiency of these stations. Typically, such hybrid systems combine wind turbines and solar PV power with grid electricity, harnessing the advantages of RE while ensuring a reliable power supply. The optimal design of these systems involves determining the appropriate size and capacity of wind and PV installations relative to the number of charging ports, as well as incorporating energy storage solutions to mitigate the variability in RE generation [37, 43, 44].

2.4.2 Electric vehicle charging and swapping configuration

EV charging and swapping configurations represent a critical component in the transition to sustainable transportation. At its core, these configurations ensure that EVs can be efficiently and reliably powered, whether through traditional charging methods or battery-swapping systems. The design typically involves careful planning of electrical infrastructure, communication protocols, and user interfaces, all essential for managing energy flows and optimizing vehicle uptime.

In a traditional EV charging configuration, multiple charging levels are available to accommodate various user needs and vehicle capabilities. For instance, Level 1 charging uses standard household power, while Level 2 charging involves higher power delivery suitable for home and public installations. Fast-charging systems, often classified as DC fast chargers, can quickly recharge a battery by delivering high-voltage direct current. Each of these configurations requires specific hardware, safety mechanisms, and control systems that monitor energy delivery, thermal management, and grid interactions, ensuring a seamless charging experience while maintaining the longevity of the battery systems [45].

Battery swapping configurations offer an alternative approach, such as replacing the depleted EV battery with a fully charged one in minutes. This method relies on a modular design in which EV batteries are standardized to fit in a wide range of vehicles, allowing for quick interchangeability. BSSs are equipped with automated systems and mechanical interfaces that handle the physical removal and installation of battery packs. These stations often integrate sophisticated battery management systems (BMS) that track the state of each EV battery and ensure that each unit meets quality and performance standards before being deployed again. The overall configuration thus supports rapid turnaround and minimizes downtime, which is particularly beneficial in commercial fleet operations [46, 47].

Modern infrastructure increasingly moves toward hybrid models combining charging and battery swapping capabilities. These integrated configurations allow operators to provide the flexibility of traditional charging alongside the rapid service of battery swapping. Advanced energy management systems, often linked with innovative grid technologies, dynamically allocate resources to manage peak loads and optimize energy consumption. Interoperability between charging standards and networked control systems is key to this approach, enabling centralized monitoring and real-time adjustments that improve overall efficiency and reduce energy costs.

Despite the clear advantages, both charging and swapping configurations face several challenges. Standardization remains a critical hurdle as manufacturers and service providers work to agree on standard battery formats and charging protocols. Additionally, integrating these systems with existing power grids requires robust cybersecurity measures and adaptive control systems to ensure reliability under varying demand conditions. As technology evolves, emerging trends such as wireless charging and improved battery chemistries are poised to reshape these configurations further, promising even faster, safer, and more convenient solutions for electric mobility [48].

2.4.3 Electric vehicle battery swapping approach perspective

The perspective of the BSS approach is based on dynamic collaboration between key stakeholders, including EV owners, station operators, and power systems. EV owners demand a rapid swap, replacing a depleted EV battery with a fully charged one within minutes to minimize downtime. At the same time, station operators must effectively manage electricity costs to keep recharging expenses low. This significant interdependency between the swapping station and the power system requires carefully coordinated strategies. The following sections examine the BSS concept and its benefits from multiple perspectives.

2.4.3.1 Electric vehicle owner perspective

In the context of sustainable mobility, the primary objective of deploying EVs is to provide the level of service that owners expect. To achieve this, EVs draw electrical energy from the utility grid, store it in onboard EV batteries, and then convert that stored energy into the propulsion energy required for operation [22, 49]. From the perspective of an EV owner, BSSs offer a promising solution to address the challenges of EV charging. BSSs have several key advantages and considerations that can significantly influence the adoption and usage of EVs such that:

- **Faster EV battery charging**: Swapping depleted EV batteries at a BSS can be as quick as refuelling a conventional gasoline-powered vehicle, drastically reducing recharge time.
- **Extended trip distance**: Access to fast battery swapping allows EV owners to travel longer distances without requiring lengthy charging stops.
- **Battery lifetime management**: The BSS operator employs advanced control strategies to maintain EV battery health and prevent sequential damages, alleviating concerns about EV battery longevity.
- **Lower household infrastructure costs**: By utilizing BSS, EV owners can avoid the expense of upgrading their home infrastructure to accommodate high-power chargers.
- **Reduced selling price of EVs**: Since the BSS owns the EV batteries, the upfront cost of purchasing an EV is significantly lowered.

These advantages collectively enhance the convenience and cost-effectiveness of owning an EV, making BSS a valuable component in the broader adoption of EVs.

2.4.3.2 Station owner perspective

The rapid advancement in battery technology is driving down the costs of EV batteries and their associated infrastructure, making BSS increasingly viable. For a BSS owner, understanding and optimizing various aspects of the operation is crucial for maximizing benefits and profitability [22, 50]. Here are some key considerations and advantages from the BSS owner's perspective:

1. **Initial investment and EV battery management**:
    - The BSS owner must determine the optimal initial number of batteries to purchase. Expected demand, vehicle types, and battery lifespan influence this decision.
    - A time-scheduled charging strategy based on fluctuating electricity prices can significantly reduce operational costs. The owner can minimize expenses by charging batteries during off-peak hours when electricity is cheaper.
2. **Grid services and ancillary revenue streams**:
    - The storage capability of batteries presents an opportunity for the BSS owner to participate in electricity markets. The BSS owner can generate additional revenue by returning stored energy to the grid during peak demand periods.
    - Providing ancillary services, such as demand response and spinning reserve, further enhances profitability. These services help stabilize the grid and can be a lucrative source of income.
3. **Real estate and space optimization**:
    - Unlike traditional charging stations that require large parking spaces, BSS can operate in more compact areas. This reduces real estate costs and allows for more flexible location choices, including urban areas where space is premium.
4. **Convenience and standardization**:
    - BSS offers a convenient solution for EV owners by providing quick battery swaps, reducing downtime compared to traditional charging methods.
    - The adoption of consistent battery standards ensures compatibility across different EV models, making the swapping process more efficient and reliable for customers.
5. **Environmental and sustainability benefits**:
    - By promoting the use of EVs, BSS contributes to reducing greenhouse gas emissions and supports sustainability initiatives. This can enhance the owner's reputation and attract environmentally conscious customers.

6. **Technological integration and innovation**:

    - Integrating advanced technologies like internet of things (IoT) and artificial intelligence (AI) can optimize battery management, predict maintenance needs, and enhance operational efficiency.
    - Staying updated with the latest battery technologies and market trends allows the owner to adapt and innovate, maintaining a competitive edge.

Deploying a BSS offers numerous benefits for the owner, including cost savings, additional revenue streams, and operational efficiencies. The BSS owner can achieve a sustainable and profitable business model by strategically managing battery inventory, leveraging grid services, and optimizing space utilization.

2.4.3.3 Power system perspective

The behaviour of EV owners is inherently stochastic and unpredictable, making it challenging to implement a controlled strategy for charging and discharging batteries when an EV is in plug-in mode. This uncontrolled charging can significantly impact the power system, increasing peak load and network congestion. In contrast, the BSS approach offers a controlled charging strategy to schedule battery charging times. This means that the BSS can postpone battery charging to nighttime or off-peak hours, thereby mitigating the aforementioned problems. The potential peak demand or overloading caused by the increasing penetration of EVs can be effectively managed by treating the BSS as a large, flexible load from the power system perspective. The BSS achieves this by determining an intelligent charging schedule that does not require upgrading the current grid infrastructure. This controlled approach helps flatten the demand curve and ensures that the power system operates more efficiently. By strategically scheduling the charging and discharging times of batteries, the BSS can play a crucial role in stabilizing the utility grid and accommodating the growing number of EVs without compromising the reliability of the power supply. This controlled charging strategy is supported by research highlighting BSS's benefits in managing EV integration into the power grid. Studies have shown that by implementing such strategies, it is possible to optimize the use of existing infrastructure while minimizing the adverse effects on the power system. This approach benefits the power grid and provides a convenient and efficient solution for EV owners, ensuring that their vehicles are charged and ready for use during peak hours [22, 47].

2.5 Hybrid renewable energy systems for battery swapping station

EVs and RE generation are two independent technologies, but when integrated together they can bring considerable benefits like the reduction of costs and ecological footprint. Eventually, the synergy between the two could also stimulate the development of each technology. Moreover, RE electricity has the advantage of being generated at both medium and low voltage levels within power systems, which additionally

reinforces the idea of embedding RE generation with EVs. A smart control strategy is necessary to optimize the power flows in the system, mostly by adapting the EV charging to variations from renewable energy generation. For example, with photovoltaic energy, the main idea can be to exploit daytime hours, when the solar radiation is at its peak, to store solar power in car batteries for future usage and eventually discharge part of its battery capacity back at the right time. Therefore, a key element in these strategies is the ability of EVs to use bidirectional flow, known as vehicle-to-grid (V2G) [51].

The first step of a smart strategy consists in defining an objective of the strategy. An objective can be either monetary, for example, decreasing electricity costs, or physical, such as reducing the ecological footprint or increasing energy efficiency. The ecological footprint can be direct or indirect emissions of CO_2, while energy efficiency can be the reduction of grid power imports [51]. The literature identifies two possible control modes for the coordination of EVs and renewable energy, which are centralized and decentralized modes. The following are the explanations of different modes:

- Centralised mode: an agent, usually called an aggregator, manages the scheduling of the EV fleet charging. An aggregator could be, for example, the charging station or the BSS itself. The drawback is the necessity to have a heavy communication architecture handling large amounts of data.
- Decentralised mode: EVs set up their charging themselves by reacting to incentives of an aggregator, such as dynamic changes in the electricity prices. On one hand, this requires a less complex communication architecture, on the other hand, the system events are less predictable.

In the latter case, EVs are not directly coordinated by a central entity controlling all charging processes. EVs belong to individuals with specific preferences and constraints, who would not allow control of the charging process without being properly compensated. This happens in the case of plug-in charging mechanisms, where EV owners have the right and chance to charge their vehicle at any time, therefore creating an impossibility for the central power supplier to control and coordinate the charging times directly. In fact, a BSS can act as an aggregator, collecting discharged batteries from EVs and deciding to schedule the charging of such batteries to the best available time frame, avoiding peak demand by proper coordination with the grid. This, of course, should consist of a trade-off, where the BSS tries to avoid excessive loads while keeping a certain amount of charged batteries to ensure service at any time.

With the help of V2G technology, EVs, and RE generation could achieve multiple benefits if combined together, as in the case of the BSS. The BSS can serve as an energy storage station or controllable load, in addition to providing EV users with battery swapping services. Therefore, the cooperation between RE and BSS could not only benefit the power grid but also promote the evolution of the RE business and the electric vehicle industry [52, 53].

2.6 Energy management in battery swapping stations

An effective energy management system (EMS) is essential for optimizing the performance of a BSS by coordinating energy resources efficiently. EMS functions as the intelligence behind BSS operations, collecting data from various energy sources and demand points to ensure an optimal energy balance. The complexity of BSS energy management comes from the integration of multiple energy sources, including renewable generation, grid supply, and battery storage, while accounting for economic and technical constraints. A well-designed EMS within a BSS must address multiple operational scenarios, including utility grid integration, energy forecasting uncertainties, and the dynamic interaction between charging stations and battery swapping operations. Incorporating RESs, such as solar PV and wind power, plays a crucial role in reducing dependence on the power grid and minimizing operational costs. The EMS must dynamically schedule power generation and consumption to ensure a reliable and cost-effective energy supply. In this context, the objective is to maximize the profitability of BSS while ensuring cost-effective energy availability for EV users [54].

The IoT can significantly enhance EMS capabilities by enabling real-time energy monitoring, predictive maintenance, and automated energy flow control. By integrating IoT-based EMS, energy can be efficiently allocated from various renewable sources to meet load demand while maintaining a strategic reserve of charged batteries. Energy transactions in BSS can be further optimized through multiple operational strategies, including Grid-to-Battery (G2B), Battery-to-Grid (B2G), Battery-to-Battery (B2B), RES-to-Battery, and RES-to-Grid, each of which must consider constraints such as battery state-of-charge (SoC) and quality-of-service requirements [55].

Real-time EMS strategies transform complex energy scheduling into single-optimization problems by accommodating dynamic electricity prices, load variability, and forecast uncertainties. This approach not only enhances the economic viability of BSS by integrating aggregator models and advanced IoT-enabled control systems but also enables flexible energy trading that maximizes profit and supports sustainable energy practices. Furthermore, incorporating G2V, V2G, and vehicle-to-vehicle (V2V) functionalities can strengthen the financial sustainability of BSS. Aggregators act as intermediaries between EV users and the utility grid, leveraging price differences to maximize profits while ensuring energy availability. However, improper scheduling in aggregator-based models can lead to unreliable operations and increased greenhouse gas emissions, highlighting the need for precise optimization techniques [56].

2.7 Optimization and control strategies in electric vehicle battery swapping station

BSSs are critical infrastructures to accelerate the adoption of EVs by addressing range anxiety and long charging times, necessitating advanced optimization and control methods to ensure operational efficiency, cost-effectiveness, and grid stability. These stations face challenges such as fluctuating user demand, heterogeneous EV battery SoC levels, dynamic electricity pricing, and integration with RESs, requiring robust

algorithms to balance supply-demand mismatches. Optimization frameworks often employ mixed-integer linear programming (MILP) or stochastic dynamic programming to schedule battery swaps, prioritize charging cycles, and allocate resources while minimizing energy costs and maximizing throughput [57]. Predictive analytics, leveraging historical usage patterns and machine learning (ML), forecast peak demand periods to pre-charge EV batteries and optimize inventory management, reducing wait times and enhancing user satisfaction. Real-time control systems utilize IoT sensors and distributed control architectures to monitor battery health, temperature, and SoC, ensuring safe charging and discharging rates [58, 59].

To address uncertainties in EV arrival times and grid electricity prices, stochastic optimization models incorporate probabilistic scenarios, while reinforcement learning adapts policies dynamically based on real-time feedback. EMS integrate RES and BESS to reduce grid dependency, using model predictive control (MPC) to align RES generation with charging schedules and store surplus energy. Dynamic pricing strategies encourage off-peak battery charging and swaps, helping to balance demand and reduce grid stress during high-tariff periods, by making energy consumption during off-peak hours cheaper [60, 61]. EV battery degradation is mitigated through multi-objective optimization that balances fast charging with longevity, using electrochemical models to limit C-rates and depth-of-discharge (DoD). Queuing theory models, such as Markov decision processes, optimize station layout and workforce allocation, ensuring minimal idle time for EVs and efficient battery retrieval. Vehicle-to-grid (V2G) integration enables bidirectional energy flow, allowing BSS to participate in demand response programs, stabilize grid frequency, and generate ancillary revenue streams. Decentralized control architectures, like multi-agent systems, coordinate multiple BSS nodes across a network, optimizing regional energy distribution and load sharing.

Cybersecurity protocols embedded in control systems safeguard against data breaches and ensure reliable communication between EVs, station controllers, and grid operators. Digital twins simulate BSS operations under varying scenarios, enabling proactive maintenance and algorithm refinement without disrupting live systems. Economic dispatch algorithms prioritize low-cost grid or RESs while adhering to carbon emission caps, aligning with sustainability goals. Finally, heuristic algorithms like genetic algorithm (GA) and particle swarm optimization (PSO) resolve combinatorial complexities in battery assignment and routing, achieving near-optimal solutions with reduced computational overhead. Together, these methods create a resilient, scalable BSS ecosystem that supports mass EV adoption while enhancing grid reliability and operational profitability [62].

2.8 Summary

This chapter provided a theoretical foundation for understanding the key technological and operational aspects of BSSs within the broader context of EV charging infrastructure. It examined fundamental EV charging technologies, the configuration and functionality of BSSs, and their integration with hybrid renewable energy systems. Additionally, the chapter explored optimization and control strategies essential for improving the efficiency, reliability, and sustainability of BSS operations.

By establishing this theoretical background, the chapter highlights the significance of BSSs in addressing challenges such as long charging durations, grid stress, and renewable energy integration. These insights lay the groundwork for further discussions on the implementation, optimization, and economic feasibility of BSSs in subsequent chapters.

Chapter 3

LITERATURE REVIEW

3.1 Chapter Overview

The energy consumption of EV BSSs has been a key focus in industrial energy efficiency research for over a decade. Various studies have explored the design and operation of EV battery swapping stations and the effectiveness of demand-side management (DSM) interventions in optimizing energy consumption. This chapter reviews existing EV BSS energy consumption literature, examining research on design principles, operational strategies, and DSM techniques. It highlights key findings from previous studies, identifies research gaps, and provides insights into the role of optimization and energy management strategies in improving the efficiency and sustainability of EV charging infrastructure.

Section 3.2 reviews the existing literature on the BSS, summarizing key findings and identifying research gaps. while Section 3.3 concludes the literature study.

3.2 Review on previous studies related to the battery swapping station

3.2.1 Development and implementation of BSSs

The growing demand for sustainable transportation has led to an increasing focus on BSSs as a viable alternative to conventional plug-in charging. Various companies worldwide are currently undertaking pilot projects to develop and implement BSSs [24, 63–66]. For example, in Taiwan, companies like Kymco and Gogoro have actively promoted the adoption of electric scooters by developing advanced battery swapping stations. These companies have launched smart electric scooters that allow users to quickly swap their depleted batteries for fully charged ones. These BSS are integrated with smartphone applications, enabling efficient battery management and enhancing the overall convenience and operational performance

for riders [65]. In China, company such as NIO has played an important role in the advancement of electric vehicle technology by introducing a comprehensive battery swapping system. The company operates a vast network of fully automated Power Swap Stations, allowing drivers to exchange depleted batteries for charged ones in just a few minutes. Its latest stations, equipped with advanced LiDAR (Light Detection and Ranging) and high-performance computing systems, are capable of performing hundreds of swaps per day. By mid 2024, NIO had deployed more than 2,400 of these stations across cities and highways, with expansion plans that include rural areas. These stations accommodate various battery sizes and vehicle types and offer high-speed charging through advanced cooling and automation, providing a fast and convenient alternative to traditional charging methods [66]. Several studies highlight the cost-effectiveness of BSS compared to traditional plug-in charging. For instance, [23] proposed proposed a robust optimization model for an EV-integrated RES incorporating BSSs. Their approach introduced an enhanced uncertainty set that integrates source–load distribution and employs a multi-time-scale scheduling method to minimize system costs while ensuring stable operation. Using a nested column and constraint generation algorithm, the model reduces conservatism in uncertainty modeling, resulting in improved economic efficiency and stable operation while meeting EV charging demands. Similarly, [56] developed a real-time energy management strategy for a smart community microgrid integrating BSSs. Their novel Lyapunov optimization framework based on queuing theory demonstrated that a dual purpose BSS could improve the economics of the overall system and facilitate the integration of RE. [67] explored optimal BSS sizing and placement under power reliability and load fluctuations. The results of their study revealed that BSSs contribute to reduced EV waiting times, improved EV battery recharging, and improved grid regulation especially in microgrids. Their analytical model, based on Berlin's transit data, identified optimal locations that maximize revenue while supporting ancillary services. Furthermore, [68] developed an energy management strategy for an EV charging station integrated with a PV system at the University of Trieste, Italy. The system maximizes solar power consumption using real-time data and a rule-based approach while demonstrating a reduction in grid dependence from 28.82% to 5.66% .

3.2.2 Optimization and energy management in BSSs

Optimization models for BSS operations have been a central research focus. [69] developed an inventory-based charging/discharging (IIC) model that optimizes BSS allocation under load uncertainty. Their data-driven addressed the tradeoff between depleted and fully charged EV batteries. The simulation results indicate that the IIC model effectively balances economic performance with robustness in inventory management. Similarly, [70] proposed an optimal planning method for BSS that integrates dynamic power distribution reconfiguration with technical grid considerations. Their multi-objective framework determines optimal placement and capacity while addressing power quality, grid constraints, and operational costs. The results from their case studies showed that this approach reduces system losses, improves voltage stability, and mitigates environmental impacts, underscoring its benefits for both EV users and grid operators. [71] introduced a distributed decision-making framework to jointly optimize power distribution networks and BSS under uncertainty. Their method minimizes worst-case costs while addressing fluctuations in wind and PV power. By reformulating the problem as a MILP using affine decision rules,

duality theory, and analytical target cascading, the approach preserves information privacy and proves less conservative than traditional robust optimization. Case studies confirm its effectiveness in coordinating operations and reducing costs. Additionally, [72] developed an optimization strategy for PV-powered BSSs using spare transformer capacity, thus avoiding new transformer investments. Their approach developed load models, charging rules, and segmented pricing to incentivize off-peak transformer rental. Simulation results demonstrate improved profitability, greater swapping capacity, and more effective peak load reduction. [73] formulated a multi-objective optimization model for a hybrid BSS integrating grid, PV, and biogas energy to maximize profitability and efficiency. Using mixed-integer programming, the model optimizes battery charging schedules and battery-to-grid operations, increasing daily net profit by up to 20 times compared to the base case. Allowing grid discharge further boosts profits by 8%. The study highlights BSS as a solution to EV range anxiety while promoting RE adoption, reducing greenhouse gas emissions, and accelerating EV market acceptance. [74] proposed a multi-objective optimization method for a centralized battery swap charging system (CBSCS) integrated with PV. Using a modified non-dominated sorting genetic algorithm III (NSGA-III), their developed model minimizes total operational costs by considering opportunity and inventory costs of reserve EV batteries. Simulation results show that PV integration reduces costs and grid impacts, with the modified NSGA-III generating superior pareto fronts compared to traditional algorithms. Further, [75] developed a mathematical model to address uncertainty constraints in BSSs, focusing on optimizing operation costs through demand shifting. Their simulation results validated the feasibility of minimizing energy expenses while ensuring battery availability and to assess its practicality in terms of reaching the lowest possible operating cost. [76] explored risk-aware energy management for microgrids incorporating BSSs, demonstrating that BSS can act as bulk storage while improving revenue under uncertainty. Responsive loads further improve revenue under uncertainty. [77] proposed an optimization model for scheduling BSSs in isolated microgrids powered by distributed energy sources. Using YALMIP + CPLEX, their model optimizes charging during low-load periods to reduce power purchase costs, grid losses, and voltage fluctuations while improving stability. Simulation results demonstrate that orderly BSS charging enhances grid security and efficiency, preventing peak overloads. Similarly, [78] introduced a demand response management framework for BSSs, optimizing battery swapping schedules to reduce peak-valley load differences in local power grids. Their time series analysis model predicts battery swapping demand, while an optimal scheduling model enhances grid stability and RE utilization. The study highlights benefits such as improved grid response, enhanced user experience through faster energy replenishment, and better EV battery management at BSS, extending EV battery life. [79] employed particle swarm optimization (PSO) to optimize BSS placement and sizing but note its limitations in dynamic grid reconfiguration. To address asynchronous EV battery swapping and centralized charging in isolated microgrids, they propose a service model leveraging backup batteries. They further introduce a quantum-behavior PSO (QPSO) algorithm, which improves BSS reliability and profitability compared to traditional methods.

3.2.3 Identified research gaps

Despite significant advancements in EV BSS research, several gaps remain unaddressed:

1. **Limited utilization of BSSs for RE integration and energy trading**: Most studies focus on hybrid RE generation for BSSs but fail to explore the potential of integrating multiple RESs for efficiently charging EV batteries before swapping.
2. **Underexplored impact of frequent EV battery discharging on battery life cycle costs**: Existing research often overlooks the effects of repeated charging and discharging on battery degradation, which directly affects operational costs and long-term economic feasibility.
3. **Insufficient consideration of market-based energy dispatch and pricing strategies**: While optimization models focus on cost reduction, there is limited research on leveraging real-time electricity pricing and energy trading mechanisms to maximize revenue generation.
4. **Need for multi-objective optimization approaches**: Most studies focus on single-objective cost minimization, whereas a more comprehensive multi-objective approach is necessary to balance operational efficiency, economic viability, and sustainability.

To address these gaps, this research work proposes a multi-objective optimization model that minimizes the design and operational costs of EV BSSs while maximizing revenue through optimal energy dispatch. The model will:

- Strategically integrate RE and grid power supply systems.
- Optimize energy sales to the utility grid based on market price signals.
- Incorporate dynamic energy trading mechanisms to enhance economic viability.
- Improve energy management strategies to ensure sustainability and efficiency.

This novel approach will support the widespread adoption of EVs while enhancing the financial and operational feasibility of BSS deployment.

3.3 Summary

A review of the literature on BSSs reveals substantial progress in optimizing their internal operational aspects, including rapid EV battery swapping, extended battery life, and enhanced EV range through advanced charging methodologies and renewable integration. However, most studies have primarily focused on internal factors such as scheduling and revenue generation while overlooking external challenges, including dynamic RE integration and its impact on overall utility grid efficiency.

To achieve maximum energy efficiency in EV charging infrastructure, it is essential to optimize not only the core operations of BSSs but also their interactions with external power networks and energy markets. Properly integrating RESs and implementing effective demand-side management strategies can enhance system reliability, reduce operational costs, and improve the overall sustainability of EV charging systems.

The subsequent chapter proposes novel methodologies for the optimal design and techno-economic feasibility of EV BSS intergrated with grid-connected wind-solar PV system. The proposed approach aims to minimize the total life cycle cost and energy consumption costs from the utility grid while maximizing system reliability through effective demand-side management strategies. By addressing these challenges, this research contributes to the development of more efficient, cost-effective, and sustainable BSS solutions, ultimately supporting the transition toward a cleaner and more resilient EV ecosystem.

Chapter 4

OPTIMAL DESIGN AND TECHNO-ECONOMIC FEASIBILITY OF GRID-CONNECTED WIND-SOLAR ENERGY SYSTEM FOR BATTERY SWAPPING STATION

4.1 Chapter overview

The content of this chapter is adapted from our previously published work [80], titled "Techno-economic feasibility and optimal design approach of grid-connected hybrid power generation systems for electric vehicle battery swapping stations." This chapter focuses on evaluating the technical and economic performance of a grid-connected wind-solar power supply system for an electric vehicle battery swapping station. The mathematical models of the components of the proposed system are presented to investigate the viability of the hybrid system as an alternative energy source. The objective is to evaluate its potential for cost savings and overall cost-effectiveness by minimizing total life-cycle cost, reducing dependence on the utility grid, and maximizing system reliability. To achieve this, an optimal control model is designed and solved using MILP. Decision variables include the power drawn from the utility grid, the number of

wind turbines, and the number of solar PV panels. The effectiveness of this model is verified through a case study, with simulation results demonstrating the desirable performance of the proposed system. The optimal number of wind turbines and solar PV panels leads to energy cost savings for the case studied. The results of the LCC analysis indicate a payback period demonstrates that the proposed hybrid system is economically and technically feasible. It is important to note that this chapter does not consider the battery energy storage system (BESS).

The remainder of this chapter is structured as follows: An overview of the mathematical model formulation of the proposed system is given in Section 3.2. The case data used are introduced in Section 3.3. Following that, Section 3.4 analyzes the simulation results and discusses the optimization findings. Lastly, Section 3.5 concludes the chapter.

4.2 Mathematical model formulation

A mathematical model has been developed to evaluate the feasibility and performance of the proposed hybrid power supply system for an EV BSS. This model aims to optimize system operation by minimizing the total life cycle cost while ensuring a reliable power supply. The formulation incorporates key decision variables, including grid power consumption, the number of WTs, and the number of solar PV panels. Constraints related to power balance, system reliability, and economic feasibility are considered. The optimization problem is solved using mixed-integer linear programming, ensuring an efficient allocation of resources and cost-effective system operation

4.2.1 Schematic model layout

Figure 4.1 illustrates the schematic layout of the proposed grid-connected wind–photovoltaic hybrid power generation system designed for the EV BSS. The main components of the proposed system are the vertical wind turbines (WTs), the solar photovoltaic generator (PV), the inverters, and the battery swapping station (BSS), which comprises the charging apparatus and swapping service for the depleted EV batteries. For such a proposed system, the size of the hybrid renewable power generation system depends on the charging and swapping demand service at the BSS. The BSS uses three distinct sources of electrical energy to recharge the depleted swapped EV batteries. These sources include the electric power generated by vertical WT, the electric power generated by the solar PV generator, and the electric power acquired from the utility grid. To ensure that the demand for swapping depleted EV batteries is met efficiently, it is crucial to accurately determine the properties of power sources utilized to charge the depleted EV batteries. By doing so, the charging process can be optimized to effectively replenish the EV batteries and meet the needs of the drivers. The depleted EV batteries are charged with the utmost priority using clean and renewable energy generated by the vertical WT and solar PV generator. This ensures optimal charging of depleted EV batteries while minimizing electricity use from the utility grid. However, the charging process depends on the accessibility of sufficient resources. In other words, if the electric

power generated by the vertical WT and solar PV generator is inadequate, the utility grid supplies the necessary power to charge the depleted EV batteries. Suppose the electric power generated by the vertical WT and solar PV generator exceeds the charging demand of the depleted EV batteries. In that case, the excess electricity can be sold back to the utility grid. The fluctuating electricity prices throughout the day significantly influence the overall cost of the charging process. Implementing a time-of-use (TOU) tariff helps to manage this cost by strategically selecting the power source for recharging depleted EV batteries. The TOU tariff is strategically designed to incentivize power consumption during off-peak periods when electric power prices are at their lowest. This approach serves the dual purpose of minimizing stress on the utility grid during peak hours and optimizing the cost-effectiveness of the charging process. Depending on the prevailing TOU tariffs, the BSS can be supplied by either hybrid power generation or the utility grid. This flexibility enables the BSS to draw power from the utility grid during off-peak periods, leading to cost savings. By doing so, the power flow from the utility grid is managed efficiently and cost-effectively, maintaining reliability and stability. This strategic utilization of the TOU tariff and power source selection not only minimizes operational costs but also contributes to the overall sustainability and resilience of the EV charging infrastructure. The decision to charge the depleted EV batteries is determined by multiple factors, such as the power flow's limitations and the TOU electricity tariff within the utility grid. The power flow's limitations depend on the available power capacity and the current power demand in the system. The TOU tariff considers the cost of electricity at different times of the day, where charging the depleted EV batteries during off-peak periods can be more cost-effective. On the other hand, the decision to replace the depleted EV batteries with fully charged ones is determined by the EV driver's arrival or the swapping service demand at the BSS. The BSS can offer a convenient solution for EV drivers who want to continue their journey without waiting for their EV battery to charge. In this chapter, the electrical energy generated by the renewable hybrid power generation system is deliberately not reintegrated into the utility grid.

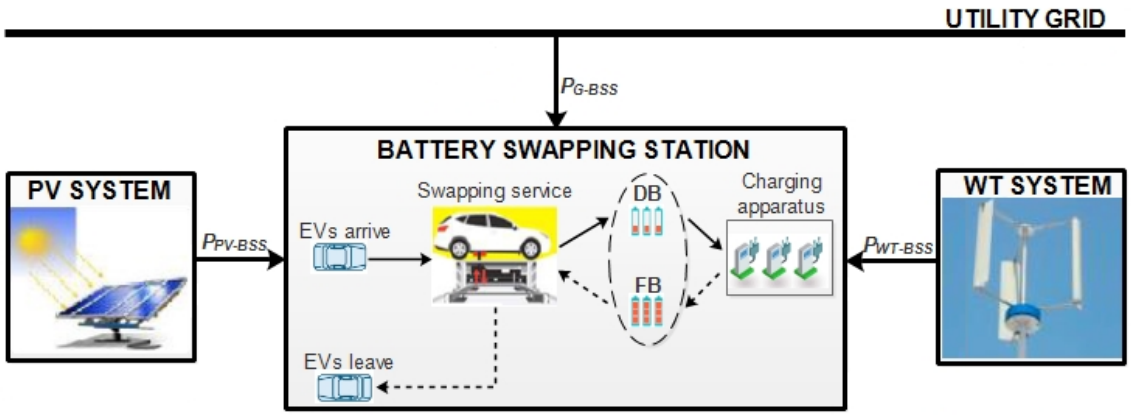


FIGURE 4.1: Schematic layout of the proposed system.

4.2.2 Wind turbine system

In wind energy systems, the air is moved to generate power through its kinetic energy. Wind energy is a resource that has the potential to be abundant and that might be easily harvested and converted into useful energy using standard technology. In addition to enabling the efficient utilization of distributed resources, wind energy systems offer the potential to make energy supply systems more flexible, robust, secure, stable, and profitable [81]. As a result, it is crucial to have a reliable assessment of the resources available at a wind farm to generate electricity there. In general, when the wind speed ranges between the "cut-in wind speed" (V_{ci}) and the "rated wind speed" (V_r), the power output of the WT is proportional to the cube of the wind speed. The model used to determine the power output of the WT is displayed in Figure 4.2. When the wind speed is below the cut-in speed, the WT is unable to generate electricity. Once the wind speed surpasses the cut-in speed, the power generated by the WT increases with the cube of the wind speed, reaching its maximum output at the rated speed. It is known as the rated power (Pr_{WT}), and it is the power for which the wind turbine is designed. As shown in Figure 4.2, the wind speed is very high at some given time, which is dangerous for wind turbines. This is referred to as "cut-out wind speed" (V_{co}). The wind turbine operation must stop at this point because it has reached the (V_{co}). Equation (4.1) represents a description of the simplest straightforward model of this behavior to simulate the power output of the WT [82]:

$$p_{WT}(t) = \begin{cases} 0 & V(t) \leq V_{ci} \\ Pr_{WT}\dfrac{V(t) - V_{ci}}{V_r - V_{ci}} & V_{ci} \leq V(t) \leq V_r \\ Pr_{WT} & V_r \leq V(t) \leq V_{co} \\ 0 & V(t) \geq V_{co} \end{cases} \tag{4.1}$$

where $V(t)$ denotes the wind speed at sampling time t, V_r denotes the rated wind speed, V_{ci} denotes the cut-in wind speed, V_{co} denotes the cut-out wind speed, and Pr_{WT} denotes the rated power of the wind generator. If the wind speeds and rated power are known, Equation (4.1) can be used to calculate the power output of the WT. Thus, the rated power of the WT generator can be expressed as

$$Pr_{WT} = \frac{1}{2}\eta_t \eta_g \varphi_a C_p A_{WT} V_r^3 \tag{4.2}$$

where η_t denotes the gearbox efficiency, η_g denotes the generator efficiency, φ_a denotes the density of air, C_p denotes the power coefficient of the WT, which is the ratio of the power output of the wind generator divided by maximum power, and A_{WT} denotes the sweeping area of the turbine rotor. In contrast, V_r denotes the rated wind speed.

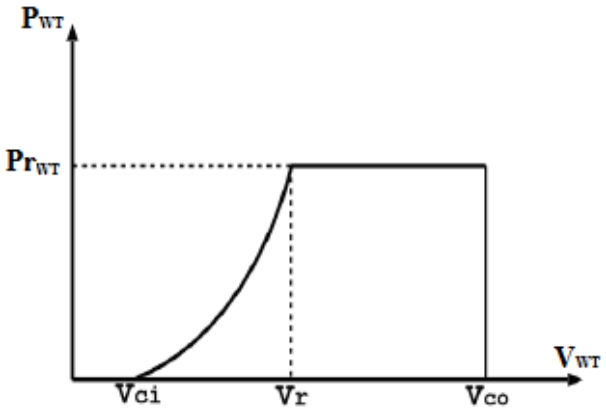


FIGURE 4.2: Wind generator power curve.

Adjustments to the wind speed profile may be required to optimize energy generation from the WT system depending on the turbine's height. The wind speed profiles can be simulated using two mathematical models: the logarithmic law and the power law. As a standard analytical approach in the field, this paper employs the power-law model to calculate wind speed at the hub height [83]. When applying this model, the wind speed at the hub height is calculated from

$$\frac{V}{V_{ref}} = \left(\frac{h}{h_{ref}}\right)^{\alpha} \tag{4.3}$$

where V_{ref} denotes the wind speed measured at the reference height (h_{ref}), V denotes the wind speed measured at the hub height (h), and α denotes the coefficient of ground surface friction, which has a value of more than 0.25 in forested areas and less than 0.1 in flat or watery areas [83].

Multiple WTs can be coupled in parallel to meet the proposed system requirements. One of the design variables is the number of WTs (N_{WT}) when operating in parallel. The size of the WT is among the variables that influence the power output of the WT. When N_{WT} is taken into account as the number of WTs, the power output generated by the WT at sampling time (t) is calculated from

$$P_{WT}(t) = N_{WT}\ p_{WT}(t) \tag{4.4}$$

Under varying operational conditions, the net power supply of the WT to the power system is limited by boundaries, which can vary between zero and the maximum power output generated. This relationship can be mathematically expressed as

$$0 \leq P_{WT}(t) \leq P_{WT}^{max}(t) \tag{4.5}$$

where 0 is the minimum capacity of the power output generated by the WT and P_{WT}^{max} is the maximum capacity of the power output generated by the WT.

Furthermore, the limited availability in number of WTs is constrained so that

$$N_{WT}^{min} \leq N_{WT} \leq N_{WT}^{max} \tag{4.6}$$

where N_{WT}^{min} is the minimum number of WTs taken as zero and N_{WT}^{max} is the maximum number of WTs that can fit into the allocated area as provided by

$$N_{WT}^{max} = \frac{AT_{WT}}{A_{WT}} \tag{4.7}$$

where AT_{WT} is the total sweeping area available for the WT at the EV BSS and A_{WT} is the sweeping area of the WT rotor.

4.2.3 Solar photovoltaic system

By definition, PV is a technology that converts the radiant (photon) energy from sunlight into DC power [84]. A PV cell is a crucial element in converting light energy directly into electrical energy through a chemical and physical process called the PV effect. The term describes a device whose electrical properties change when exposed to light, such as voltage, current, or resistance. Solar PV panels, also known as solar PV modules, comprise solar PV cells. A solar PV module or solar PV panel comprises several solar PV cells arranged in an integrated group, all facing the same direction. In contrast, an array or solar PV array comprises the solar PV module or solar PV panel connected in parallel, series, or a combination of the two [85]. The size of the PV panel, its efficiency, solar radiation, and the surrounding temperature all affect how much electricity the PV system can generate. The power output generated by a solar PV array is provided by [85]

$$p_{PV} = \eta_{PV} A_{PV} I_{PV} \tag{4.8}$$

where p_{PV} is the power output generated by the PV array, A_{PV} is the area of the PV array exposed to solar radiation, I_{PV} is the solar radiation that reaches the PV array, and η_{PV} is the energy conversion efficiency of the PV generator.

It is possible to express the solar irradiation according to the time during the day using

$$I_{PV}(t) = R_B \left[I_B(t) + I_D(t) \right] + I_D(t) \tag{4.9}$$

where R_B is a geometric factor used to indicate the ratio between plane-tilted beams' irradiation incident and plane-horizontal beams' standard irradiation, $I_D(t)$ is the diffuse irradiation, and $I_B(t)$ is the hourly global irradiation.

The ambient temperature and hourly isolation impact the solar PV generator energy conversion efficiency η. It can be stated that

$$\eta_{PV} = \eta_r \eta_{pc} \left[1 - \beta \left(T_c - T_{c_{ref}} \right) \right] \tag{4.10}$$

where β denotes the temperature factor for PV generator efficiency, which ranges from 0.004 to 0.006 per °C, $T_{c,ref}$ denotes the reference cell temperature, η_{pc} denotes the efficiency of power conditioning, T_c denotes the cell temperature, and η_r denotes the manufacturer-rated efficiency of the solar array module.

The cell temperature is

$$T_c = T_a + \left(\frac{T_{NOCT} - 20}{800}\right) I_{PV}(t) \tag{4.11}$$

where T_{NOCT} is the nominal cell operating temperature, while T_a is the ambient temperature.

The power output of a PV array depends on the number of installed PV panels (N_{PV}). Factors such as the size of the panels and others influence the total power generated by the PV system. When considering N_{PV} as the number of solar PV panels, the total power output generated by the PV panels at a given sampling time (t) can be calculated from

$$P_{PV}(t) = N_{PV}\ p_{PV}(t) \tag{4.12}$$

Depending on the operation conditions, the net power supply of the solar photovoltaic panels to the power system is determined by sizing and optimal positioning, and it can vary between zero and the maximum power output generated. This can be stated in the following way:

$$0 \leq P_{PV}(t) \leq P_{PV}^{max}(t) \tag{4.13}$$

where 0 and P_{PV}^{max} represent the minimum and maximum capacity of the solar PV panel, respectively.

Furthermore, the limited availability number of solar PV arrays is constrained so that

$$N_{PV}^{min} \leq N_{PV} \leq N_{PV}^{max} \tag{4.14}$$

where N_{PV}^{min} is the minimum number of solar PV panels taken as zero and N_{PV}^{max} is the maximum number of solar PV panels that can fit into the allocated area as provided by

$$N_{PV}^{max} = \frac{AT_{PV}}{A_{PV}} \tag{4.15}$$

where AT_{PV} denotes the total available surface area for the solar PV panel at the EV BSS and A_{PV} denotes the area of the PV array that is exposed to solar radiation.

4.2.4 Inverter

The inverter is a very important device in grid-connected renewable energy systems. It is used to synchronize the output power and set the output voltage. Inverters convert DC power sources to AC power and vice versa. The power output of the WT is AC, which is converted into DC by the inverter for later use. Therefore, it is essential to have high inverter efficiency. The inverter efficiency is provided by [86]

$$\eta_{INV} = \frac{P_{out}(t)}{P_{in}(t)} \tag{4.16}$$

where η_{INV} is the efficiency of the inverter, P_{out} is the power out from the inverter, and P_{in} is the power that enters into the inverter. In order to ensure safe operation and efficiency, the inverter's rated power should often be oversized by 10% to 30% [87]. Therefore, the inverter-rated power is

$$Pr_{INV} = \sum_{t=1}^{N} P_{in}(t) K_{INV} \tag{4.17}$$

where K_{INV} is the oversized coefficient of the inverter. The inverter lifetime is less than the installation lifespan. The total number of inverter replacements required over the system's operational lifetime can be quantified as

$$N_{Rep,INV} = \frac{L_p}{L_{INV}} - 1 \quad , \tag{4.18}$$

where L_p is the lifetime of the installation project, while L_{INV} is the lifetime of the inverter.

4.2.5 Utility grid power supply system

The current utility grid was not designed to accommodate the charging demand of depleted EV batteries [88]. In contrast to household loads, the full charge of the depleted EV batteries requires high power levels and substantial amounts of energy [89,90]. Charging the depleted EV batteries can have a significant impact on voltages, component loads, and losses depending on the supplied loads and the design of the utility grid. The impacts on the utility grid are significantly influenced by the charging power and penetration level of the EVs. The number of EV batteries as a percentage of all EVs at the BSS is the general definition of the penetration level. The power from the utility grid is modeled as an all-time available power source for recharging depleted EV batteries at the BSS. The total energy supplied by the utility grid is provided by

$$E_g = \sum_{t=1}^{N} P_{G-BSS}(t)\ \Delta t \tag{4.19}$$

where P_{G-CSS} is the power flow from the utility grid to charge the depleted EV batteries at the BSS and Δt is the sampling time.

Therefore, the energy cost that can be extracted from the utility grid is established by the local electricity market policy and time of use (TOU) tariff. Two parameters are required for utility grid modeling: the utility grid's maximum power demand (measured in kW), which defines the upper limit of electricity that can be drawn, and the energy procurement cost (expressed in ZAR/kWh), representing the cost of electricity supplied by the utility grid. The energy cost C_{Eg} that can be drawn from the utility grid when charging the depleted EV batteries can be calculated from

$$C_{Eg} = p_e(t) \sum_{t=1}^{N} P_{G-BSS}(t)\ \Delta t \tag{4.20}$$

where $P_e(t)$ is the TOU electricity price at the t-th sampling interval per kWh. Additionally, the power drawn from the utility grid can be constrained to a limited range using

$$0 \leq P_{G-BSS}\,(t) \leq +\infty \tag{4.21}$$

4.2.6 Battery swapping station power demand

An EV BSS is a facility designed for EV owners to efficiently exchange their depleted EV batteries for fully charged ones in just several minutes. This innovative concept has emerged as a potential solution to address the challenges associated with traditional plug-in charging methods for EVs [91, 92]. A standard EV BSS has one or more battery swapping units, enabling multiple EVs to exchange their depleted EV batteries simultaneously. Several factors, such as the charging and swapping processes of depleted EV batteries and the specific characteristics of the EV batteries themselves, typically influence the power demand of a BSS. These specific characteristics encompass parameters such as EV battery capacity, EV battery technology, and the depleted EV battery's state of charge (SoC) before charging [93]. Proper modeling of power demand at the BSS is crucial, especially during the charging period of depleted EV batteries, to ensure sufficient supply for swapping demand when EVs arrive. Equations (4.22) and (4.23), respectively, represent the total charged and discharged power of depleted EV batteries at the BSS. These equations calculate the cumulative power by summing the power contributions or power outputs of all depleted EV batteries present at the BSS [94].

$$P_{c,BSS}(t) = \sum_{EV,b=1}^{n} P_{c,(EV,b)}(t) \tag{4.22}$$

$$P_{d,BSS}(t) = \sum_{EV,b=1}^{n} P_{d,(EV,b)}(t) \tag{4.23}$$

where n is the total number of depleted EV batteries at the BSS, $P_{c,BSS}(t)$ is the total charging power of the depleted EV batteries at the BSS, $P_{d,BSS}(t)$ is the total discharging power of the depleted EV batteries at the BSS, $P_{c,(EV,b)}(t)$ is the charging power of one depleted EV battery at the BSS, and $P_{d,(EV,b)}(t)$ is the discharging power of one depleted EV battery at the BSS. Each depleted EV battery undergoes a charging or discharging process similar to a conventional battery. The charging process of depleted EV batteries is determined by their state of charge (SoC) at specific time intervals, representing the available capacity relative to the maximum capacity when fully charged. Taking these factors into account, the SoC of every EV battery at t^{th} sampling interval inside the BSS can be generally expressed by [75, 94]

$$SOC_{EV,b}(t) = SOC_{EV,b}(t-1) + \left(P_{c,(EV,b)}(t) - \frac{P_{d,(EV,b)}(t)}{\eta_{EV,b}}\right) \times I_{dur}(t) \tag{4.24}$$

where $I_{dur}(t)$ is the duration of time interval in minutes and $\eta_{EV,b}$ is the efficiency of one EV battery (%) and provided by Equation (4.25).

$$\eta_{EV,b} = \frac{\sum_{t=1}^{N} P_{d,(EV,b)}(t) \times I_{dur}(t)}{\sum_{t=1}^{N} P_{c,(EV,b)}(t) \times I_{dur}(t)} \tag{4.25}$$

The battery swapping procedure at a BSS involves replacing a depleted EV battery with a fully charged one from an incoming EV. This swap period prevents the EV battery from charging or discharging as the swapping operation progresses. As a result, the EV battery's power and SoC are reset to zero during the swapping period, as defined by Equation (4.26).

$$\begin{cases} P_{c,(EV,b)}(t) = 0 \\ P_{d,(EV,b)}(t) = 0 \\ SoC_{EV,b}(t) = 0 \end{cases} \qquad \forall t = t_{swap} \tag{4.26}$$

Before the battery swapping period, the depleted EV battery must be fully charged in preparation for the next swap. Thus, the energy management system must guarantee that an adequate number of fully charged EV batteries are available at each time interval to meet the demand for upcoming swaps. This requirement is articulated in Equation (4.27).

$$SoC_{EV,b}(t) = SoC_{EV,b}(t-1) \qquad \forall t = (t_{swap} - 1) \tag{4.27}$$

The total power demand at the BSS is based on the power capacity of the charging station. The discretized charging power demand for each depleted EV battery is added together to determine the overall charging power demand. In other words, the total expected power demand required to charge all n depleted EV batteries at the BSS during time t can be calculated using Equation (4.28).

$$P_{Ld,BSS}(t) = \sum_{EV,b=1}^{n} \left(P_{c,(EV,b)}(t) - P_{d,(EV,b)}(t) \right) \tag{4.28}$$

where $P_{Ld,BSS}(t)$ is the total expected power demand of all depleted EV batteries charged at time (t) and n is the total number of depleted EV batteries at the BSS.

4.2.7 Economic evaluation parameters of the proposed system

The economic evaluation indicators are mathematical methods used to compare the costs and benefits of the installations in terms of economic, commercial, and social aspects. These indicators play a crucial role in the optimization design of grid-connected hybrid systems [95, 96]. This chapter considers the economic parameter based on the life cycle cost (LCC) concept as the economic criterion to evaluate the financial viability of the installation system. The LCC method accounts for the time value of money and the system's lifespan by discounting all future cash flows to their present value. In other words, the LCC covers all the

cash inflows and outflows into the proposed system in its entire lifetime. It evaluates initial investment options and determines the most cost-effective alternative over a year x [97,98]. The costs included in the LCC evaluation are the initial capital investment cost (I_{IVST}), operation and maintenance cost ($C_{O\&M}$), replacement cost (C_R), and salvage cost (C_S). Mathematically, the LCC is provided by [99,100]

$$LCC = I_{IVST} + C_{O\&M} + C_R - C_S \tag{4.29}$$

The initial capital investment cost is the amount of money required to set up all components in the proposed system, which includes the cost of purchasing materials, installation of each component, and civil works. Meanwhile, the operating and maintenance cost value indicates the maintenance costs incurred throughout the proposed system's lifespan for all components to ensure proper operation. This represents the total of all yearly planned operation and maintenance costs. The operator's wage, inspections, insurance, and any necessary planned maintenance are all included in the operation and maintenance cost. A general formula for calculating the present value of the $C_{O\&M}$ of a hybrid system is provided by [101,102]

$$C_{O\&M} = \begin{cases} C_{(O\&M)_0} \times \dfrac{1+r}{i-r}\left[1 - \left(\dfrac{1+r}{1+i}\right)^{L_P}\right] & \text{for} \quad i \neq r \\ C_{(O\&M)_0} \times L_p & \text{for} \quad i = r \end{cases} \tag{4.30}$$

where $C_{(O\&M)_0}$ is the operation and maintenance cost in the first year, r is the inflation rate, i is the interest rate, and L_P is the lifespan of the installation. The replacement cost is a cautionary expense over the lifetime of the proposed system for replacing any components. During the lifespan of the proposed system, some components, like the inverter, could need to be changed. Again, the price of these components is liable to change in the future. The present value of C_R can be determined by incorporating the real interest rate (i) and accounting for the inflation rate (r_0) of the component to be replaced [101,102]. It can be expressed as

$$C_R = C_{unit}\ C_{nom} \sum_{y=1}^{N_{rep}} \left[\frac{(1+r_0)}{(1+i)}\right] \left(\frac{L_y}{N_{rep}+1}\right) \tag{4.31}$$

where C_{unit} is the capital cost of the component per wh, C_{nom} is the nominal capacity of the replacement system component in wh, r_0 is the inflation rate of the component replaced taken equal to r, y is the index of the components, L_y is the lifetime of the components, and N_{rep} is the number of replacements of each component over the system lifespan period of the installation (L_p). Finally, the cost incurred at the end of the system's lifespan is known as the salvage cost. This includes the cost of removal and disposal and the proposed system's salvage value.

Assessing the economic viability of the hybrid system requires calculating its overall life cycle cost. This is achieved by summing the LCC of each component so that

$$LCC_{Tot} = LCC_{WT} + LCC_{PV} + LCC_{INV} \tag{4.32}$$

where LCC_{WT} is the life cycle cost of the WT, LCC_{PV} is the life cycle cost of the solar PV generator, and LCC_{INV} is the life cycle cost of all the inverters.

(a) **LCC of the wind turbine system**

The initial capital investment cost of the wind turbine system includes the cost of purchasing and installing the wind turbine at the BSS. The purchase cost of the wind turbine may vary depending on its size, efficiency, and brand. In addition, installation costs can vary based on various factors, including the site's location and the complexity of the installation process. Overall, the initial capital investment cost of the WT system can be estimated by factoring in the cost of purchasing and installing the WT, as shown in (4.33).

$$I_{IVST,WT} = IC_{WT} + I_{INST} \tag{4.33}$$

where $I_{IVST,WT}$ is the initial capital investment cost of the WT generator system, IC_{WT} is the initial cost of the WT, and I_{INST} is the installation cost of the WT. If the installation cost is assumed to be 20% of the initial cost of the WT generator [103, 104], then the initial capital investment cost for the WT generator can be expressed as

$$I_{IVST,WT} = 1.2\ \gamma\ N_{WT}\ Pr_{WT} \sum_{t=1}^{N} P_{WT}(t) \tag{4.34}$$

where γ is the capital cost of the WT generator per kW, N_{WT} is the total number of WT generators, and Pr_{WT} is the power rating of the WT. It is assumed that the operation and maintenance cost of the WT generator ($C_{O\&M,WT}$) will be 5% of its initial capital investment cost [103, 104]. Considering the annual cost of WT generator increasing at the inflation rate (r), the net present value of the $C_{O\&M,WT}$ can be calculated using

$$C_{O\&M,WT} = 0.06\ \gamma\ N_{WT}\ Pr_{WT} \sum_{t=1}^{N} P_{WT}(t) \times \Gamma \tag{4.35}$$

with $\Gamma = \left[\dfrac{1+r}{i-r}\left(1 - \left(\dfrac{1+r}{1+i}\right)^{L_p}\right)\right]$

Assuming that the installation lifespan and the wind turbine generator lifetime are equal, the replacement cost of the wind turbine generator is zero ($C_{R,WT} = 0$). The salvage cost is neglected. As a result, by using (4.34) and (4.35), the LCC of the WT generator (LCC_{WT}) can be obtained from

$$LCC_{WT} = (1.2 + 0.06\ \Gamma)\,\gamma\ N_{WT}\ Pr_{WT} \sum_{t=1}^{N} P_{WT} \tag{4.36}$$

(b) **LCC of the photovoltaic system**

The initial capital investment cost of the PV system includes the purchase and installation costs of the solar panel at the BSS. The purchase cost of the solar panel may vary depending on its size, efficiency, and brand. Additionally, installation costs may vary based on various factors, including the site's location

and the complexity of the installation process. Overall, the initial capital investment cost of solar PV system can be estimated by factoring in the cost of purchasing and installing the solar panel, as shown in (4.37).

$$I_{IVST,PV} = IC_{PV} + I_{INST} \tag{4.37}$$

where $I_{IVST,PV}$ is the initial capital investment cost of the solar PV system, IC_{PV} is the initial cost of the solar panel, and I_{INST} is the installation cost of the solar panel. Some studies indicate that solar PV system installation cost represents approximately 40% of total initial cost [103, 104]. By considering the installation costs along with other associated expenses, the initial capital investment cost of the solar PV panel is provided by

$$I_{IVST,PV} = 1.4\ \delta\ N_{PV}\ Pr_{PV} \sum_{t=1}^{N} P_{PV}(t) \tag{4.38}$$

where δ is the capital cost of the solar PV panel pekW, N_{PV} is the total number of solar PV panels, Pr_{PV} is the power rating of the solar PV, and $P_{PV}(t)$ is the output power generated by the solar PV panel at each instant t. The $C_{O\&M}$ of solar PV panels is assumed to be 1% of their initial capital investment cost [103, 104]. Considering the annual cost of solar PV panels increasing at the inflation rate (r), the net present value of the operation and maintenance cost ($C_{O\&M,PV}$) can be calculated from

$$C_{O\&M,_{PV}} = 0.014\ \delta\ N_{PV}\ Pr_{PV} \sum_{t=1}^{N} P_{PV}(t) \times \Gamma \tag{4.39}$$

with $\Gamma = \left[\dfrac{1+r}{i-r}\left(1 - \left(\dfrac{1+r}{1+i}\right)^{L_p}\right)\right]$

If it is assumed that the installation and the solar PV panels have the same lifetime, then the replacement cost of the solar PV panel is zero ($C_{R,PV} = 0$). The salvage cost is ignored. By using Equations (4.38) and (4.39), the overall LCC of the PV power generation system (LCC_{PV}) is provided by

$$LCC_{PV} = (1.4 + 0.014\ \Gamma)\ \delta\ N_{PV}\ Pr_{PV} \sum_{t=1}^{N} P_{PV}\,(t) \tag{4.40}$$

(c) **LCC of the inverters**

The initial capital investment cost of the inverter ($I_{IVST,INV}$) includes all the expenses incurred in the purchase and installation of the inverter at the BSS. This includes the cost of the inverter unit, as well as any additional equipment, parts, and labor required to complete the installation. The $I_{IVST,INV}$ is provided by

$$I_{IVST,INV} = I_{C,INV} + I_{INST} \tag{4.41}$$

where $I_{IVST,INV}$ is the initial capital investment cost of the inverter, $I_{C,INV}$ is the initial cost of the inverter, and I_{INST} is the installation cost of the inverter. This paper does not take into account the

installation cost of the inverters. Then, the initial capital investment cost can be calculated from

$$I_{IVST,INV} = \lambda K_{INV}\eta_{INV}\times \left[N_{PV}\ Pr_{PV}\sum_{t=1}^{N}P_{PV}(t) + N_{WT}\ Pr_{WT}\sum_{t=1}^{N}P_{WT}(t)\right] \tag{4.42}$$

where λ is the capital cost of the inverter per kW, K_{INV} is the oversize coefficient of the inverter, and η_{INV} is the efficiency of the inverter. The inverter lifespan (L_{INV}) is less than the installation lifespan of the proposed system. Additional investment is required before the end of the installation project. Then, the net present value of the replacement cost of the inverter $C_{R,INV}$ is provided by

$$C_{R,INV} = \lambda\ K_{INV}\eta_{INV}\times \left[N_{PV}\ Pr_{PV}\sum_{t=1}^{N}P_{PV}(t) + N_{WT}\ Pr_{WT}\sum_{t=1}^{N}P_{WT}(t)\right]\times\Pi \tag{4.43}$$

where $\Pi = \sum_{y=1}^{N_{rep}}\left(\frac{(1+r_0)}{(1+i)}\right)^{\left(\frac{L_y}{N_{rep}+1}\right)}$.

In this chapter, the operation and maintenance cost of the inverter, as well as its salvage cost, have not been taken into account. The LCC of the inverter (LCC_{INV}), in general terms, is provided by

$$LCC_{INV} = \lambda K_{INV}\eta_{INV}\times \left[N_{PV}\ Pr_{PV}\sum_{t=1}^{N}P_{PV}(t) + N_{WT}\ Pr_{WT}\sum_{t=1}^{N}P_{WT}(t)\right]\times[1+\Pi] \tag{4.44}$$

4.2.8 Reliability consideration of the proposed system

This paper evaluates the reliability of the proposed system using the loss of power supply probability (LPSP). LPSP is a statistical parameter that represents the inability of a distributed power system to meet the required charging demand [105]. The reliability of grid-connected hybrid systems is sized and evaluated using the LPSP approach as one of the technology-implemented criteria. For a given period N, the LPSP is the ratio of the total loss of power supply (LPS) accumulated during that period N to the overall charging demand. Due to the proximity of the substation and the installation area for the proposed system to the EV BSS, wiring losses within the distribution network are assumed to be insignificant. The LPSP is provided by [106, 107]

$$LPSP = \frac{\sum_{t=1}^{N}LPS(t)}{\sum_{t=1}^{N}P_{Ld,BSS}(t)} \tag{4.45}$$

where $LPS(t)$ is the loss of power supply at sampling time t_s and $P_{Ld.BSS}(t)$ is the hourly load demand of the charging demand of depleted EV batteries at the BSS.

Assuming that the LPSP is between 0 and 1, a value of 1 indicates that the charging demand at the BSS is never met. On the other hand, the charging demand is always satisfied when the LPSP is equal to 0.

Therefore, the LPS is provided by

$$LPS = P_{PV-BSS}(t) + P_{WT-BSS}(t) + P_{G-BSS}(t) - P_{Ld,BSS}(t) \tag{4.46}$$

where P_{G-BSS} is the power flow from the utility grid charging the depleted EV batteries at the BSS, P_{PV-BSS} is the power flow from the solar PV system charging the depleted EV batteries at the BSS, and P_{WT-BSS} is the power flow from the wind turbine charging the depleted EV batteries at the BSS.

4.2.9 Objective function

The objective function of the optimization model is to minimize the total life cycle cost (LCC_{Tot}) of the proposed system and the electricity cost purchased from the utility grid (C_{EG}) to recharge the depleted EV batteries at the BSS through optimal power flow control within the demand-side management framework while maximizing its reliability. The objective function is provided in (4.47), in which the first part represents the total LCC and the second part is the electricity cost purchased from the utility grid.

$$\min Z = \xi \; LCC_{Tot} + (1 - \xi) \; C_{Eg} \tag{4.47}$$

where ξ is a weighting factor. The weighting factor ξ transforms the multi-objective optimization problem into a single-objective framework, which should generate one optimal solution. This paper assigns equal weighting to the LCC_{Tot} and the C_{Eg}, ensuring a balanced consideration of both factors. Thus, the weighting factor is 0.5. The decision variables are the hourly power from the utility grid $P_{G-BSS}(t)$, the number of WT (N_{WT}), and the number of solar PV panels (N_{PV}). N_{WT} and N_{PV} depend on the total surface area (AT_{WT}) for the WT and (AT_{PV}) for the solar PV panel available in the EV BSS. The hourly power from the utility grid is a continuous variable, while N_{WT} and N_{PV} must be integer values. The objective function in Equation (4.47) can thus be reformulated in light of these decision variables as

$$\begin{aligned} \min Z = & \xi \left\{ [1.2 + 0.06\Gamma]\gamma N_{WT} Pr_{WT} \sum_{t=1}^{N} P_{WT}(t) + [1.4 + 0.014\Gamma]\delta N_{PV} Pr_{PV} \sum_{t=1}^{N} P_{PV}(t) \right. \\ & \left. + \lambda K_{INV} \eta_{INV} \left(N_{WT} Pr_{WT} \sum_{t=1}^{N} P_{WT}(t) + N_{PV} Pr_{PV} \sum_{t=1}^{N} P_{PV}(t) \right) \right\} \Delta t \\ & + (1 - \xi) p_e(t) \sum_{t=1}^{N} P_{G-BSS}(t) \Delta t \end{aligned} \tag{4.48}$$

where δ denotes the capital cost of the solar PV generator per kW, N_{PV} denotes the number of solar PV panels, $P_{PV}(t)$ denotes the output power generated by the solar PV panel at sampling time t, Pr_{PV} denotes the power rating of a solar PV generator, γ denotes the capital cost of the WT generator per kW, N_{WT} denotes the number of WTs, $P_{WT}(t)$ denotes the output power generated by the WT at sampling time t, Pr_{WT} denotes the power rating of a WT, λ denotes the capital cost of the inverter per kW, η_{INV} denotes the efficient of the inverter, K_{INV} denotes the oversize coefficient of the inverter, N the

sampling period, P_{G-CS} denotes the power from the utility grid, Δt is the sampling time, and ξ is the weighting factor.

4.2.10 System Constraints

As a result of power supply generation and charging demand at the EV BSS, the objective function has some operational, technical, and reliability constraints. These constraints are mathematically represented as follows:

► Reliability : To enhance the reliability of the proposed hybrid system, the LPSP is subject to the following constraints:

$$\begin{cases} LPSP \geq 0 \\ P_{PV-BSS}(t) + P_{WT-BSS}(t) + P_{G-BSS}(t) - P_{Ld,BSS}(t) \geq 0 \\ P_{PV-BSS}(t) + P_{WT-BSS}(t) + P_{G-BSS}(t) \geq P_{Ld,BSS}(t) \\ -\left[P_{PV-BSS}(t) + P_{WT-BSS}(t) + P_{G-BSS}(t)\right] \leq -P_{Ld,BSS}(t) \end{cases} \tag{4.49}$$

► The power flow limits For safety reasons, all the power flows connected to various components should be kept within the manufacturer's requirements. Therefore, at any sampling time t, the power flows can be within a specific limited range of zero to their rated power, and these can be represented as follows:

$$0 \leq P_{PV}(t) \leq P_{PV}^{max}(t) \tag{4.50}$$

$$0 \leq P_{WT}(t) \leq P_{WT}^{max}(t) \tag{4.51}$$

$$0 \leq P_{G-BSS}\,(t) \leq +\infty \tag{4.52}$$

► Wind turbine numbers The limited number of WTs bounded by the maximum and minimum units of WTs considered. The economic constraints define the upper limit, while the configuration considered determines the lower limit. This means

$$0 \leq N_{WT} \leq N_{WT}^{max} \tag{4.53}$$

► Solar photovoltaic panel numbers The limited number of solar PV panels bounded by the maximum and minimum units of solar PV panels considered. The economic constraints define the upper limit, while the configuration considered determines the lower limit:

$$0 \leq N_{PV} \leq N_{PV}^{max} \tag{4.54}$$

4.2.11 Algorithm formulation

The optimization model developed in this paper is structured as MILP problem. Since N_{WT} and N_{PV} must be integers and, at the same time, P_{G-BSS} must be a continuous value, the optimization problem is solved using the solving constraint integer program (SCIP) solver in the Matlab R2024a OPTI Toolbox [1]. The algorithm for solving an MILP problem using the SCIP solver involves several key steps. Initially, SCIP reads and parses the problem, converting it into an internal representation. This is followed by preprocessing, where SCIP simplifies the problem by removing redundant constraints and variables, tightening bounds, and detecting infeasible sub-problems. The core of the algorithm is the branch-and-bound method, which iteratively divides the problem into smaller sub-problems by branching on fractional variables. At each node of the branch-and-bound tree, SCIP uses linear programming (LP) relaxations to obtain bounds and employs cutting planes to improve these bounds. Additionally, heuristics are applied to find feasible solutions quickly, and primal and dual bounds are updated to guide the search process. SCIP also integrates constraint propagation techniques to further reduce the search space. The process continues until all sub-problems are either solved or pruned, resulting in the optimal solution to the MILP problem [108, 109]. A scalarization technique is necessary to solve multi-objective optimization problems using MILP. This technique employs weight factors to convert multiple objective functions into a single aggregated objective function [110, 111]. Therefore, the objective function and constraints can be formulated using the canonical form as follows:

$$\min f^T(x) \tag{4.55}$$

subject to

$$\begin{cases} Ax \leq b \text{ ; linear inequality constraint} \\ lb \leq x \leq ub \text{ ; lower and upper bounds} \\ x \text{; integer decision variables} \\ x = N_{PV}, N_{WT}, P_{G-BSS}(t) \\ N_{PV} \in N \\ N_{WT} \in N \\ P_{G-BSS}(t) \in R \end{cases} \tag{4.56}$$

where $f^T(x)$ represents the objective function, x is the vector containing the decision variables representing the optimal number of wind turbines and solar panels, as well as the cost of the energy purchased from the utility grid, A and b are the coefficients associated with inequality constraints, and lb and ub are the lower and upper bounds of the decision variables.

4.3 Case study

A case study is conducted using real-world data from an operational BSS network to validate the feasibility and effectiveness of the proposed system, as illustrated in Figure 4.1. The choice of data sources is

[1] https://www.mathworks.com/help/optim/ug/intlinprog.html(accessed on 15 August 2024)

constrained by data availability. This data provides reliable and practical input parameters for analysis and simulations, making it ideal for addressing this multi-optimization problem. The study leverages RES to demonstrate the applicability and benefits of the developed model. The charging demand at the EV BSS is met through a combination of vertical WTs, solar PV panels, and the utility grid. Notably, this chapter does not consider feeding the generated energy back into the utility grid.

The subsequent sections present the daily load profile of the EV BSS power demand, followed by an introduction to the necessary input data used in the model for simulating hybrid renewable power output and the time-of-use (TOU) electricity tariff for the selected location

4.3.1 EV BSS power demand load profile

To accurately assess the energy requirements of the EV BSS, a detailed load profile was constructed using historical data from an operational BSS. The chosen EV BSS is a heavy-duty truck swapping station situated at a central logistics hub in Shanghai Port, China, where energy consumption patterns reflect the high and variable demand associated with commercial EV operations. The data from Shanghai Port were readily accessible and reliable for the respective purposes, making them practical choices for this optimisation problem. The data were recorded over a representative period, capturing daily and seasonal demand variations. Figure 4.3 illustrates the daily energy consumption at the EV BSS, highlighting peak demand periods that coincide with high traffic volumes and operational hours. The background colors in Figure 4.3 are designated as green for off-peak, yellow for standard, and light red for peak periods. The load profile serves as the basis for sizing the hybrid renewable energy system and determining the optimal mix of energy sources.

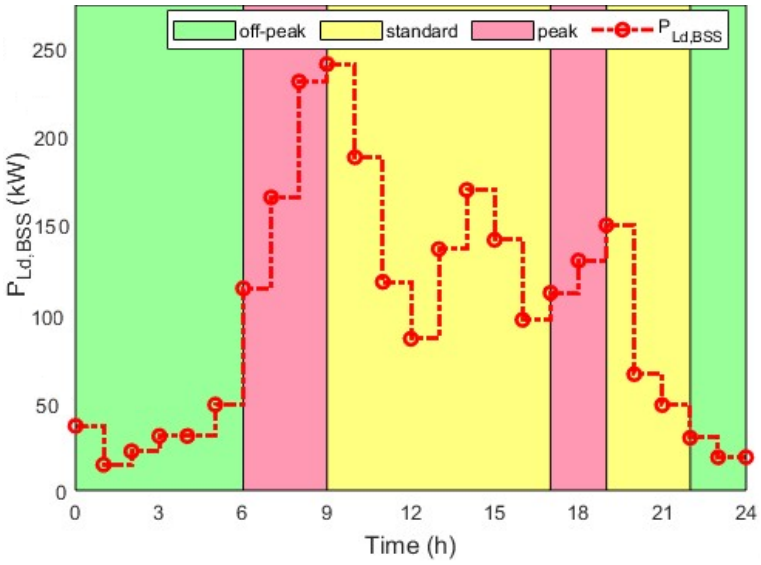


FIGURE 4.3: Charging patterns of electric vehicles battery swapping station.

.

4.3.2 Renewable energy power supply

The proposed hybrid system incorporates WTs and solar PV panels as primary energy sources, supplemented by grid electricity, to ensure a reliable supply. The input parameters for WT system power generation, such as the wind speed, and for solar PV power generation, such as the solar radiation and ambient temperature, are obtained from a typical day in the low-demand season in Cape Town, South Africa, as referenced in [112]. Figure 4.4 illustrates the hourly average wind speed measured at a height of 10 m above ground level. The wind speed varies throughout the day, with a daily average of 2.46 m/s. The windiest period occurs between 2:00 and 3:00 PM, with an average wind speed of 4.6 m/s, while the calmest period is observed between 1:00 and 2:00 AM, with an average wind speed of 1.08 m/s. For more information, the average hourly wind speed over the year is presented in Figure 4.5. Additionally, the daily average for PV generation is depicted in Figure 4.6, indicating that the peak incident shortwave radiation for solar PV power generation reaching the ground's surface over a wide area is approximately 0.42 kW/m^2 around 12:45 PM. For more information, the annual shortwave radiation for solar PV power generation reaching the ground's surface over a wide area is presented in Figure 4.7, which provides significant seasonal variation, with the brightest peak around December and the darkest period around June. respectively. The proposed hybrid power system is designed to ensure that the EV BSS charging demand is met at any given time, particularly when electricity from the utility grid is expensive. The sizing of the WT and solar PV system is tied to the initial equipment cost and available capital, directly impacting power generation and reducing energy costs from the utility grid.

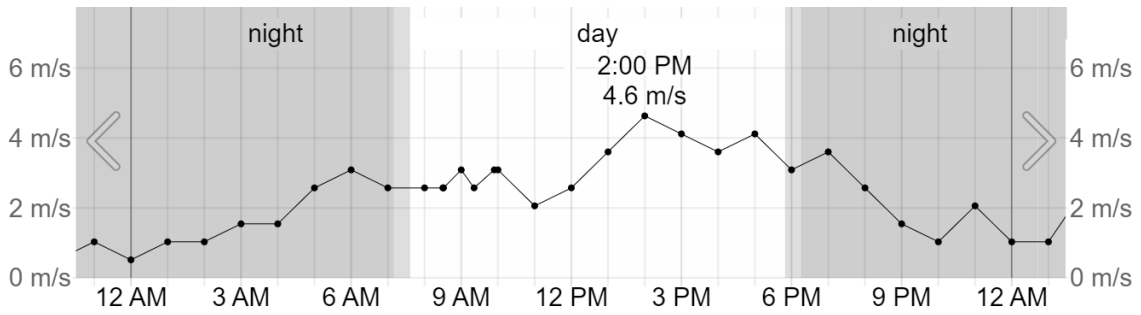


FIGURE 4.4: Average hourly wind speed.

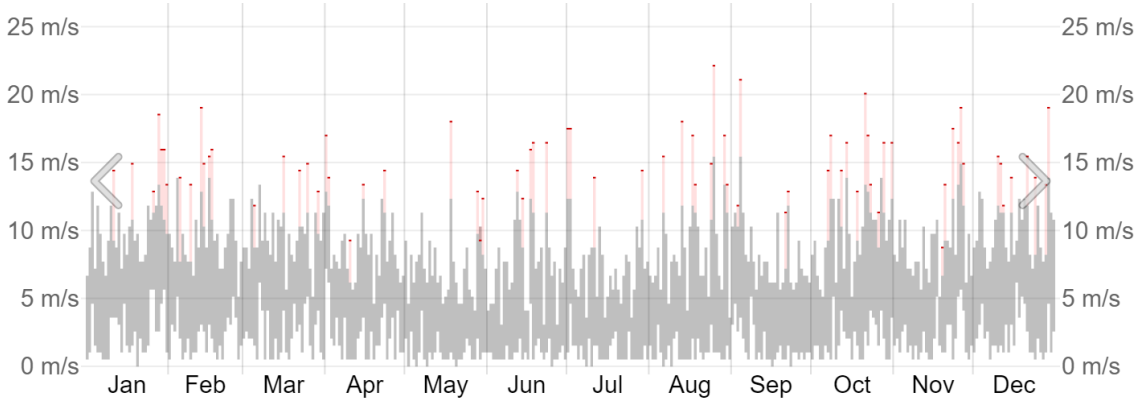


FIGURE 4.5: Monthly average wind speed.

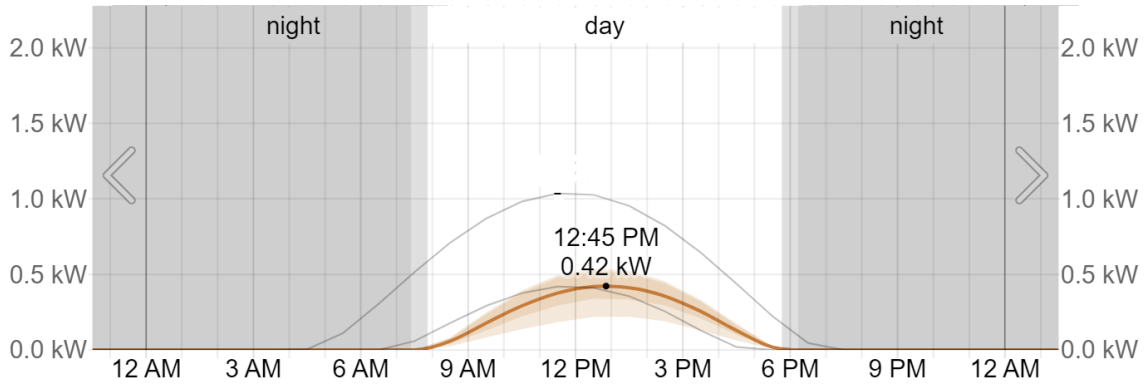


FIGURE 4.6: Daily average shortwave solar power.

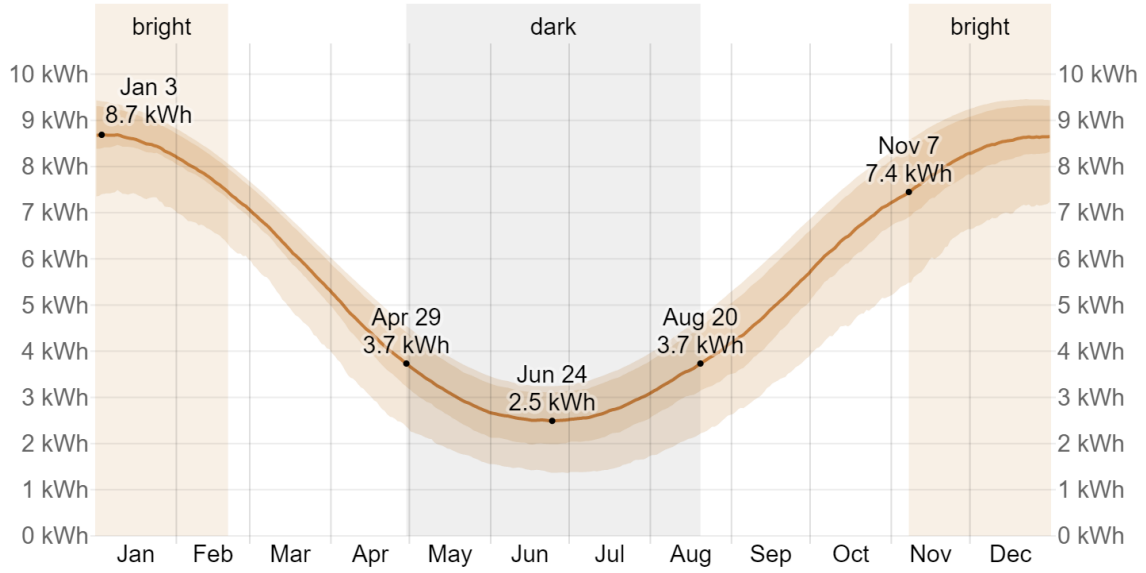


FIGURE 4.7: Monthly average shortwave solar energy.

4.3.3 Time-of-use electricity tariff

The South African power grid is operated by the national utility company "Eskom", Sandton, South Africa, while electricity tariffs are regulated by the National Energy Regulator of South Africa (NERSA). Eskom's tariff structure typically includes both flat and dynamic TOU pricing systems. TOU pricing is a demand-side management strategy that reflects the varying costs of electricity production throughout the day and is divided into three periods: off-peak ($p_{e\ off}$), standard-peak ($p_{e\ std}$), and on-peak ($p_{e\ pk}$). These periods correspond to times when electricity demand and generation costs are low, moderate, and high, respectively. In the context of the optimization problem, the TOU electricity tariff significantly influences the energy efficiency of the EV BSS. This chapter considers the Eskom Megaflex TOU tariff scheme, which applies to urban and industrial consumers who both consume energy from the utility grid and generate energy at the same point of supply. For this case study, the 2023/2024 Eskom Megaflex electricity tariff for high-demand season (from June to August) weekdays is used as the basis for the TOU electricity tariff

analysis given as [2]

$$p_{e(t)} = \begin{cases} p_{e\ off} = 1.0370\ ZAR/\text{kWh}\ ;\ \text{if}\ t \in [00:00, 06:00) \cup [22:00, 24:00), \\ p_{e\ std} = 1.8991\ ZAR/\text{kWh}\ ;\ \text{if}\ t \in [09:00, 17:00) \cup [19:00, 22:00), \\ p_{e\ pk} = 6.2421\ ZAR/\text{kWh}\ ;\ \text{if}\ t \in [06:00, 09:00) \cup [17:00, 19:00). \end{cases} \tag{4.57}$$

with ZAR being the South African currency (Rand) and t representing the time of day in hours.

4.4 Results and discussion

The following section breaks down the simulation results from the optimization model presented in the previous section. The simulation results regarding the system's performance, cost-effectiveness, and reliability are analyzed. Additionally, the impact of varying key input parameters, such as the number of WTs, PV panels, and TOU electricity tariffs, is also discussed. The outcomes provide insights into the optimal design and management strategies for a grid-connected wind–solar hybrid power supply system for the EV BSS. Furthermore, a comprehensive economic analysis is conducted by assessing the payback period and cost-effectiveness of installing the proposed system. Table 4.1 presents the overall simulation parameters used in this chapter.

[2] https://www.eskom.co.za/distribution/wp-content/uploads/2023/03/Schedule-of-standard-prices-2023_24-140323.pdf (accessed on 20 August 2024)

Table 4.1: Simulation parameters used in this chapter.

Parameters	**Symbol**	**Values**
Installation lifetime	L_p	20 years
Sampling period	N	24
Sampling time	Δt	1 h
Weighting factor	ξ	0.5
Upper bound	ub	[481 2802 ∞]
Lower bound	lb	[0 0 0]
Inflation rate	r	4.60%
Interest rate	i	8.25%
Photovoltaic systems		
Lifetime of the PV system	L_{PV}	25 years
Rated power of the PV panel	Pr_{PV}	0.545 kW
Conversion efficiency of the PV panel	η_{PV}	19.4%
Rated efficiency of the PV panel	η_r	18.1%
Initial cost of the PV panel	$IC_{INVT,PV}$	ZAR 3 199.99
Annual O & M cost of PV	$C_{O\&M,_{PV}}$	1% of $IC_{INVT,PV}$
Capital cost of the solar PV per kW	δ	ZAR 8 220.16/kW
Wind turbine systems		
Lifetime of the WT system	L_{WT}	25 years
Rated power of the WT generator	Pr_{WT}	8 kW
Rated WT speed	V_r	12 m/s
Cut-in WT speed	V_{ci}	2.5 m/s
Cut-out WT speed	V_{co}	25 m/s
WT gearbox efficiency	η_T	90%
WT generator efficiency	η_g	80%
Air density	φ_a	1.225 kg/m^3
WT power coefficient	C_p	0.48
Initial cost of the WT	$IC_{INVT,WT}$	ZAR 10,580.63
Annual O & M cost of WT	$C_{O\&M,_{WT}}$	5% of $IC_{INVT,WT}$
Capital cost of the WT per kW	γ	ZAR 15,403/kW
Inverter		
Lifetime of the inverter	L_{INV}	15 Years
Efficiency of the inverter	η_{INV}	98%
Inverter factor	K_{INV}	1.25
Initial cost of the inverter	$I_{C,INV}$	ZAR 38,860.00
Capital cost of inverter per kW	λ	ZAR 3 108.80/kW

4.4.1 Optimal hybrid power system sizing and management strategy

The optimization problem, formulated as an MILP, is solved through the SCIP solver within MATLAB's R2024a OPTI Toolbox during a 24 h horizon with a sampling interval $\Delta t = 1$ h. The objective is to determine the most cost-effective and reliable design for the hybrid system, focusing on the optimal sizing of WTs and solar PV panels to meet the charging demand while minimizing reliance on the utility grid. The simulation utilized technical and economic input parameters, as outlined in Table 4.1, to identify the optimal configuration of the hybrid system. With a weighting factor of 0.5, the simulation results indicate that the optimal configuration for the hybrid systems consists of 64 WTs and 402 solar PV panels, resulting in a total LCC of ZAR 1,963,520.12. This configuration remains optimal for weighting factor values within the range of 0.27 to 0.71. For weighting factors below 0.27, the hybrid system is prioritized over the utility grid, potentially leading to excess energy absorbed by the utility grid. Conversely, weighting factors above 0.71 prioritize the utility grid, resulting in an oversized hybrid system with all the charging power supplied by the utility grid.

Figure 4.8 illustrates the power generated by the hybrid power system over a 24 h period. It shows that both wind and PV power sources exhibit diurnal patterns, with peaks occurring at different times of the day. The PV power generation starts increasing in the morning, reaching its peak between 12:00 and 15:00 when solar irradiance is at its highest. It gradually decreases towards the evening as sunlight diminishes, showing a typical bell-shaped curve. In contrast, the WT power output exhibits more variability throughout the day, with multiple peaks occurring at different times, reflecting the intermittent nature of wind speed. Notably, wind power generation complements the PV output by producing power during the early morning and late afternoon hours when solar power is negligible, demonstrating a synergistic effect that enhances the overall renewable energy availability. This complementary behavior benefits hybrid renewable systems as it can reduce dependency on grid power.

Figure 4.9 presents the simulation results of the charging demand along with the optimal output power flows from each source over a 24 h period. It can be observed that the charging demand fluctuates throughout the 24 h, with peak demands occurring around 10 AM, 3 PM, and 8 PM. Hybrid power generation systems supply a significant portion of the power required to meet this charging demand, thereby substantially reducing the operational costs associated with the utility grid. During the off-peak hours (00:00–06:00), hybrid power generation is minimal due to low wind speeds and the unavailability of solar PV, resulting in higher reliance on the utility grid to meet the charging demand. As the wind speed increases from 06:00 onwards, WTs contribute more significantly to the power supply, reducing utility grid dependency. The solar PV system begins generating power at sunrise, reaching its peak around noon. During these hours, the combined contribution of solar PV and WTs is sufficient to meet the charging demand of the EV BSS, significantly decreasing the operational cost of the system. The utility grid supplements any remaining deficit power. Between 17:00 and 19:00, there is another peak in charging demand. Solar PV generation declines at this time, and WTs partially compensate for the power deficit. However, some reliance on the utility grid is necessary to meet the demand. The system's optimization strategy ensures

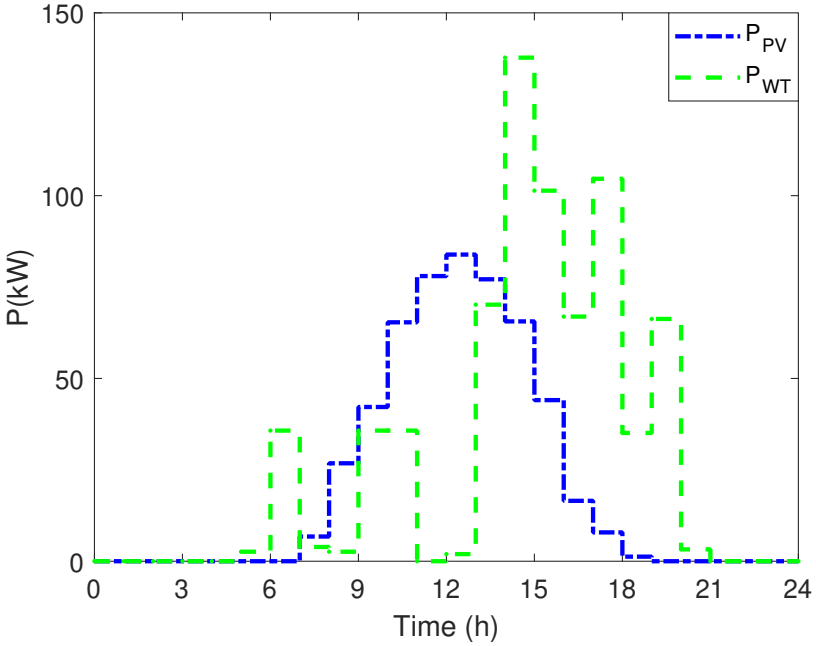


FIGURE 4.8: Wind and photovoltaic power generated by the hybrid systems.

.

that electricity is predominantly drawn from renewable sources whenever available, limiting the use of expensive grid electricity during peak TOU tariff periods.

Applying Eskom's TOU electricity tariff to the proposed system generates a daily electricity cost of R7 676.39 for the charging demand. Incorporating the optimization model reduces this cost to ZAR 4483.53, representing 41.6% of the daily cost savings. Table 4.2 and Table 4.3 summarize the simulation results, including the number of WTs, PV panels, total LCC, and cost savings achieved through optimal control intervention. These results are based on the average daily cost in the case study, with the daily cost annualized to reflect an average yearly amount. The results demonstrate the feasibility and effectiveness of integrating wind and solar energy, significantly reducing the dependency on the utility grid and offering a sustainable and resilient solution for EV charging and swapping infrastructure.

TABLE 4.2: Simulation results of the proposed system.

Number of WTs	**Number of PV panels**	**Total life cycle cost**
64	402	1 963 520.12 ZAR

TABLE 4.3: Daily optimal energy and annual cost savings of the proposed system.

	Baseline cost	**Optimal cost**	**Cost saving**
Daily	7 676.39 ZAR	4 483.53 ZAR	3 192.5 ZAR
Annualized			1 165 262.5 ZAR

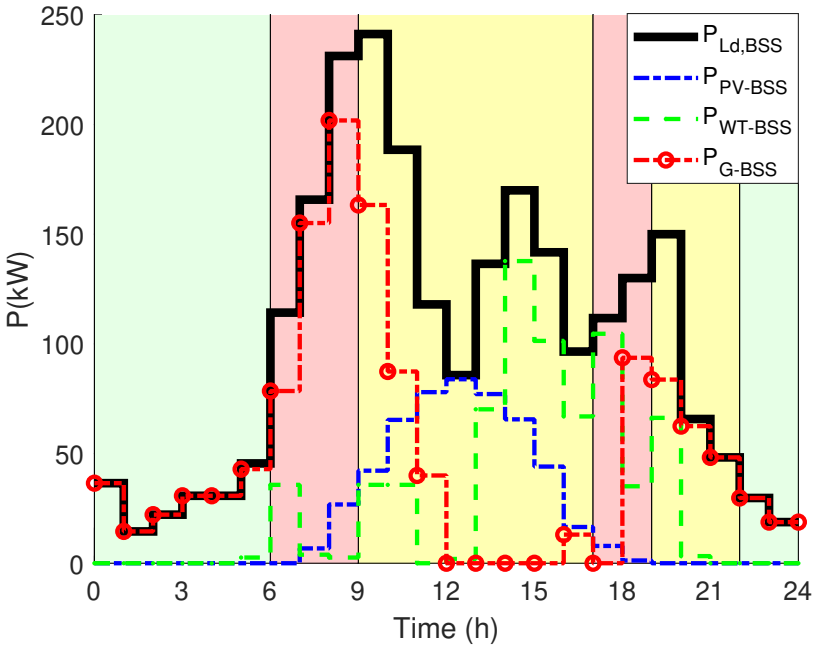


FIGURE 4.9: Load side power flows at EV-BSS.

.

The proposed optimization model is tailored to a specific region but has been demonstrated as operational in the existing literature. An analysis of the methodology and simulation results indicates that the model effectively demonstrates the techno-economic feasibility and provides an optimal design approach for managing grid-connected hybrid power generation systems in EV BSSs over multiple days under different operational scenarios. Although the optimization model is designed for a particular use case, the simulation results suggest that its straightforward structure enables adaptation to a more generalized framework that is applicable to various electricity markets.

The study's findings highlight that integrating grid-connected hybrid wind–PV systems into EV BSSs aligns with South Africa's energy objectives, particularly the Integrated Resource Plan (IRP, 2023) [113], which emphasizes RE diversification and emission reductions in the transport sector. These findings augment the country's broader policy aspirations of reducing dependence on fossil fuels and implementing distributed generation systems, promoting energy security through minimized grid dependency. To fully capture such innovations, strategic policy changes are required. Governments can provide economic incentives, such as tax rebates and low-interest loans, to help lower hybrid system adoption barriers. Streamlining the permitting procedure and reforming TOU tariff prices would also promote off-peak RE consumption, matching economic benefits with sustainable strategies. Encouraging public–private partnerships and investing in adaptive grid technologies could create a regulatory environment that accelerates infrastructure development with rapid technological advancements. Collaboration among policymakers, utilities (e.g., Eskom), and private stakeholders is equally vital. Collaborative efforts in co-funding pilot trials and developing harmonized technical standards would close the gap between research and large-scale deployment and align with national climate change policies [113] and energy security agendas.

4.4.2 LCC analysis for the payback period

Economic feasibility is assessed through a cost–benefit analysis of cash outflows and inflows associated with installing the proposed system. The installation feasibility can be evaluated using various methods, considering both environmental benefits and economic indicators [114–116]. The LCC method considers the time value of money and the lifespan of the installation by converting all the future cash flows into their present value through discounting. The comparative advantage of LCC is that it covers all the cash inflows and outflows into the system in its lifetime. As a result, the discounted present value (DPV) of a cash flow occurring in a future period (z-th year) can be expressed as

$$DPV(z) = \frac{FV(z)}{(1+d)^z} \tag{4.58}$$

where DPV is the discounted present value of the future cash flow, FV is the nominal value of a cash flow amount in a future period (z-th year), d is the discount rate, and z is the time in years before the future cash flow occurs. In this LCC analysis, d represents the time value of money or the cost of holding capital and may also account for the risk of not receiving the full payment. The actual d is calculated as the difference between the average interest rate and the inflation rate. The interest rate (r) reflects the opportunity cost of time, representing the compensation required to delay spending from the current to a future year. On the other hand, the inflation rate (i) indicates the percentage change in prices over a specific period, typically measured monthly or annually, and shows how quickly prices increased during that time. The i is an essential parameter in the LCC analysis of an installation project, and, thus, the unit cost of generation is an essential parameter. In this chapter, the average interest rate [3] is 8.25%, and the inflation rate [4] is 4.6%, reflecting the time value of money in South Africa as of July 2024. The component prices are based on South African market rates. In this LCC economic analysis of energy efficiency projects, both operational and maintenance costs, as well as cost savings, are considered. Once FV (z) is determined, the net present value (cumulative cash flow) is calculated as follows [116]:

$$NPV_{z=1}^{m} = \sum_{z=1}^{m} DPV(z) - CC \tag{4.59}$$

where NPV is the net present value (or cumulative cash flow) and CC is the total investment capital cost. Subsequently, the discounted payback period (PBP) can be determined using the following equation [116]:

$$PBP = m_y + \frac{-NPV_{z=1}^{m}}{DPV(m_y+1)} \tag{4.60}$$

where m_y denotes the last year with a negative NPV. Table 4.4 provides the approximate prices of the various components of the proposed system, leading to a total investment capital cost.

[3] https://tradingeconomics.com/south-africa/interest-rate(accessed on 20 September 2024)
[4] https://tradingeconomics.com/south-africa/inflation-cpi (accessed on 20 September 2024)

TABLE 4.4: Costs components of the proposed system.

Components	**Costs (ZAR)**
Wind turbines	677 160.32
Solar photovoltaic	1 286 359.80
Inverters	77 720
Installation cost	649 975,98
Accessories	3 000 000
Total investment capital cost	**5 691 216.10**

Certain assumptions are made when conducting the LCC analysis for the proposed system. It is assumed that the annual operation and maintenance costs $C_{O\&M}$, as well as the annual optimal cost–benefit, will increase proportionally over the installation service lifetime. The annual cost–benefit represents the amount the EV BSS owner would have spent each year without implementing the proposed system. Table 4.5 presents the LCC analysis of the proposed system under the optimal control strategy, with the salvage cost neglected when calculating the PBP. As shown in Table 4.5, the projected total investment capital cost is recorded as a negative cash flow in brackets as (ZAR 5,691,216.10) in the financial statement. The cash flows and PBP are calculated following the assumptions that the annual optimal cost–benefit and $C_{O\&M}$ will increase proportionately during the lifetime of the proposed system. The cumulative cash flows decrease as negative ones until they eventually turn positive. The PBP occurs when the cumulative cash flow reaches zero, and, at this point, the total invested capital cost has been fully recovered. For the proposed system, the PBP occurs after 5 years and 6 months. Afterward, the cumulative cash flow becomes positive, and all the revenue in the following years represents pure profit or benefit. Suppose that the proposed system installation has a lifetime of 20 years and a payback period of approximately 5 years and 6 months. In that case, the EV BSS owner can recover the total capital investment within a reasonable timeframe and will have over 10 years to generate guaranteed profit.

4.5 Summary

This chapter presented a novel techno-economic evaluation and optimal design approach for a grid-connected wind-solar PV hybrid power supply system tailored for EV BSS. The proposed optimization model, developed using MILP, aims to minimize the total LCC and the cost of electrical energy consumption from the utility grid while maximizing system reliability. The decision variables considered include the number of wind turbines, solar PV panels, and power drawn from the utility grid. For the case study, the optimal solution consists of 64 WTs and 402 solar PV panels, resulting in a total LCC of 1,963,520.12 ZAR. The results demonstrate that the implementation of energy cost management under a TOU electricity tariff yields substantial savings, reducing electricity costs from the utility grid by 41.58%. A cost-effectiveness analysis performed using LCC as the economic performance indicator reveals a payback period of 5 years and 6 months, highlighting the financial benefits of the proposed hybrid system. Furthermore, this optimization approach not only significantly reduces energy costs but also ensures high

TABLE 4.5: Life cycle cost analysis and payback period of the proposed system .

Years	**Total investment capital cost**	**Annual O & M cost**	**Annual optimal cost benefit**	**Total**	**Discount factor $(1+d)^{-L_p}$**	**Discounted cash flows**	**Cumulative cash flows**
0	(5 691 216.10)				1.00	(5 691 216.10)	(5 691 216.10)
1		(46 721.61)	1 165 390.25	1 118 668.64	0.96	1 079 275.10	(4 611 941.01)
2		(47 389.73)	1 182 055.33	1 134 665.60	0.93	1 056 158.93	(3 555 782.07)
3		(48 067.40)	1 198 958.72	1 150 891.32	0.90	1 033 537.87	(2 522 244.20)
4		(48 754.77)	1 216 103.83	1 167 349.07	0.87	1 011 401.32	(1 510 842.89)
5		**(49 451.96)**	**1 233 494.12**	**1 184 042.16**	**0.84**	**989 738.89**	**(521 104.00)**
6		(50 159.12)	1 251 133.08	1 200 973.96	0.81	968 540.43	447 436.43
7		(50 876.40)	1 269 024.29	1 218 147.89	0.78	947 796.00	1 395 232.43
8		(51 603.93)	1 287 171.33	1 235 567.40	0.75	927 495.88	2 322 728.31
9		(52 341.87)	1 305 577.88	1 253 236.02	0.72	907 630.56	3 230 358.87
10		(53 090.35)	1 324 247.65	1 271 157.29	0.70	788 190.71	4 018 549.58
11		(53 849.55)	1 343 184.39	1 289 334.84	0.67	869 167.24	4 887 716.82
12		(54 619.60)	1 362 391.92	1 307 772.33	0.65	850 551.21	5 738 268.03
13		(55 400.66)	1 381 874.13	1 326 473.47	0.63	832 333.90	6 570 601.93
14		(56 192.89)	1 401 634.93	1 345 442.04	0.61	814 506.78	7 385 108.72
15		(56 996.44)	1 421 678.31	1 364 681.86	0.58	797 061.48	8 182 170.20
16		(57 811.49)	1 442 008.31	1 384 196.82	0.56	779 989.84	8 962 160.04
17		(58 638.20)	1 462 629.03	1 403 990.83	0.54	763 283.83	9 725 443.87
18		(59 476.72)	1 483 544.62	1 424 067.90	0.52	746 935.64	10 472 379.50
19		(60 327.24)	1 504 759.31	1 444 432.07	0.51	730 937.60	11 203 317.10
20		(61 189.92)	1 526 277.37	1 465 087.45	0.49	715 282.20	11 918 599.30
						Payback is 5 years plus 6 months (6.45636)	

system reliability. This techno-economic feasibility and design optimization offers an adaptable solution in various applications. The developed system can be extended to different locations, proving its flexibility in optimizing grid-connected wind-PV hybrid power systems, especially in areas where storage system may be prohibitive. The proposed system offers a cost-effective and reliable solution for EV BSS, with promising potential for widespread implementation in South Africa's roadways, driving both economic and environmental benefits.

The next chapter discusses the optimal operation control of a grid-connected wind-solar energy system designed for battery swapping stations. It presents advanced control strategies and optimization techniques that balance renewable generation with grid reliability, ensuring efficient and cost-effective energy management.

Chapter 5

OPTIMAL OPERATION CONTROL OF GRID-CONNECTED WIND-SOLAR POWER GENERATION WITH STORAGE SYSTEM FOR BATTERY SWAPPING STATION

5.1 Chapter overview

In this chapter, an integrated approach to optimizing the operation and control of a grid-connected wind-solar hybrid power system coupled with a BESS for an EV BSS is presented. It begins by describing the overall system architecture, including WT, solar PV arrays, and the BESS, all of which are interconnected with the utility grid. The proposed model builds upon previous chapter that focused on minimizing the total LCC and the cost of electrical energy consumption from the utility grid while maximizing system reliability. Here, the optimal operation control problem is formulated with key objectives such as minimizing operational associated with the power flow drawn from the utility grid and the wear cost of the hybrid system due to the frequent charging and discharging of the BESS, and maximizing the use of locally generated RE. Simulation results illustrate the cost savings, energy efficiency gains, and emissions reductions

achieved through the proposed control strategy under scenarios where the objectives are equally weighted. This chapter is a substantial extension of the short version presented at the Southern African Universities Power Engineering Conference (SAUPEC 2025) [117].

For the remainder of this chapter, an overview of the optimal operation modelling is given in Section 4.2. The case data used are introduced in Section 4.3. Following that, Section 4.4 analyzes the results and discusses the optimization findings. Lastly, Section 4.5 concludes the chapter.

5.2 Operation modelling and problem formulation

5.2.1 Schematic model layout

The proposed grid-connected wind–solar hybrid power generation system with storage comprises four main components: a vertical-axis WT system, a solar PV generator, a battery energy storage system (BESS), and an EV BSS. The EV BSS includes both the charging apparatus and the battery swapping service for depleted EV batteries. Figure 5.1 illustrates the schematic layout of this hybrid power system, where the arrows indicate the direction of power flow among the components. Specifically, P_1 represents the power flow from the PV generation to the EV BSS, P_2 represents the power flow from the PV generation to the BESS, P_3 represents the power flow from the PV generation to the utility grid, P_4 represents the power flow from the WT to the EV BSS, P_5 represents the power flow from the WT to the BESS, P_6 represents the power flow from the WT to the utility grid, P_7 represents the power flow discharging from the BESS to the EV BSS, and P_8 represents the power flow from the utility grid to the EV BSS. In the proposed hybrid system, various inverters are essential to match voltage and current levels. Compared to the configuration in Figure 4.1, the BESS has been added to store surplus energy generated by the PV and WT systems, thereby enhancing the reliability and efficiency of the EV BSS power supply. The proposed design aims to integrate RESs (PV and WT), a BESS, and utility grid support to consistently meet the charging demands of depleted EV batteries while reducing reliance on the grid. Under normal conditions, renewable energy sources serve as the primary power supply, with any excess energy directed to the BESS for later use. During periods when renewable generation is insufficient, the stored energy in the BESS is dispatched to ensure uninterrupted operation of the EV BSS. In the event that both the RESs and the BESS are unable to meet demand, the utility grid provides supplemental power as a backup. Finally, when the EV BSS charging demand are satisfied and the BESS is fully charged, any remaining surplus power is exported back to the utility grid, further optimizing overall energy utilization and system resilience.

5.2.2 Wind turbine system

Wind turbines harness the mechanical energy of the wind to generate electrical power. The wind turbine operates as an AC generator, with its efficiency depending on the speed and height of the wind. The wind turbine begins to generate power at a specific wind speed known as the cut-in wind speed (V_{ci}). As the

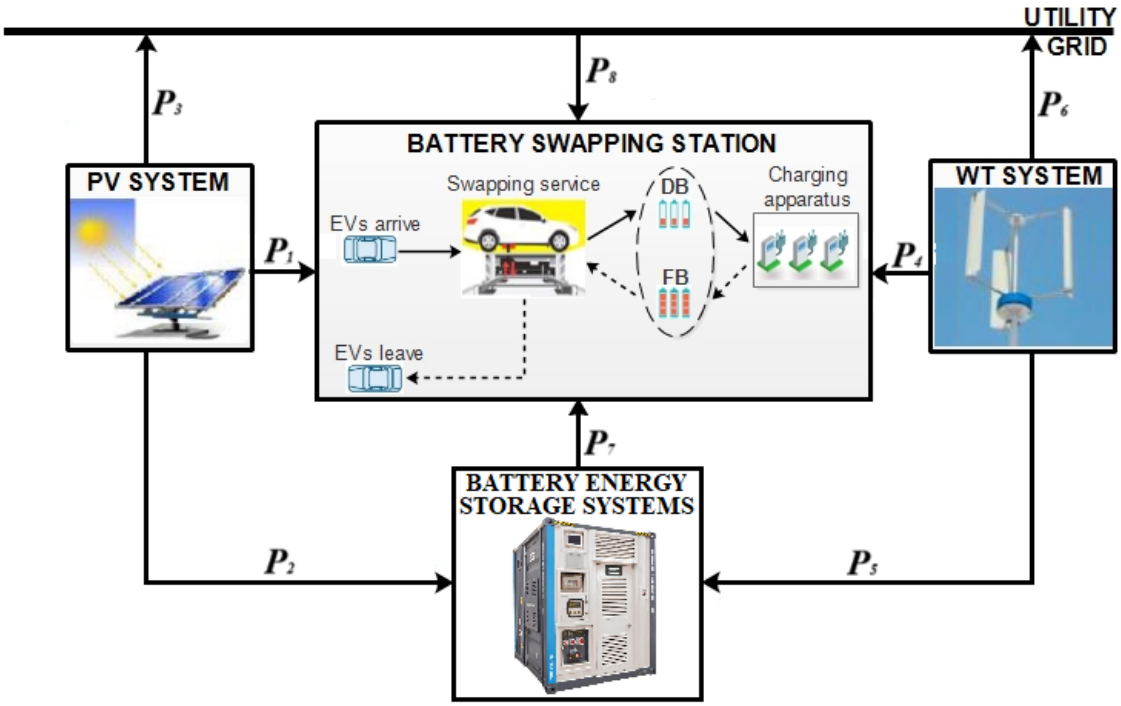


FIGURE 5.1: Schematic layout of the proposed system.

wind speed increases, the generated power increases until it reaches the rated capacity of the turbine. At this rated wind speed (V_r), further increases in wind speed do not affect the output power, which remains constant. When the wind speed exceeds a critical point, called the cut-out wind speed (V_{co}), the turbine is shut down to protect the rotor from damage. The relationship between wind speed and turbine power generation can be expressed mathematically as follows [82]:

$$P_{WT}(t) = \begin{cases} 0 & V(t) \leq V_{ci} \\ Pr_{WT}\frac{V(t)-V_{ci}}{V_r-V_{ci}} & V_{ci} \leq V(t) \leq V_r \\ Pr_{WT} & V_r \leq V(t) \leq V_{co} \\ 0 & V(t) \geq V_{co} \end{cases} \tag{5.1}$$

where $V(t)$ is the wind speed at a given sampling time t, V_r is the rated wind speed, V_{ci} is the cut-in wind speed, V_{co} is the cut-out wind speed, and Pr_{WT} is the rated power of the wind turbine, which is further expressed by:

$$Pr_{WT}(t) = 0.5\eta_t\eta_g\varphi_a C_p A_{WT} V_r^3 \tag{5.2}$$

where η_t and η_g are the efficiencies of the turbine's gearbox and generator, respectively, φ_a is the air density (measured in kg/m^3), C_p is the power coefficient (also known as the Betz limit), which represents the ratio of the actual power output to the theoretical maximum, A_{WT} is the swept area of the turbine rotor, and V_r is the rated wind speed. The power generation capacity of a wind turbine is influenced by

its height, which makes the turbine's height a crucial parameter to consider. The wind speed data at a specific height can be adjusted to other heights using the following relation:

$$\frac{V}{V_{ref}} = \left(\frac{h}{h_{ref}}\right)^{\alpha} \tag{5.3}$$

where V is the wind speed measured at a hub height (h), V_{ref} is the wind speed measured at a reference height (h_{ref}), and α represents the ground surface friction coefficient, ranging from values above 0.25 in forested areas to below 0.1 in flat or water-covered areas [83].

The wind turbine system supplies power $P_4(t)$ to the EV BSS, $P_5(t)$ to the BESS, and $P_6(t)$ to the utility grid. The power balance for the wind turbine system is given by Equation 5.4.

$$P_4(t) + P_5(t) + P_6(t) \leq P_{WT}(t) \tag{5.4}$$

The power generated by the wind turbine is constrained between a minimum and a maximum power limit. The minimum power output is zero, which indicates that there is no generation when wind speeds are too low to produce electricity. The maximum power output is capped at the turbine's rated capacity, beyond which it cannot generate additional power. This constraint can be expressed as shown in Equation 5.5.

$$0 \leq P_{WT}(t) \leq P_{WT}^{max}(t) \tag{5.5}$$

5.2.3 Solar PV system

The solar PV cell converts solar irradiation into direct current (DC) electrical energy and is modelled as an intermittent DC power generator. The power output of a solar PV system fluctuates based on solar irradiation, making its reliability dependent on both the availability and intensity of sunlight. The power generated by the solar PV system is influenced by solar irradiation, ambient temperature, efficiency of the PV collector, and its surface area. The output power generated by the solar PV array is given by [85]:

$$p_{PV} = \eta_{PV} A_{PV} I_{PV} \tag{5.6}$$

where p_{PV} is the power output generated by the solar PV array, A_{PV} is the area of the solar PV array exposed to solar irradiation, I_{PV} is the solar irradiation incident on the solar PV array, and η_{PV} is the energy conversion efficiency of the solar PV system. The energy conversion efficiency is expressed by:

$$\eta_{PV} = \eta_r \left[1 - 0.98\beta \left(\frac{I_{PV}}{I_{PV,NT}}\right) (T_{c,NT} - T_{A,NT}) - \beta (T_A - T_R)\right] \tag{5.7}$$

where η_r is the reference efficiency of the PV generator at a standard cell temperature T_R (typically 25°C), β is the temperature coefficient for cell efficiency (typically 0.004–0.005 per °C), $I_{PV,NT}$ represents the

average hourly solar irradiation incident on the array under nominal test conditions (0.8 kWh/m^2), and $T_{c,NT}$ (typically 45°C) and $T_{A,NT}$ (20°C) are the cell and ambient temperatures at nominal test conditions, respectively. The solar irradiation received by a solar PV array varies on an hourly basis and is influenced by several factors, including the time of day, the season, the tilt and azimuth angles of the array, the geographical latitude of the site, and the components of global solar irradiation, both direct (beam) and diffuse. The total hourly solar irradiation incident on the PV array is given by:

$$I_{PV}(t) = [I_B(t) + I_D(t)]\, R_B + I_D(t) \tag{5.8}$$

where $I_B(t)$ and $I_D(t)$ are the hourly beam and diffuse irradiation, respectively, and R_B is a geometric factor representing the ratio of beam irradiation on a tilted plane to that on a horizontal plane.

The total output power generated by a solar PV array depends on the number of PV panels installed. Considering N_{PV} as the total number of PV panels, the overall output power generated by the solar PV system at a given sampling time (t) is given by:

$$P_{PV}(t) = N_{PV}\ p_{PV}(t) \tag{5.9}$$

The PV system supplies power $P_1(t)$ to the EV BSS, $P_2(t)$ to the BESS, and $P_3(t)$ to the utility grid. The power balance for the PV system is given by Equation 6.10.

$$P_1(t) + P_2(t) + P_3(t) \leq P_{PV}(t) \tag{5.10}$$

The installed capacity of a solar PV system depends on its size and optimal positioning, and its power output is constrained from zero to its maximum rated power, as shown in Equation 6.11.

$$0 \leq P_{PV}(t) \leq P_{PV}^{max}(t) \tag{5.11}$$

5.2.4 Battery energy storage system

The process of charging the depleted EV batteries harms the power distribution utility grid. These reduce the efficiency of the power grid and increase stress on its infrastructure. The integration of a BESS within a BSS enhances the system's reliability and operational flexibility. The BESS acts as a buffer between the intermittent RE supply, the EV battery swapping demand, and the utility grid, ensuring the uninterrupted availability of energy during periods of peak demand. This strategy reduces the dependence on the power grid while enhancing the utilization of RES, such as solar PV and wind power. Additionally, the BESS facilitates energy arbitrage by storing excess RE generated during low-demand periods and discharging it during high-demand or low-renewable generation periods, optimizing the system's overall operational cost. A BESS is typically characterized by its SoC, which increases with charging power and decreases with discharging power over each time step duration. The SoC increases when surplus power from RESs

is available for charging, and it decreases when the stored energy is used to meet the charging demand of depleted EV batteries at the BSS. This dynamic response ensures efficient energy utilization and helps stabilize the power supply within the system. To accurately determine the real SoC of a BESS, it is essential to know the initial SoC, as well as the charging and discharging power. However, most BESSs are not ideal, as losses occur during charging, discharging, and even during idle storage periods. Considering these factors, the SoC of the BESS at time $(t+1)$ can be generally expressed as follows [118]:

$$SoC(t+1) = SoC(t) \times (1 - d_b) + \left\{ \frac{\eta_C}{E_{Nom}} [P_{chg}(t)] - \frac{1}{\eta_D \times E_{Nom}} [P_{dis}(t)] \right\} \Delta t \tag{5.12}$$

where $SoC(t)$ is the state of charge of the BESS at any sampling time t, d_b is the self-discharged rate of the BESS, η_C is the BESS charge efficiency, E_{Nom} is the BESS nominal energy, η_D is the BESS discharge efficiency, P_{chg} and P_{dis} are the charging and discharging power at time t respectively, Δt is the sampling time. By applying inductive reasoning from equation (5.12), the dynamics of the BESS SoC at t^{th} sampling interval can be expressed in terms of its initial value $SoC(0)$ using the following equation [118]:

$$SoC(t) = SoC(0) \times (1 - d_b) + \left\{ \frac{\eta_C}{E_{Nom}} \sum_{\tau=0}^{t-1} [P_{chg}(\tau)] - \frac{1}{\eta_D \times E_{Nom}} \sum_{\tau=0}^{t-1} [P_{dis}(\tau)] \right\} \Delta t \tag{5.13}$$

where $SoC(0)$ is the initial SoC of the BESS. The following Equations (5.14) and (5.15) describe the charging and discharging power flow of the BESS, respectively.

$$P_2(t) + P_5(t) = P_{chg}(t) \tag{5.14}$$

$$P_7(t) = P_{dis}(t) \tag{5.15}$$

where $P_2(t)$ is the power flow from the PV system to the BESS, $P_4(t)$ is the power flow from the WT system to the BESS, $P_5(t)$ is the power flow from the BESS to the EV BSS, and $P_6(t)$ is the power flow from the BESS to the utility grid. Additionally, at any given sampling interval, the BESS must adhere to specific constraints to ensure safe and reliable operation. These constraints stipulate that the BESS capacity must not fall below the minimum allowable capacity nor exceed the maximum permissible capacity, as defined in Equations (5.16), (5.17), and (5.18), respectively.

$$SoC^{min} \leq SoC(t) \leq SoC^{max} \tag{5.16}$$

$$0 \leq P_{chg}(t) \leq P_{chg}^{max}(t) \tag{5.17}$$

$$0 \leq P_{dis}(t) \leq P_{dis}^{max}(t) \tag{5.18}$$

where SoC^{min} and SoC^{max} are the minimum and maximum allowable states of charge, respectively, $P_{chg}^{max}(t)$ is the maximum allowable charging power to the BESS, and $P_{dis}^{max}(t)$ is the maximum allowable discharging power from the BESS. The SoC^{min} is related to the BESS depth of discharge (DoD), which is given by:

$$SoC^{min} = (1 - DoD)\ SoC^{max} \tag{5.19}$$

where DoD denotes the depth of discharge given in percentage.

5.2.5 Utility Grid

The utility grid system serves as a critical source of power for charging depleted EV batteries, especially when renewable energy sources like wind and solar PV systems are unavailable or insufficient to meet the charging demand. In this context, the power from the utility grid is modelled as an all-time available power source supplying the charging demands at the EV-BSS. The grid system in this setup not only supplies power for charging depleted EV batteries but also facilitates the selling of excess electricity back to the utility grid, providing an additional revenue stream. This bidirectional flow of energy allows for better integration of renewable sources like wind and solar PV systems, optimizing the use of generated power. The energy drawn from the utility grid for charging EV batteries can be modelled mathematically to determine its impact on the total cost and energy optimization of the system. The energy purchased from the utility grid, denoted as $E_g(t)$, is calculated based on the power demand of the depleted EV battery charging process at any time t and is expressed as:

$$E_g = \sum_{t=1}^{N} P_8(t)\ \Delta t \tag{5.20}$$

where P_8 is the power flow from the utility grid to supply the depleted EV batteries at the BSS, and Δt is the sampling time. Therefore, the energy cost that can be extracted from the utility grid is determined by the local electricity market policy and time of use (TOU) tariff. The cost of energy C_{Eg} that can be drawn from the utility grid when charging the depleted EV batteries can be calculated from

$$C_{Eg} = p_e(t) \sum_{t=1}^{N} P_8(t)\ \Delta t \tag{5.21}$$

where $P_e(t)$ is the TOU electricity price at the t-th sampling interval per kWh.

On the other hand, the energy sold back to the utility grid, denoted as $E_{g_{in}}(t)$, is expressed as:

$$E_{g_{in}} = [P_3(t) + P_6](t)\ \Delta t \tag{5.22}$$

where P_3 is the power flow from the PV generation to the utility grid at time t, P_6 is the the power flow from the WT to the utility grid at time t. The revenue generated from selling electricity back to the utility grid, R, is calculated by:

$$R = p_{r1}(t) \sum_{t=1}^{N} P_3(t)\ \Delta t + p_{r2}(t) \sum_{t=1}^{N} P_6(t)\ \Delta t \tag{5.23}$$

where $p_{r1}(t)$ represents the feed-in tariff for the solar PV at time t, $p_{r2}(t)$ represents the feed-in tariff for the WT at time t. This model helps optimize energy exchange with the utility grid, balancing costs and revenue to enhance the overall economic performance of the hybrid renewable power system. Additionally, the power from the utility grid can be constrained to a limited range which is given by:

$$0 \leq P_8\,(t) \leq +\infty \tag{5.24}$$

5.2.6 Battery swapping station power demand

An EV BSS is a facility designed to allow EV drivers to quickly exchange depleted batteries for fully charged ones, addressing the challenges of traditional plug-in charging methods [91, 92]. A standard EV BSS features multiple battery swapping units, allowing simultaneous battery exchanges for several EVs. The power demand at the BSS is influenced by the charging and swapping processes and the characteristics of EV batteries, such as capacity, technology and initial SoC [93]. Accurate modelling of power demand is crucial, especially during the charging of depleted EV batteries, to meet the swapping requirements when EVs arrive. The total charging and discharging power of depleted EV batteries at the BSS are represented by Equations (5.25) and (5.26), respectively:

$$P_{c,BSS}(t) = \sum_{EV,b=1}^{n} P_{c,(EV,b)}(t) \tag{5.25}$$

$$P_{d,BSS}(t) = \sum_{EV,b=1}^{n} P_{d,(EV,b)}(t) \tag{5.26}$$

where n is the total number of the depleted EV batteries, $P_{c,BSS}(t)$ is the total charging power of the depleted EV batteries, $P_{d,BSS}(t)$ is the total discharging power of the depleted EV batteries, $P_{c,(EV,b)}(t)$ is the charging power of one depleted EV battery, $P_{d,(EV,b)}(t)$ is the discharging power of one depleted EV battery. Each depleted EV battery undergoes charging and discharging processes akin to a conventional battery. The charging of these depleted EV batteries is determined by their SoC during specific time intervals, which quantifies the available capacity relative to the maximum capacity when fully charged. Taking into account these factors, the SoC of the EV battery at the t^{th} sampling interval can be generally expressed as [75, 94]:

$$SoC_{EV,b}(t) = SoC_{EV,b}(t-1) + \left(P_{c,(EV,b)}(t) - \frac{P_{d,(EV,b)}(t)}{\eta_{EV,b}} \right) \times I_{dur}(t) \tag{5.27}$$

where $I_{dur}(t)$ is the duration of time interval, $\eta_{EV,b}$ is the EV battery efficiency (%), calculated as:

$$\eta_{EV,b} = \frac{\sum_{t=1}^{N} P_{d,(EV,b)}(t) \times I_{dur}(t)}{\sum_{t=1}^{N} P_{c,(EV,b)}(t) \times I_{dur}(t)} \tag{5.28}$$

During the battery swapping process, the power and SoC of the EV battery are set to zero, as described by Equation (5.29).

$$\begin{cases} P_{c,(EV,b)}(t) = 0 \\ P_{d,(EV,b)}(t) = 0 \\ SoC_{EV,b}(t) = 0 \end{cases} \qquad \forall t = t_{swap} \tag{5.29}$$

Prior to the battery swapping period, the depleted EV battery must be fully charged to prepare for the next swap. Consequently, the energy management system must ensure that an adequate number of fully charged EV batteries are available at each time interval to meet the demand for upcoming swaps. This requirement is formalized in Equation (5.30).

$$SoC_{EV,b}(t) = SoC_{EV,b}(t-1) \qquad \forall t = (t_{swap} - 1) \tag{5.30}$$

The total power demand at the BSS, which is based on the power capacity of the charging station, is determined by summing the discretized charging power requirements for each depleted EV battery. Consequently, the total expected power demand for all n depleted EV batteries charged at the BSS at time t can be estimated using Equation (5.31).

$$P_{Ld,BSS}(t) = \sum_{EV,b=1}^{n} \left(P_{c,(EV,b)}(t) - P_{d,(EV,b)}(t) \right) \tag{5.31}$$

where $P_{Ld,BSS}(t)$ is the total expected power demand of all depleted EV batteries charged at time (t).

5.2.7 Objective function and constraints

The optimization problem addressed in this chapter is a multi-objective function problem. The objective function aims to simultaneously minimize the operational costs associated with power purchased from the utility grid and the wear-related costs of the hybrid system while maximizing revenue from electricity sold back to the grid. This is achieved by determining the optimal operation strategy that meets the charging demand of the EV BSS, ensuring its continuous operation. The wear-related cost of the hybrid system is influenced by the frequent charging and discharging cycles of the battery energy storage system, which directly affects its operational lifespan. The mathematical formulation of the objective function is

presented as follows:

$$\min J = \left(\xi_1 \sum_{t=1}^{N} p_e(t) P_8(t) + \xi_2 \sum_{t=1}^{N} [\phi(P_7(t) + 24a] - \xi_3 \sum_{t=1}^{N} [p_{r1}(t) P_3(t) + p_{r2}(t) P_6(t)] \right) \Delta t \tag{5.32}$$

where ξ_1, ξ_2, ξ_3 are weighting factors respectively, $p_e(t)$ is the electricity price under the TOU tariff, $p_{r1}(t)$ is the feed-in tariff for the solar PV, $p_{r2}(t)$ is the feed-in tariff for the WT, P_7 is the power flow from the utility grid to the EV BSS, P_5 is the power flow from the BESS to the EV BSS, P_6 is the power flows from the BESS to the utility grid, Δt is the sampling time, N is the sampling period number, ϕ is the wearing cost coefficient of the hybrid system, and a is the hourly wearing cost of other components. The TOU electricity tariff and the feed-in tariff are key parameters in the optimization process. The weighting factor is adjusted according to the EV BSS's preferred outcomes where $\xi_1 + \xi_2 + \xi_3 = 1$.

5.2.8 Constraints

The objective function has some operational constraints, and these constraints are mathematically represented as follows:

- ***Power balance***: At any sampling time t at the EV BSS, the total charging demand must be met by the combined power supplied from the utility grid, PV system, wind turbine, and BESS, as expressed in Equation 4.33:

$$P_1(t) + P_4(t) + P_7(t) + P_8(t) = P_{Ld,BSS}(t) \tag{5.33}$$

- ***Wind turbine power supply***: At any sampling time t, the total power supplied by the wind turbine to both the EV BSS and the BESS must not exceed the total power generated by the wind turbine, as expressed in the following equation:

$$P_4(t) + P_5(t) + P_6(t) \leq P_{WT}(t) \tag{5.34}$$

- ***Solar PV power supply***: At any sampling time t, the total power supplied by the solar PV to the EV BSS, the BESS, and the one feedback to the utility grid must not exceed the total power generated by the solar PV, as expressed in the following equation:

$$P_1(t) + P_2(t) + P_3(t) \leq P_{PV}(t) \tag{5.35}$$

- ***State of charge of the BESS***: At any sampling time t, the SoC of the BESS must remain within acceptable limits as indicated in the following equation:

$$SoC^{min}(t) \leq SoC(t) \leq SoC^{max}(t) \tag{5.36}$$

- ***The power flow limits***: At any sampling time t, the power output from each source is constrained within a specific controllable range, from zero up to its maximum available instantaneous power. These constraints ensure that the power flow remains within feasible operational limits. The mathematical representation of these limits is given in Equation 5.37, which defines the upper and lower bounds for each source's power output.

$$0 \leq P_i(t) \leq P_i^{max}(t), \tag{5.37}$$

  where i = 1,2,3,..,8 is the index of power flows, $P_i^{max}(t)$ is the maximum limits for each decision variable $P_i(t)$ at the sampling time t.

- ***Fixed-final state condition for the BESS***: Equation 5.38 enforces a fixed-final state condition for the BESS, ensuring that the total energy inflows and outflows remain balanced over the simulation horizon. This constraint is essential for maintaining a stable SoC at the beginning of each simulation cycle, which enhances the accuracy and reliability of performance modeling. By stabilizing the SoC, this condition enables repeatable and balanced BESS operation, supporting optimal operation and effective battery storage management.

$$\sum_{t=1}^{N} P_7(t) - P_5(t) - P_2(t) = 0 \tag{5.38}$$

5.2.9 Algorithm formulation

An optimal control method is used to manage the power flows P_i in all sampling time to minimize the electricity cost consumption from the grid of the objective function 6.32, subject to constraints from 5.33 to 5.38. Because the objective function and constraints are linear, therefore, the optimization problem can be solved using the OPTI toolbox SCIP algorithm in MATLAB R2024a [1]. The objective function is formulated in the following canonical form:

$$\min f^T(x) \tag{5.39}$$

subject to:

$$\begin{cases} Ax \leq b \text{ ; linear inequality constraint} \\ A_{eq}x = b_{eq} \text{ ; linear equality constraint,} \\ lb \leq x \leq ub \text{ ; lower and upper bounds} \end{cases} \tag{5.40}$$

where $f^T(x)$ represents the objective function, A and b represent the coefficients corresponding to the inequality constraints, A_{eq} and b_{eq} represent the coefficients corresponding to the equality constraints, lb and ub are the lower and upper bounds of the decision variables.

[1] https://www.mathworks.com/help/optim/ug/intlinprog.html(accessed on 05 December 2024)

5.3 Case study

A case study using real-world data from an operational BSS network is conducted to validate the feasibility and effectiveness of the proposed system. The charging demand at the EV BSS is met through a combination of wtS, solar PV panels, and the utility grid, with surplus energy fed back into the utility grid or stored in the BESS for late use. This subsequent section presents the daily load profile, input data for hybrid renewable power generation, and the time-of-use (TOU) electricity tariff for the selected location.

5.3.1 EV BSS power demand load profile

To accurately assess the energy requirements of the EV BSS, a detailed load profile was constructed using historical data from an operational BSS. The chosen location is a heavy-duty truck swapping station at a central logistics hub in Shanghai Port, China, where energy consumption patterns reflect the high and variable demand associated with commercial EV operations. The data was recorded over a representative period, capturing daily and seasonal demand variations. Figure 6.2 and Figure 5.3 illustrate the daily energy consumption for one day in the weekday and weekend at the EV BSS, highlighting peak demand periods that coincide with high traffic volumes and operational hours. The load profile serves as the basis for sizing the hybrid renewable energy system and determining the optimal mix of energy sources.

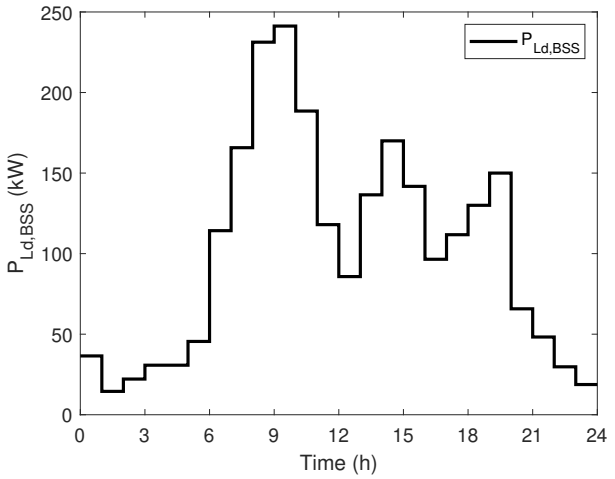


FIGURE 5.2: Charging patterns of the electric vehicle battery swapping station on a weekday.

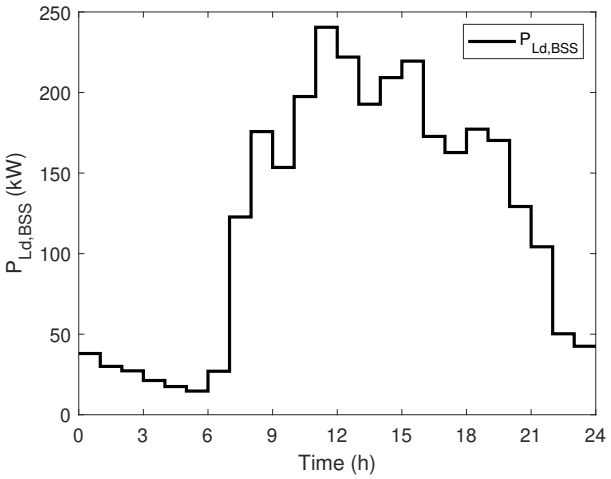


FIGURE 5.3: Charging patterns of the electric vehicle battery swapping station on a Weekend.

5.3.2 Renewable energy power supply

The proposed hybrid renewable power generation system incorporates wind turbines and solar PV panels as primary energy sources, supplemented by grid electricity to ensure a reliable supply. The input parameters for WT system power generation, such as the wind speed, and for solar PV power generation, such as the solar radiation and ambient temperature, are obtained from a typical day in the low-demand season in

Cape Town, South Africa, as referenced in [112]. Figure 6.3 presents the hourly average wind speed at 10 m above the ground in high demand season. The wind speed varies throughout the day, with a daily average of 2.54 m/s. The windiest period occurs between 2:00 PM and 4:00 PM, with an average wind speed of 4.6 m/s, while the calmest period is observed between 0:00 and 1:00 AM, with an average wind speed of 0.48 m/s, while Figure 6.4 presents the hourly average wind speed at 10 m above the ground in low demand season. The wind speed varies throughout the day, with a daily average of 3.27 m/s. The windiest period occurs between 9:00 AM and 10:00 AM, with an average wind speed of 3.81 m/s, while the calmest period is observed between 11:00 PM and 3:00 AM, with an average wind speed of 2.72 m/s. For more information, the average hourly wind speed over the year is presented in Figure 6.7. Additionally, the daily average for PV generation is depicted in Figure 6.5, indicating that the peak incident short-wave radiation for solar PV power generation reaching the ground's surface over a wide area is approximately 0.67 kW/m^2 around noon in high demand season, while Figure 6.6 indicating that the peak incident short-wave radiation for solar PV power generation reaching the ground's surface over a wide area is approximately 0.79 kW/m^2 between 1PM and 2PM in low demand season. For more information, The annual short-wave radiation for solar PV power generation reaching the surface of the ground over a wide area is presented in Figure 6.8, which gives significant seasonal variation with the peak brighter and lowest darker period of the year around December and June, respectively. The hybrid power system is designed to ensure that the EV BSS charging demand is met at any given time, particularly when electricity from the utility grid is expensive. The sizing of the wind and PV system is tied to the initial equipment cost and available capital, directly impacting power generation and reducing energy costs from the utility grid.

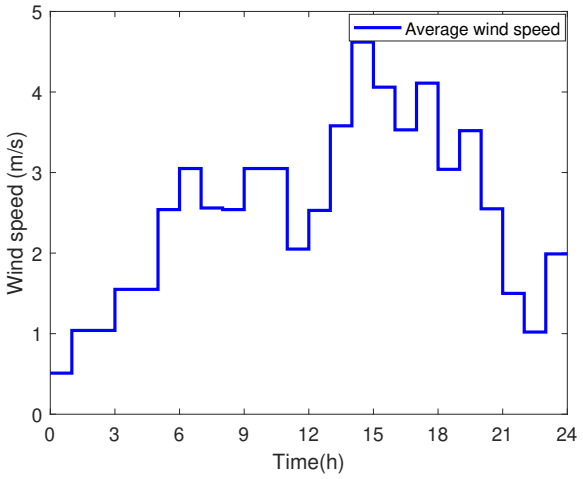


FIGURE 5.4: Average hourly wind speed HD.

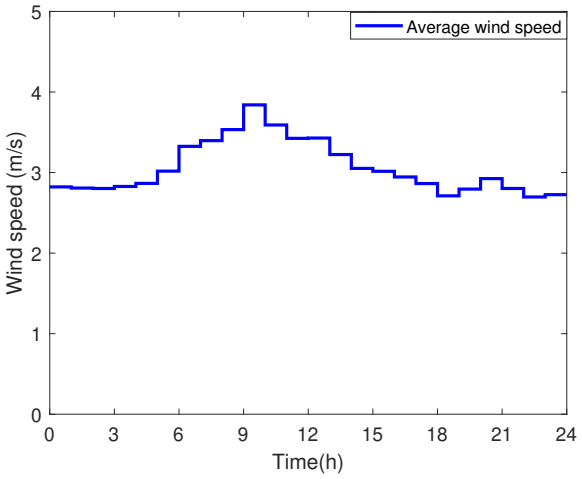


FIGURE 5.5: Average hourly wind speed LD.

5.3.3 Time-of-use electricity tariff

The South African power grid is managed by the national utility, "Eskom", with electricity tariffs regulated by the National Energy Regulator of South Africa (Nersa). Eskom's tariff structure typically includes both flat and dynamic TOU pricing systems. TOU pricing is a demand-side management strategy that reflects

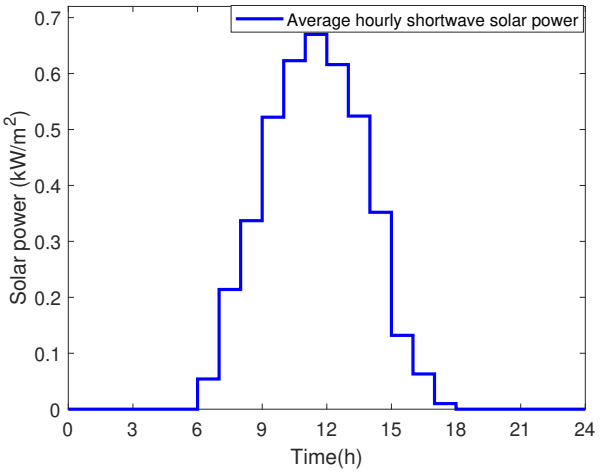


FIGURE 5.6: Daily average shortwave solar power HD.

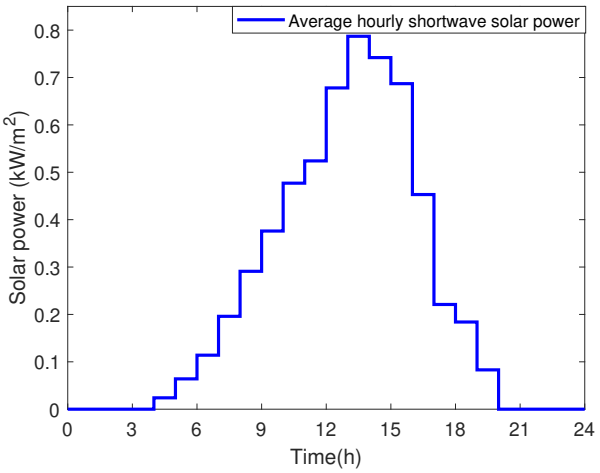


FIGURE 5.7: Daily average shortwave solar power LD.

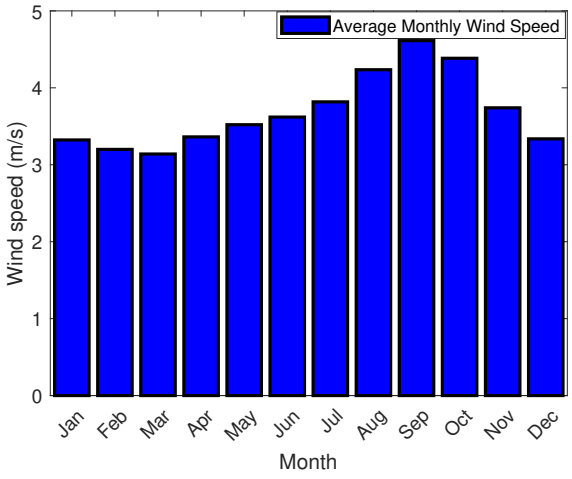


FIGURE 5.8: Monthly average wind speed.

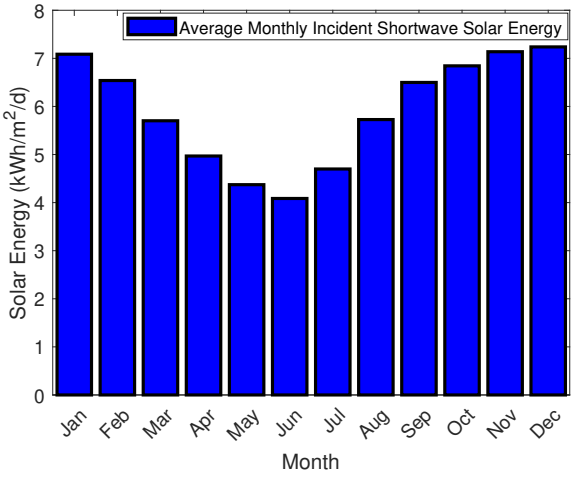


FIGURE 5.9: Monthly average shortwave PV power

the varying costs of electricity production throughout the day and is divided into three periods: off-peak ($p_{e\ off}$), standard-peak ($p_{e\ std}$), and on-peak ($p_{e\ pk}$). These periods correspond to times when electricity demand and generation costs are low, moderate, and high, respectively, implementing in a seasonal price variation. In the seasonal pricing, the winter months of June to August are classified as high demand season and electricity prices per unit are higher, while the remaining months of the year, September to May are classified as low demand season with lower electricity prices. In the context of our optimization problem, the TOU electricity tariff significantly influences the energy efficiency of the EV BSS. The 2023/2024 Eskom Megaflex TOU tariff scheme, which applies to industrial consumers who both consume energy from the utility grid and generate energy at the same point of supply is considered for the case study for the high and low-demand season weekday and weekend is used as the basis for the TOU electricity tariff analysis

given by (6.55) to (5.44), respectively [2]:

High demand season for weekdays and weekends:

$$p_{e(t)} = \begin{cases} p_{e\ off} = 1.0370\ ZAR/kWh\ ;\ \text{if}\ t \in [00:00, 06:00) \cup [22:00, 24:00)\ , \\ p_{e\ std} = 1.8991\ ZAR/kWh\ ;\ \text{if}\ t \in [09:00, 17:00) \cup [19:00, 22:00)\ , \\ p_{e\ pk} = 6.2421\ ZAR/kWh\ ;\ \text{if}\ t \in [06:00, 09:00) \cup [17:00, 19:00)\ . \end{cases} \tag{5.41}$$

$$p_{e(t)} = \begin{cases} p_{e\ off} = 1.0370\ ZAR/kWh\ ;\ \text{if}\ t \in [00:00, 07:00) \cup [12:00, 18:00) \cup [20:00, 00:00)\ , \\ p_{e\ std} = 1.8991\ ZAR/kWh\ ;\ \text{if}\ t \in [07:00, 12:00) \cup [18:00, 20:00)\ , \end{cases} \tag{5.42}$$

Low demand season for weekdays and weekends:

$$p_{e(t)} = \begin{cases} p_{e\ off} = 0.8992\ ZAR/kWh\ ;\ \text{if}\ t \in [00:00, 06:00) \cup [22:00, 24:00)\ , \\ p_{e\ std} = 1.4104\ ZAR/kWh\ ;\ \text{if}\ t \in [06:00, 07:00) \cup [10:00, 18:00) \cup [20:00, 22:00)\ , \\ p_{e\ pk} = 2.0440\ ZAR/kWh\ ;\ \text{if}\ t \in [07:00, 10:00) \cup [18:00, 20:00)\ . \end{cases} \tag{5.43}$$

$$p_{e(t)} = \begin{cases} p_{e\ off} = 0.8992\ ZAR/kWh\ ;\ \text{if}\ t \in [00:00, 07:00) \cup [12:00, 18:00) \cup [20:00, 00:00)\ , \\ p_{e\ std} = 1.4104\ ZAR/kWh\ ;\ \text{if}\ t \in [07:00, 12:00) \cup [18:00, 20:00)\ , \end{cases} \tag{5.44}$$

where ZAR is the South African currency (Rand), t represents the time of day in hours, and $p_{e(t)}$ represents the daily electricity price. One can notice that in both high and low demand seasons on the weekend (5.42) and (5.44), respectively, the TOU electricity pricing has only two periods, which are off-peak and standard-peak periods. There is no on-peak period. The utility grid can accommodate excess power generated by the wind and solar PV systems while supplementing renewable resources to meet the charging demand of the EV BSS. The feed-in tariff for distributed renewable energy sources (DREs) is regulated by the National Energy Regulator of South Africa (NERSA) [3], which oversees the establishment of feed-in tariffs for RE in the country. The current feed-in tariff is 1.12 ZAR/kWh for solar PV power generation and 1.0398 ZAR/kWh for WT power generation. The power is supplied to the utility grid to maximize sales when charging demand within the control horizon, which has been met at different times of the day. This strategy benefits the utility grid by enabling optimal network operation and reducing system losses.

[2] https://www.eskom.co.za/distribution/wp-content/uploads/2023/03/Schedule-of-standard-prices-2023_24-140323.pdf

[3] https://www.nersa.org.za/

5.4 Simulation results and discussion

This section presents and analyzes the simulation results obtained from the optimization model, focusing on the system's performance and efficiency. The impact of key input parameters, including the power capacity of WTs, solar PV panels, the utility grid, and TOU electricity tariffs, is examined to provide insights into optimal operational strategies for the grid-connected wind-solar hybrid power system with BESS supplying the EV BSS. The optimization problem is solved using the SCIP solver in MATLAB's OPTI Toolbox over a 24-hour horizon, with a sampling interval of $\Delta t = 1$h, starting at midnight. Table 5.1 presents the parameters used in the simulation. Furthermore, four operational scenarios are considered to minimize the daily operational cost of the proposed system.

Table 5.1: Simulation parameters used in this chapter.

Parameters	**Symbol**	**Values**
Sampling period	N	24
Sampling time	Δt	1 h
Weighting factor	ξ_1	0.35
Weighting factor	ξ_2	0.3
Weighting factor	ξ_3	0.35
Rated power of the PV panel	Pr_{PV}	0.545 kW
Conversion efficiency of the PV panel	η_{PV}	19.4%
Rated efficiency of the PV panel	η_r	18.1%
Total number of PV panels	N_{PV}	402
Rated power of the WT generator	Pr_{WT}	8 kW
Rated WT speed	V_r	12 m/s
Cut-in WT speed	V_{ci}	2.5 m/s
Cut-out WT speed	V_{co}	25 m/s
WT gearbox efficiency	η_T	90%
WT generator efficiency	η_g	80%
Air density	φ_a	1.225 kg/m^3
WT power coefficient	C_p	0.48
Total number of WTs	N_{WT}	64
Wearing cost coefficient of the hybrid system	ϕ	0.001
Hourly wearing cost of other components	a	0.002
BESS nominal capacity	E_{nom}	600 kWh
BESS maximum SoC	SoC^{max}	90%
BESS minimum SoC	SoC^{min}	30%
BESS initial SoC	$SoC(0)$	50%
BESS charging efficiency	η_C	90%
BESS discharging efficiency	η_D	80%

5.4.1 High demand electricity pricing season

5.4.1.1 Scenario 1: Optimal operation strategy of the proposed system in high demand season for one day on the weekday (June to August).

Figure 5.10 illustrates the power generation and supply dynamics of the grid-connected wind-solar hybrid system with BESS, ensuring optimal operation of the EV BSS for a selected day in winter over a weekday. The figure presents the contributions of solar PV power flow (P_1), WT power flow (P_4), the BESS power flow (P_7), and the utility grid power flow (P_8). During the off-peak period, early hours in the morning 00:00 to 06:00 and late 22:00 to 00:00, the charging demand of the EV batteries at the BSS relies primarily on the power flow from the utility grid due to the low electricity price first and second to minimal renewable generation. As solar radiation increases after sunrise, the power flow from the solar PV system starts to contribute significantly and reduce dependency on the utility grid. In contrast, the power flow from the WT exhibits variability throughout the day, complementing PV generation. The BESS is strategically used to store excess energy and discharge power during peak periods from 06:00 to 09:00 or low generation from the hybrid system from 17:00 to 19:00, helping to balance the power supply and charging demand. During these times, the system relies heavily on the RE and the BESS to meet the charging demand, and the power flow from the utility grid serves as a crucial backup, mainly during morning peak periods when the power from the PV, WT and the BESS are insufficient. During the standard period, from 09:00 to 17:00 and 19:00 to 22:00, the charging demand of the depleted EV batteries at the EV BSS is only met by the hybrid system, reducing reliance on the utility grid and charging the BESS.

Figure 5.11 presents the simulation results for the optimal power flows of the proposed model at the BESS side. Here, the power flows include the charging power flow from the solar PV (P_2), the charging power flow from the WT (P_5) and the discharging power flow to supply the EV BSS (P_7). When the solar PV and WT output exceed the charging demand of the depleted EV battery at the EV BSS, the surplus power is stored in the BESS. Most of the power flow from the BESS is used to meet the charging demand of the depleted EV battery during peak periods and standard periods, especially in the evening.

Figure 5.12 shows the SoC of the BESS. It can be seen that most of the SoC increases during standard periods between 09:00 and 17:00 due to the high irradiation of solar PV generation, and it decreases during peak periods when stored energy is used to meet the charging demand of the depleted EV battery and standard period of 19:00 to 22:00 due to unavailability of the solar PV. Both the SoC boundary constraint and the fixed-final state condition constraint for the BESS are satisfied throughout the simulation.

The hybrid system generally generates more power during the day than at night. In Figure 5.13, the surplus hybrid power generation shows the power sold to the utility grid with most coming from the solar PV system. When the Eskom TOU electricity tariff is applied, without the hybrid power generation, the charging demand results in a daily electricity cost of ZAR 7,676.39. However, implementing the proposed optimization model for the optimal operation of the hybrid power generation reduces the daily electricity cost to ZAR 564.81. The income of selling electricity back to the utility grid from the selected day over the

weekdays is ZAR 129.00 which priority come from the solar PV. The system effectively integrates multiple power sources to optimize power supply while complying with TOU electricity tariff constraints.

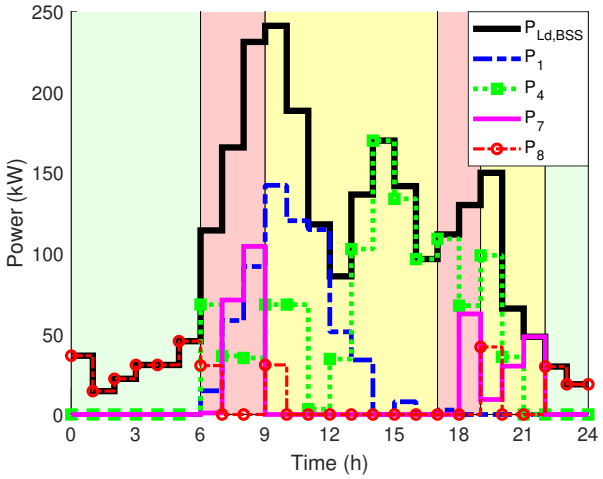


FIGURE 5.10: Charging demand side power flows.

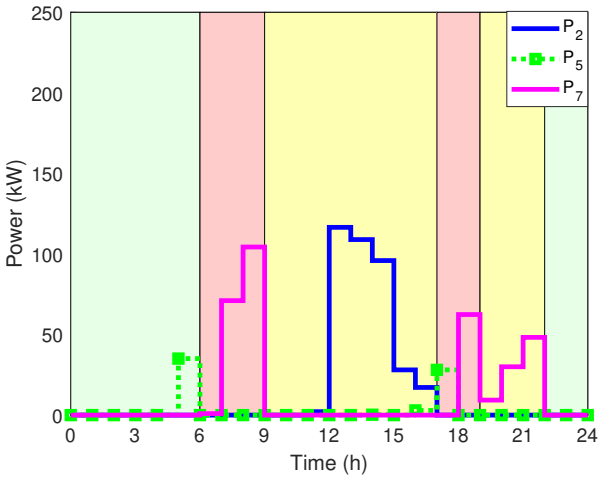


FIGURE 5.11: BESS side power flows.

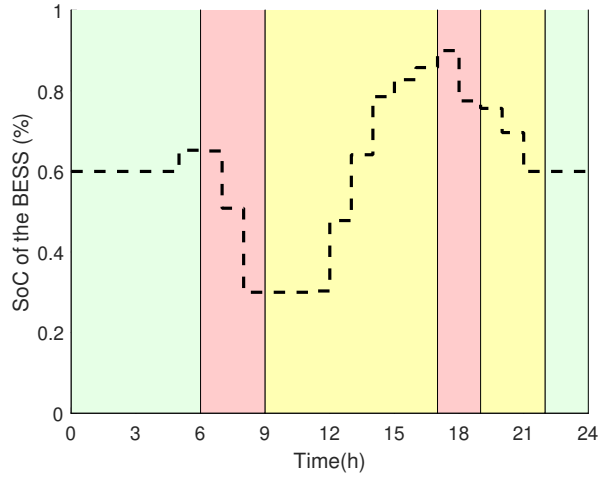


FIGURE 5.12: BESS SoC.

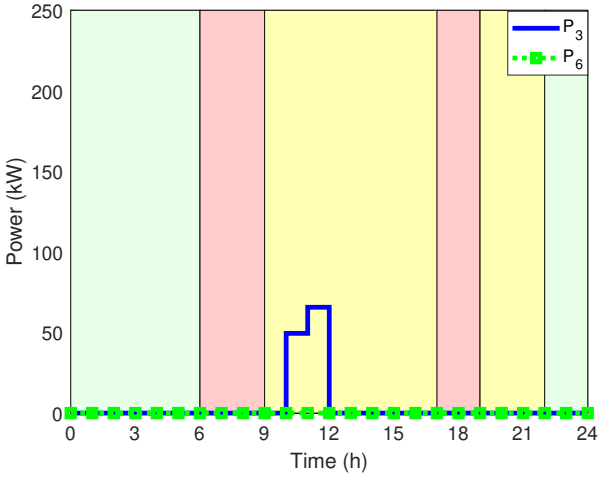


FIGURE 5.13: Hybrid power to the Grid.

5.4.1.2 Scenario 2: Optimal operation strategy of the proposed system in high demand season for one day on the weekend (June to August).

Figure 5.14 illustrates the power generation and supply dynamics of the grid-connected wind-solar hybrid system with BESS, ensuring optimal operation of the EV BSS for a selected day in winter over a weekend. The figure presents the contributions of solar PV power flow (P_1), WT power flow (P_4), the BESS power flow (P_7), and the utility grid power flow (P_8) to meet the charging demand of the EV BSS ($Ld, BSSP$). One can notice that during the weekend, there are only two peak time periods for the TOU electricity tariff, including the off-peak period and the standard-peak period. During the off-peak period, early hours from 00:00 to 07:00, 12:00 to 18:00, and late from 20:00 to 00:00, the charging demand of the EV batteries at

the BSS relies mainly on the power flow from the utility grid due to low electricity prices and minimal RE generation. During the standard period (07:00 to 12:00 and 18:00 to 20:00), as solar radiation increases after sunrise, the power flow from the solar PV system contributes significantly to meet the charging demand for depleted EV batteries at the EV BSS, reducing dependence on the utility grid. Meanwhile, the power flow from the WT varies throughout the day, complementing the PV generation. The BESS is strategically used to store excess energy and discharge power during these periods, or when renewable generation is low, helping to balance power supply and charging demand.

Figure 5.15 presents the simulation results for the optimal power flows at the BESS side. Here, the power flows include the charging power flow from the solar PV (P_2), the charging power flow from the WT (P_5), and the discharging power flow supplying the EV BSS (P_7). When solar PV and WT generation exceed the charging demand of the depleted EV batteries at the EV BSS, the surplus power is stored in the BESS. One can notice that only power flow from the WT is stored to the BESS and these happen during all off-peak periods. The stored energy is then used to meet the charging demand, particularly during standard periods. The BESS plays a key role in shifting energy availability to times of high demand, thus minimizing reliance on the utility grid and reducing operational cost.

Figure 5.16 illustrates the SoC of the BESS throughout the 24-hour period. The SoC increases significantly during the off-peak period (00:00 to 7:00 and 12:00 to 18:00) due to high WT generation, allowing surplus energy to be stored. Conversely, the SoC decreases during standard periods (07:00 to 12:00 and 18:00 to 20:00) as stored energy is utilized to meet the charging demand of the depleted EV battery at the EV BSS, reducing reliance on the utility grid. Throughout the simulation, the SoC boundary constraint and the fixed-final state condition constraint for the BESS are satisfied, ensuring optimal storage operation without overcharging or excessive discharge.

Figure 5.17 shows the surplus hybrid power generation exported to the utility grid. This power includes contributions from solar PV (P_3) and WT (P_6). Most of the exported power occurs during the midday, when solar PV generation is at its peak. The sale of excess power generation back to the utility grid generates revenue, improving the economic viability of the system. By implementing the Eskom TOU electricity tariff on the proposed optimization model, the daily electricity cost of the EV BSS is significantly reduced. Without hybrid power generation, the daily electricity cost would be ZAR 4,093.28. However, applying the optimazation model on the system reduces the daily cost to ZAR 1,330.84. Additionally, income from selling electricity back to the utility grid amounts to ZAR 643.56.

5.4.2 Low demand electricity pricing season

5.4.2.1 Scenario 3: Optimal operation strategy of the proposed system in low demand season for one day on the weekday (September to May).

Figure 5.18 illustrates the power generation and supply dynamics of the grid-connected wind-solar hybrid system with BESS, ensuring optimal operation of the EV BSS for a selected day in summer over a weekday.

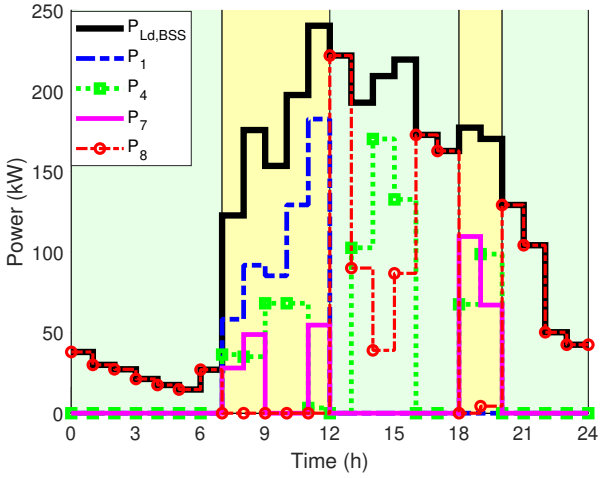


FIGURE 5.14: Charging demand side power flows.

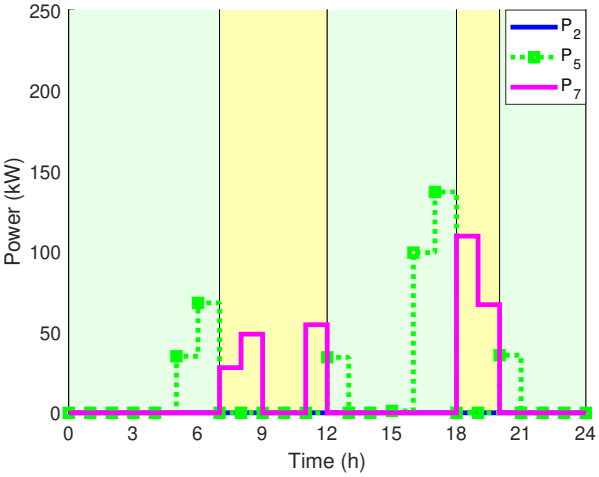


FIGURE 5.15: BESS side power flows.

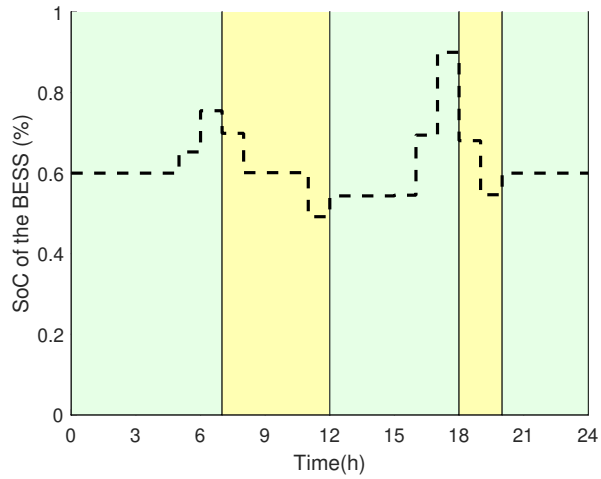


FIGURE 5.16: BESS SoC.

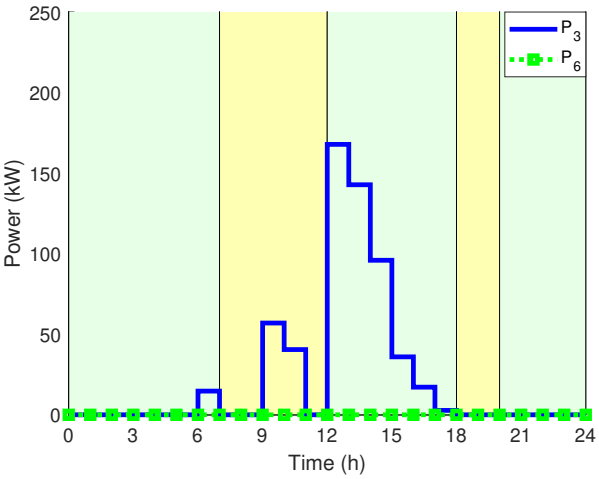


FIGURE 5.17: Hybrid power to the Grid.

The figure presents the contributions of solar PV power flow (P_1), WT power flow (P_4), the BESS power flow (P_7), and the utility grid power flow (P_8). During the off-peak period (00:00 to 06:00 and 22:00 to 00:00), the charging demand of the depleted EV batteries at the EBSS ($P_{Ld,BSS}$) primarily relies on the power flow from the utility grid due to low electricity prices and minimal RE generation. As solar radiation increases after sunrise, the power flow from the solar PV system starts contributing significantly, reducing dependency on the utility grid. The power flow from the WT exhibits variability throughout the day, complementing PV generation. The BESS is strategically used to store excess energy and discharge power during peak periods (07:00 to 10:00 and 18:00 to 20:00), balancing the power supply and charging demand. During the standard period (06:00 to 7:00, 10:00 to 18:00, and 20:00 to 22:00), the charging demand of the depleted EV battery at the EV BSS is met primarily by the hybrid system. The system relies on RE, with the power flow from the utility grid serving as a crucial backup, particularly in the morning and later in the evening standard period.

Figure 5.19 presents the simulation results for the optimal power flows at the BESS side. Here, the power

flows include the charging power flow from the solar PV (P_2), the charging power flow from the WT (P_5), and the discharging power flow supplying the EV BSS (P_7). When the output power from the solar PV and WT exceeds the charging demand at the EV BSS, the surplus power is stored in the BESS. The stored energy in the BESS is then used to meet the charging demand of the depleted EV battery, particularly during peak periods. The BESS plays a key role in shifting energy availability to times of high demand, thus minimizing reliance on the grid and reducing operational costs.

Figure 5.20 illustrates the SoC of the BESS throughout the 24-hour period. The SoC increases significantly early in the morning due to the WT generation and then after during from 11:00 to 14:00 due to high radiation of the solar PV, allowing surplus energy to be stored. Conversely, the SoC decreases during peak periods as stored energy is used to meet the charging demand, reducing reliance on the utility grid. Throughout the simulation, the SoC boundary constraint and the fixed-final state condition constraint for the BESS are satisfied, ensuring optimal storage operation without overcharging or excessive discharge.

Figure 5.21 shows the surplus hybrid power generation exported to the utility grid. This power includes contributions from solar PV (P_3) and WT (P_6). The majority of the exported power occurs during afternoon from 13:00 to 17:00), when solar PV generation is at its peak. The sale of excess power back to the utility grid generates revenue, improving the economic viability of the system. By implementing the proposed optimization model, the daily electricity cost of the EV BSS is significantly reduced. Without hybrid power generation, the daily electricity cost would be ZAR 3,883.59. However, applying the optimization model on the system reduces the daily cost to ZAR 380.89. Additionally, income from selling electricity back to the utility grid amounts to ZAR 322.78.

5.4.2.2 Scenario 4: Optimal operation strategy of the proposed system in low demand season for one day on the weekend (September to May).

Figure 5.22 illustrates the power generation and supply dynamics of the grid-connected wind-solar hybrid system with BESS, ensuring optimal operation of the EV BSS for a selected day in summer over a weekend. The figure presents the contributions of solar PV power flow (P_1), WT power flow (P_4), the BESS power flow (P_7), and the utility grid power flow (P_8) to meet the charging demand of the EV BSS ($Ld, BSSP$). One can notice that during the weekend, there are only two peak time periods for the TOU electricity tariff, including the off-peak period and the standard-peak period. During the off-peak period, early hours from 00:00 to 07:00, 12:00 to 18:00, and late from 20:00 to 00:00, the charging demand of the depleted EV batteries at the EV BSS relies mainly on the power flow from the utility grid due to low electricity prices. During the standard period (07:00 to 12:00 and 18:00 to 20:00), as solar radiation increases after sunrise, the power flow from the solar PV system contributes significantly to meet the charging demand for depleted EV batteries, reducing dependence on the utility grid. Meanwhile, the power flow from the WT varies throughout the day, complementing the PV generation. The BESS is strategically used to store excess energy and discharge power during these periods, helping to balance power supply and charging demand.

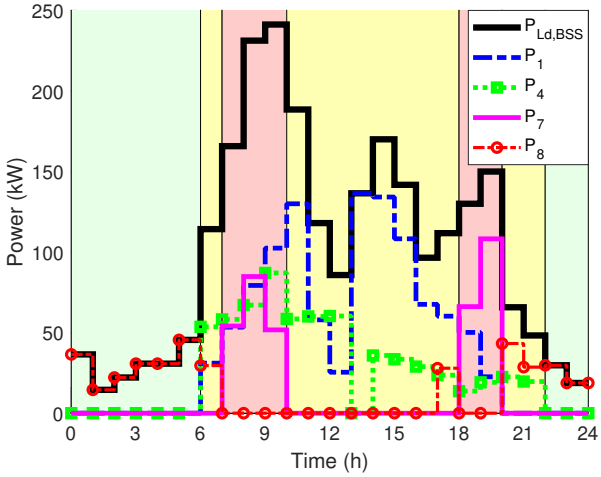


FIGURE 5.18: Charging demand side power flows.

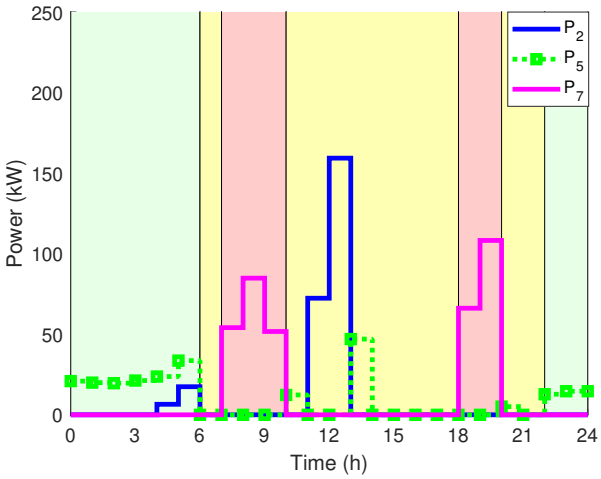


FIGURE 5.19: BESS side power flows.

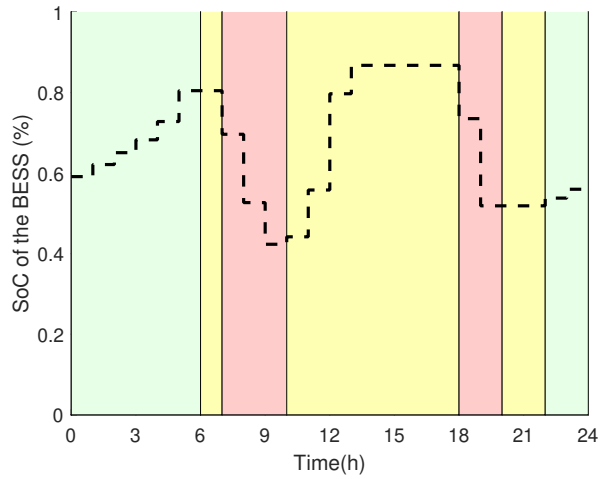


FIGURE 5.20: BESS SoC.

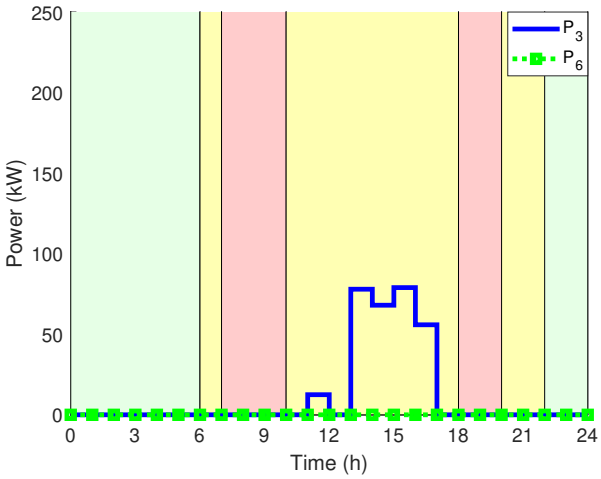


FIGURE 5.21: Hybrid power to the Grid.

Figure 5.23 presents the simulation results for the optimal power flows at the BESS side. Here, the power flows include the charging power flow from the solar PV (P_2), the charging power flow from the WT (P_5), and the discharging power flow supplying the EV BSS (P_7). When solar PV and WT generation exceed the charging demand of the depleted EV batteries at the EV BSS, the surplus power is stored in the BESS. One can notice that only power flow from the WT is stored to the BESS and these happen during all off-peak periods. The stored energy is then used to meet the charging demand, particularly during standard periods. The BESS plays a key role in shifting energy availability to times of high demand, thus minimizing reliance on the utility grid and reducing operational cost.

Figure 5.24 illustrates the SoC of the BESS throughout the 24-hour period. The SoC increases significantly during the off-peak period (00:00 to 7:00, 12:00 to 18:00, and 20:00 to 00:00) due to high WT generation, allowing surplus energy to be stored. Conversely, the SoC decreases during standard periods (07:00 to 12:00 and 18:00 to 20:00) as stored energy is utilized to meet the charging demand of the depleted EV battery at the EV BSS, reducing reliance on the utility grid. Throughout the simulation, the SoC boundary

constraint and the fixed-final state condition constraint for the BESS are satisfied, ensuring optimal storage operation without overcharging or excessive discharge.

Figure 5.25 shows the surplus hybrid power generation exported to the utility grid. This power includes contributions from solar PV (P_3) and WT (P_6). Most of the exported power occurs during the afternoon and few in the morning, when solar PV generation is at its peak. The sale of excess power generation back to the utility grid generates revenue, improving the economic viability of the system. By implementing the proposed optimization model, the daily electricity cost of the EV BSS is significantly reduced. Without hybrid power generation, the daily electricity cost would be ZAR 3,256.88. However, applying the optimization model on the system reduces the daily cost to ZAR 1,456.11. Additionally, income from selling electricity back to the utility grid amounts to ZAR 1,194.

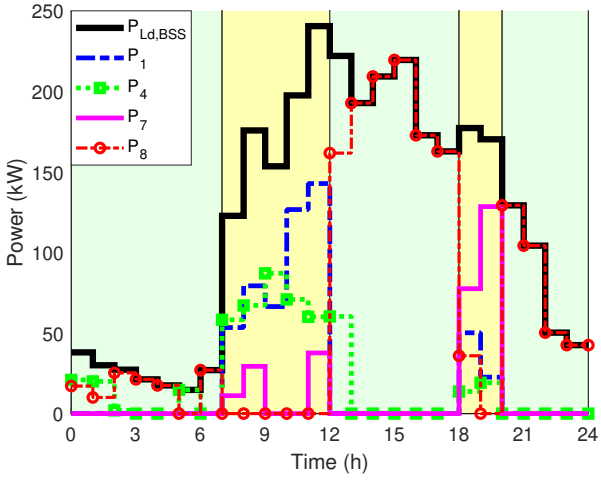


FIGURE 5.22: Charging demand side power flows.

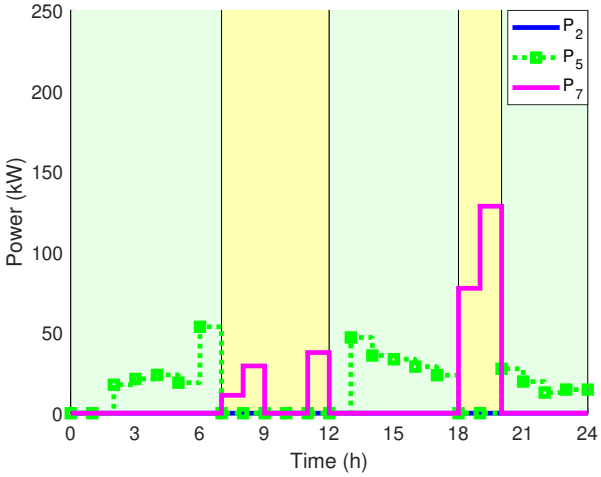


FIGURE 5.23: BESS side power flows.

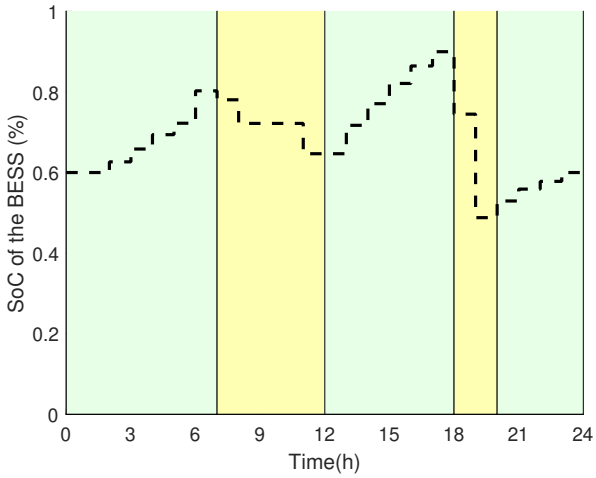


FIGURE 5.24: BESS SoC.

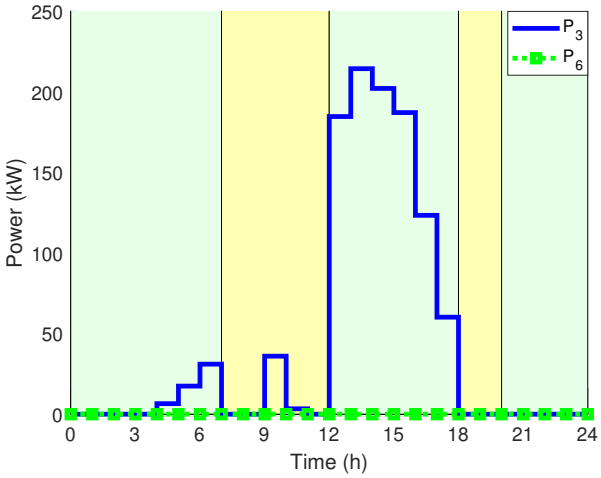


FIGURE 5.25: Hybrid power to the Grid.

5.4.3 Baseline and optimal cost saving

In order to evaluate the effectiveness of the proposed grid-hybrid wind-solar power generation with storage system for the EV BSS, four scenarios are analyzed for the baseline and optimal cost saving. The baseline assumes a conventional setup, where the charging demand of the depleted EV battery at the EV BSS relies totally on the utility grid without sophisticated scheduling or significant RE penetration. On the other hand, the optimal cost is the energy cost obtained after employing the proposed optimization model strategy presented in this chapter. The optimal cost comprises the sum of energy used to charge the depleted EV battery at the EV BSS. The hybrid energy sales are the revenue generated by selling wind and solar energy to the power grid. Not all the hybrid power generated was sold, some went to supplement the charging demand and charge the BESS. Table 6.1 summarizes the four scenarios' daily energy consumption cost savings and hybrid feed-in to the utility grid. The results clearly indicate that incorporating renewable resources and optimal scheduling reduces reliance on the utility grid, thereby lowering overall operational costs. Furthermore, the advanced control strategy leverages the BESS to store excess energy during low-tariff or in high-generation periods, which is later discharged during peak period where the TOU electricity tariff is expensive. This approach minimizes the EV BSS's electricity expenses and enhances the power supply's resilience and sustainability.

Table 5.2: Different case scenario with daily optimal energy and cost savings .

				Savings	
	Baseline cost (ZAR)	**Optimal cost (ZAR)**	**Hybrid feed-in (ZAR)**	**Energy (kWh)**	**Cost (ZAR)**
Scenario 1	7 676.39	564.81	129.00	2 092.16	7 111.58
Scenario 2	4 093.28	1 330.83	643.56	1 638.72	2 762.45
Scenario 3	3 883.59	380.89	322.78	2 071.02	3 560.81
Scenario 4	3 256.88	1 456.11	1 194.70	1 319.51	2 062.18

As shown in Table 6.1, the proposed optimization model significantly reduces daily costs compared to the baseline, primarily due to the coordinated operation of RE generation and the BESS. This optimal control strategy is particularly effective on weekdays, when peak periods occur more frequently than on weekends. In addition, the model generates considerable revenue from selling surplus hybrid energy. Usually the high feed-in energy occurs during the weekend due to low TOU electricity tariff when the utility grid is used to meet the charging demand of the depleted EV battery at the EV BSS.

Assuming daily charging demand remains constant across both weekdays and weekends, annual cost savings can be extrapolated from weekly data throughout the year. During the high-demand season (June to August, totaling 13 weeks), the weekly cost savings amount to (7 111.58 $\times$ 5) + (2 762.45 $\times$ 2) = 41 082.80 ZAR. During the low-demand season (September to May, covering 39 weeks), the weekly cost savings are (3 560.81 $\times$ 5) + (2 062.18 $\times$ 2) = 21 928.41 ZAR. Consequently, the total annual cost savings

of the proposed system are (41 082.8 × 13) + (21 928.41 × 39) = 1 389 284.39 ZAR. Table 5.3 summarizes the weekly and annual cost savings achieved by this configuration.

TABLE 5.3: Weekly and Annual cost savings.

				Savings	
	Baseline cost (ZAR)	**Optimal cost (ZAR)**	**Hybrid feed-in (ZAR)**	**Energy** (kWh)	**Cost** (ZAR)
Weekly HD	46 568.51	5 485.76	1 932.12	13 738.24	41 082.80
Weekly LD	25 931.71	4 816.67	4 003.30	12 994.12	21 928.41
Annualized			181 246.26	685 367.80	1 389 284.39

5.4.4 Economic analysis for the payback period

The optimal operation of a grid-connected hybrid renewable energy system with storage, integrated with an EV BSS, has been shown to enhance energy efficiency and reduce energy costs. A payback period analysis is conducted to assess the economic viability of the proposed system by determining the time required to recover the initial investment through energy cost savings. The baseline scenarios assume a conventional grid-powered EV BSS without optimization, while the proposed system leverages the coordinated operation of RESs and the utility grid. By contrast, the proposed optimization model achieves daily savings over the 24-hour control horizon, which are then annualized to evaluate long-term financial benefits. Throughout this analysis, the maintenance costs, as well as the annual optimal cost-benefit and the operation cost are assumed to increase proportionally over the lifetime of the system. A discounted present value approach is applied to the cash flow evaluation, ensuring that the time value of money is accurately reflected in determining the net economic gains. As a result, the discounted present value (DPV) of a cash flow occurring in a future period (z-th year) can be expressed as [80, 116]:

$$DPV(z) = \frac{FV(z)}{(1+d)^z} \tag{5.45}$$

where DPV is the discounted present value of the future cash flow, FV is the nominal value of a cash flow amount in a future period (z-th year), d is the discount rate, and z is the time in years before the future cash flow occurs. In this economic analysis, d represents the time value of money or the cost of holding capital and may also account for the risk of not receiving the full payment. The actual d is calculated as the difference between the average interest rate and the inflation rate. The interest rate (r) reflects the opportunity cost of time, representing the compensation required to delay spending from the current to a future year. On the other hand, the inflation rate (i) indicates the percentage change in prices over a specific period, typically measured monthly or annually, and shows how quickly prices increased during that time. The average interest rate [4] is 8.25%, and the inflation rate [5] is 4.6%, reflecting the time value of money in South Africa as of July 2024. Once $FV(z)$ is determined, the net present value (or cumulative

[4] https://tradingeconomics.com/south-africa/interest-rate(accessed on 20 September 2024)
[5] https://tradingeconomics.com/south-africa/inflation-cpi (accessed on 20 September 2024)

cash flow) is calculated as follows [116]:

$$NPV_{z=1}^{m} = \sum_{z=1}^{m} DPV(z) - CC \tag{5.46}$$

where NPV is the net present value (or cumulative cash flow) and CC is the total investment capital cost. Subsequently, the discounted payback period (PBP) can be determined using the following equation [116]:

$$PBP = m_y + \frac{-NPV_{z=1}^{m}}{DPV(m_y + 1)} \tag{5.47}$$

where m_y denotes the last year with a negative NPV. Table 5.4 provides the approximate prices of the various components of the proposed system, leading to a total investment capital cost (CC). The component prices are based on South African market rates[6]. Table 5.5 presents the payback period analysis of the proposed system under the optimal control strategy, with the salvage cost neglected.

TABLE 5.4: Costs components of the proposed system.

Components	**Costs (ZAR)**
Wind turbines	677 160.32
Solar photovoltaic	1 286 359.80
Storage system	159 340.00
Inverters	77 720
Installation cost	665 909.98
Accessories	3 000 000
Total investment capital cost	**5 866 490.10**

As shown in Table 5.5, the projected total investment capital cost is recorded as a negative cash flow in brackets as (ZAR 5 866 490.10) in the financial statement. The cash flows and PBP are calculated following the assumption that the annual optimal cost-benefit, the maintenance cost, and the operation cost increase proportionately throughout the lifetime of the proposed system. The cumulative cash flows decrease as negative ones until they eventually turn positive. The payback occurs when the cumulative cash flow reaches zero, and, at this point, the total investment capital cost has been fully recovered. For the proposed system, the PBP occurs after 5 years. Afterward, the cumulative cash flow becomes positive, and all the revenue in the following years represents pure profit or benefit. Suppose that the proposed system installation has a lifetime of 20 years and a payback period of approximately 5 years, in that case, the EV BSS owner can recover the total capital investment within a reasonable timeframe and will have over 15 years to generate guaranteed profit.

[6] https://www.sustainable.co.za/ (accessed on 14 March 2023)

TABLE 5.5: Payback period of the proposed system .

Years	Total investment capital cost (ZAR)	Annual cost Operation (ZAR)	Annual cost Maintenance (ZAR)	Annual revenue Optimal benefit cost (ZAR)	Annual revenue Hybrid feed-in (ZAR)	Total (ZAR)	Discount factor $(1+d)^{-L_p}$	Cash flows Discounted (ZAR)	Cash flows Cumulative (ZAR)
0	(5 866 490.10)						1.00	(5 866 490.10)	(5 866 490.10)
1		(54 688.61)	(285 357.51)	1 389 284.39	181 246.26	1 230 484.53	0.96	1 187 153.43	(4 679 336.67)
2		(55 470.66)	(289 438.12)	1 409 151.16	198 645.90	1 262 888.28	0.93	1 175 509.98	(3 503 826.69)
3		(56 263.89)	(293 577.08)	1 429 302.02	217 715.91	1 297 176.95	0.90	1 164 907.13	(2 338 919.56)
4		(57 068.47)	(297 775.23)	1 449 741.04	238 616.63	1 333 513.97	0.87	1 155 368.03	(1 183 551.53)
5		**(57 884.54)**	**(302 033.42)**	**(1 470 472.33)**	**261 523.83**	**1 372 078.20**	**0.84**	**1 146 917.90**	**(36 633.63)**
6		(58 712.29)	(306 352.50)	1 491 500.09	286 630.12	1 413 065.42	0.81	1 139 584.23	1 102 950.60
7		(59 551.88)	(310 733.34)	1 512 828.54	314 146.61	1 456 689.93	0.78	1 133 396.78	2 236 347.37
8		(60 403.47)	(315 176.83)	1 534 461.99	344 304.69	1 503 186.38	0.75	1 128 387.79	3 364 735.17
9		(61 267.24)	(319 683.85)	1 556 404.79	377 357.94	1 552 811.63	0.72	1 124 592.07	4 489 327.24
10		(62 143.36)	(324 255.3)	1 578 661.38	413 584.30	1 605 846.98	0.70	1 122 047.12	5 611 374.36
11		(63 032.01)	(328 892.18)	1 601 236.24	453 288.39	1 662 600.43	0.67	1 120 793.28	6 732 167.64
12		(63 933.37)	(333 595.34)	1 624 133.92	496 804.07	1 723 409.28	0.65	1 120 873.88	7 853 041.53
13		(64 847.62)	(338 365.76)	1 647 359.03	544 497.27	1 788 642.93	0.63	1 122 335.41	8 975 376.94
14		(65 774.94)	(343 204.39)	1 670 916.27	596 769.00	1 858 705.95	0.61	1 125 227.66	10 100 604.60
15		(66 715.52)	(348 112.21)	1 694 810.37	654 058.83	1 934 041.47	0.58	1 129 603.91	11 230 208.50
16		(67 669.55)	(353 090.21)	1 719 046.16	716 848.48	2 015 134.87	0.56	1 135 521.12	12 365 729.62
17		(68 637.23)	(358 139.40)	1 743 628.52	785 665.93	2 102 517.82	0.54	1 143 040.12	13 508 769.74
18		(69 618.74)	(363 260.80)	1 768 562.41	861 089.86	2 196 772.73	0.52	1 152 225.85	14 660 995.59
19		(70 614.29)	(368 455.43)	1 793 852.85	943 754.48	2 298 537.62	0.51	1 163 147.51	15 824 143.09
20		(71 624.07)	(373 724.34)	1 819 504.94	1 034 354.92	2 408 511.45	0.49	1 175 878.87	17 000 021.96
								Payback is 5 years plus 0 months (0.385758)	

5.5 Summary

This chapter presented an advanced optimal operation control strategy for grid-connected wind-solar power generation with a storage system for EV BSS. The proposed optimization model, developed using LP, aims to minimize the total operation costs associated with the cost of electrical energy purchased from the utility grid, and the wear cost of the hybrid system due to the frequent charging and discharging of the BESS, while maximizing the use of RE generated. Four scenarios have been considered for the case study including one day selected through the weekdays and weekend in high demand season, and on the other hand one day selected through the weekdays and weekend in low demand season. The simulation results demonstrate that integrating EV BSSs with the proposed grid-connected hybrid wind-solar PV power supply system with energy storage not only optimizes energy utilization and reduces costs, but also increases hybrid power feedback to the utility grid. This energy system offers significant advantages, including substantial energy and cost savings, while generating additional revenue through surplus power sales. A comprehensive economic analysis of the payback period is conducted to assess the feasibility of investing in the proposed system. The results indicate that the system achieves a payback period of approximately 5 years, aligning well with findings from similar studies, thereby demonstrating its economic viability. The proposed model is well suited for various locations that experience intermittent power supply, which makes it applicable in both urban and commercial areas. The proposed system provides a reliable and cost-effective solution for EV BSSs, with strong potential for widespread adoption across South African charging hubs and fleet depots.

Its implementation can drive both economic savings and environmental benefits, enhancing the sustainability of electric mobility.

However, the next chapter discusses the model predictive control strategy for a grid-connected wind-solar energy system designed for EV BSSs.

Chapter 6

MODEL PREDICTIVE CONTROL STRATEGY FOR GRID-CONNECTED WIND-SOLAR POWER GENERATION WITH STORAGE SYSTEMS FOR BATTERY SWAPPING STATION

6.1 Chapter overview

This chapter explores the application of model predictive control (MPC) to optimize the operation of a grid-connected hybrid power generation system with storage for an EV BSS. It begins by detailing the system configuration, which includes WTs, solar PV arrays, a BESS, the utility grid, and the EV BSS, comprising both the swapping system and charging infrastructure. Building on the open-loop control optimization from the previous chapter, this chapter develops an MPC-based strategy to determine the system's optimal operation while accounting for external disturbances and uncertainties. The multi-objective optimization function aims to minimize the cost of energy drawn from the utility grid under a TOU electricity tariff and the wear-related costs of the hybrid system, influenced by frequent BESS charging and discharging cycles while maximizing revenue from surplus energy sold back to the grid. A key advantage of MPC is

its ability to respond dynamically to external disturbances and uncertainties in real time through periodic re-optimization. This chapter highlights the benefits of a closed-loop approach in maintaining system stability and optimizing energy dispatch throughout the control horizon. Additionally, a comparative analysis between open-loop and closed-loop control strategies demonstrates the limitations of open-loop control in handling disturbances and the superior adaptability of closed-loop MPC in achieving a robust and cost-effective operation.

The remainder of this chapter is structured as follows: Section 5.2 presents the system modelling and formulation, Section 5.3 introduces the case study data, Section 5.4 discusses the optimization results, and Section 5.5 concludes the chapter.

6.2 System modelling and Formulation

6.2.1 Schematic model layout

Considering the model predictive control (MPC) strategy, the schematic of the proposed system is shown in Figure 6.1. The proposed grid-connected wind–solar hybrid power generation system with storage comprises four main components: a vertical-axis WT system, a solar PV generator, a BESS, and an EV BSS. The EV BSS includes both the charging apparatus and the battery swapping service for depleted EV batteries. The proposed design aims to integrate RESs (PV and WT), BESS, and utility grid to consistently meet the charging demands of depleted EV batteries while reducing reliance on the power grid. Under normal conditions, renewable energy sources serve as the primary power supply, with any excess energy directed to the BESS for later use. During periods when renewable generation is insufficient, the stored energy in the BESS is dispatched to ensure uninterrupted operation of the EV BSS. In the event that both the RESs and the BESS are unable to meet demand, the utility grid provides supplemental power as a backup. Finally, when the EV BSS charging demand are satisfied and the BESS is fully charged, any remaining surplus power is exported back to the utility grid, further optimizing overall energy utilization and system resilience. In Figure 5.1, the arrows represent the directions of the power flows of the control variables to be optimized. P_1 represents the power flow from the PV generation to the EV BSS, P_2 represents the power flow from the PV generation to the BESS, P_3 represents the power flow from the PV generation to the utility grid, P_4 represents the power flow from the WT to the EV BSS, P_5 represents the power flow from the WT to the BESS, P_6 represents the power flow from the WT to the utility grid, P_7 represents the power flow discharging from the BESS to the EV BSS, and P_8 represents the power flow from the utility grid to the EV BSS.

6.2.2 Wind turbine system

The wind turbine starts to generate power at a specific wind speed known as the cut-in wind speed (V_{ci}). As the wind speed increases, the generated power increases until it reaches the rated capacity of the

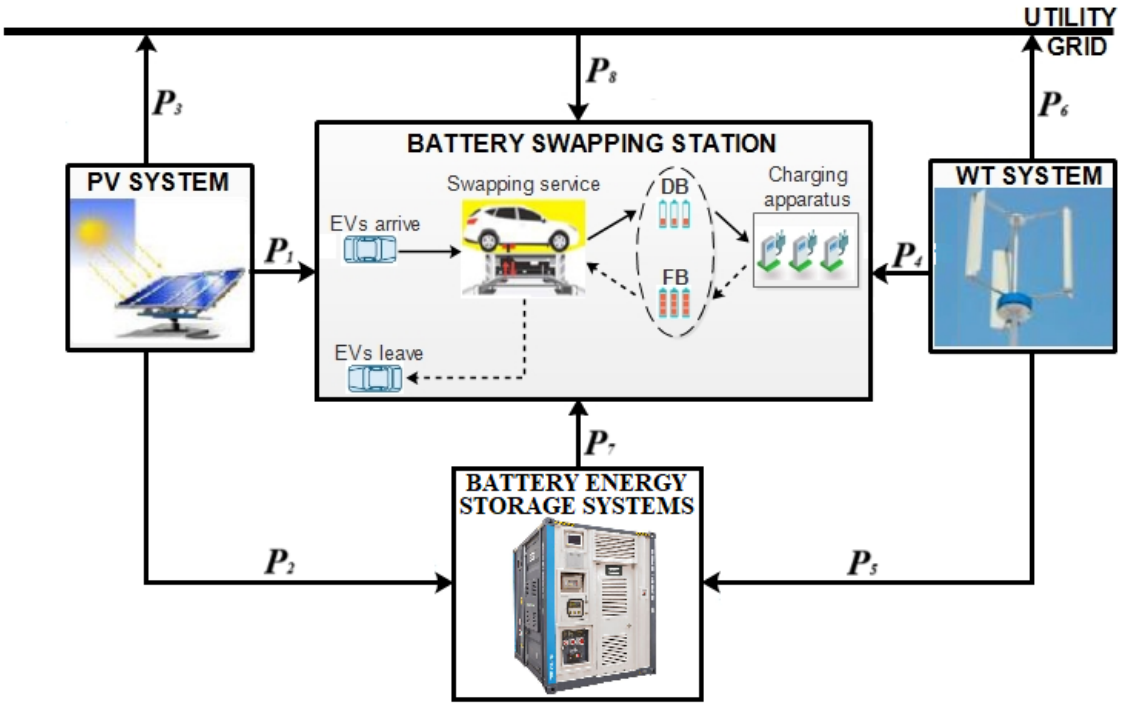


FIGURE 6.1: Schematic layout of the proposed system.

turbine. At this rated wind speed (V_r), further increases in wind speed do not affect the power output, which remains constant. When the wind speed exceeds a critical point, called the cut-out wind speed (V_{co}), the turbine is shut down to protect the rotor from damage. The relationship between wind speed and turbine power generation can be expressed mathematically as follows [82]:

$$P_{WT}(t) = \begin{cases} 0 & V(t) \leq V_{ci} \\ Pr_{WT}\frac{V(t)-V_{ci}}{V_r-V_{ci}} & V_{ci} \leq V(t) \leq V_r \\ Pr_{WT} & V_r \leq V(t) \leq V_{co} \\ 0 & V(t) \geq V_{co} \end{cases} \tag{6.1}$$

where $V(t)$ is the wind speed at a given sampling time t, V_r is the rated wind speed, V_{ci} is the cut-in wind speed, V_{co} is the cut-out wind speed, and Pr_{WT} is the rated power of the wind turbine, which is further expressed by:

$$Pr_{WT}(t) = 0.5\eta_t\eta_g\varphi_a C_p A_{WT} V_r^3 \tag{6.2}$$

where η_t and η_g are the efficiencies of the turbine's gearbox and generator, respectively, φ_a is the air density (measured in kg/m^3), C_p is the power coefficient (also known as the Betz limit), which represents the ratio of the actual power output to the theoretical maximum, A_{WT} is the swept area of the turbine rotor, and V_r is the rated wind speed. The power out generated capacity depends on its height, making it a key parameter. Wind speed at a given height can be adjusted for other heights using the following relation:

$$V = V_{ref} \left(\frac{h}{h_{ref}} \right)^{\alpha} \tag{6.3}$$

where V is the wind speed measured at a hub height (h), V_{ref} is the wind speed measured at a reference height (h_{ref}), and α represents the ground surface friction coefficient, ranging from values above 0.25 in forested areas to below 0.1 in flat or water-covered areas [83].

The WT system supplies power $P_3(t)$ to the EV BSS and $P_4(t)$ to the BESS. The power balance for the WT system is given by Equation 6.4.

$$P_3(t) + P_4(t) \leq P_{WT}(t) \tag{6.4}$$

The power output generated by the WT is constrained from zero to its maximum power, as shown in Equation 6.5.

$$0 \leq P_{WT}(t) \leq P_{WT}^{max}(t) \tag{6.5}$$

6.2.3 Solar PV system

The output power generated by the solar PV array is given by [80, 85]:

$$p_{PV} = \eta_{PV} A_{PV} I_{PV} \tag{6.6}$$

where p_{PV} is the power output generated by the solar PV array, A_{PV} is the area of the solar PV array exposed to solar irradiation, I_{PV} is the solar irradiation incident on the solar PV array, and η_{PV} is the energy conversion efficiency of the solar PV system. The energy conversion efficiency is expressed by:

$$\eta_{PV} = \eta_r \left[1 - 0.98\beta \, (\frac{I_{PV}}{I_{PV,NT}}) \, (T_{c,NT} - T_{A,NT}) - \beta \, (T_A - T_R) \right] \tag{6.7}$$

where η_r is the reference efficiency of the PV generator at a standard cell temperature T_R (typically 25°C), β is the temperature coefficient for cell efficiency (typically 0.004–0.005 per °C), $I_{PV,NT}$ is the average hourly solar irradiation incident on the array under nominal test conditions (0.8 kWh/m^2), and $T_{c,NT}$ (typically 45°C) and $T_{A,NT}$ (20°C) are the cell and ambient temperatures at nominal test conditions, respectively. The solar radiation incident on a solar PV array changes on an hourly basis and is affected by numerous factors, such as the time of day, season, tilt angle and azimuth angle of the array, the geographical latitude of the location, and the direct (beam) and diffuse components of global solar irradiation. The total hourly solar radiation incident is given by:

$$I_{PV}(t) = [I_B(t) + I_D(t)] \, R_B + I_D(t) \tag{6.8}$$

where $I_B(t)$ and $I_D(t)$ are the hourly beam and diffuse irradiation, respectively, and R_B is a geometric factor representing the ratio of beam irradiation on a tilted plane to that on a horizontal plane.

The total power output generated by a solar PV array depends on the number of PV panels installed. Considering N_{PV} as the total number of PV panels, then the total power output at any given sampling time (t) is:

$$P_{PV}(t) = N_{PV}\ p_{PV}(t) \tag{6.9}$$

The PV system supplies power $P_1(t)$ to the EV BSS and $P_2(t)$ to the BESS. The power balance for the PV system is

$$P_1(t) + P_2(t) \leq P_{PV}(t) \tag{6.10}$$

The power output generated by a solar PV array is constrained from zero to its maximum rated power, as shown in Equation 6.11.

$$0 \leq P_{PV}(t) \leq P_{PV}^{max}(t) \tag{6.11}$$

6.2.4 Battery energy storage system

The integration of a BESS within the EV BSS enhances the system's reliability and operational flexibility. The BESS acts as a buffer between the intermittent RE supply, the charging demand, and the utility grid, ensuring the uninterrupted availability of energy during periods of peak demand. This strategy reduces the dependence on the power grid while enhancing the utilization of RES. In addition, the BESS facilitates energy arbitrage by storing excess RE generated during low-demand periods and discharging it during high-demand or low-renewable generation periods. A BESS is typically characterized by its SoC, which increases when surplus power from RESs is available for charging, and it decreases when the stored energy is used to meet the charging demand of depleted EV batteries. This dynamic response ensures efficient energy utilization and helps stabilize the power supply within the system. To accurately determine the real SoC, it is essential to know the initial SoC, as well as the charging and discharging power. However, most BESSs are not ideal, as losses occur during charging, discharging, and even during idle storage periods. Considering these factors, the SoC of the BESS at time $(t+1)$ can be generally expressed as follows [118]:

$$SoC(t+1) = SoC(t) \times (1 - d_b) + \left\{ \frac{\eta_C}{E_{Nom}} \left[P_{chg}(t)\right] - \frac{1}{\eta_D \times E_{Nom}} \left[P_{dis}(t)\right] \right\} \Delta t \tag{6.12}$$

where $SoC(t)$ is the state of charge of the BESS at any sampling time t, d_b is the self-discharged rate of the BESS, η_C is the BESS charge efficiency, E_{Nom} is the BESS nominal energy, η_D is the BESS discharge efficiency, P_{chg} and P_{dis} are the charging and discharging power at time t respectively, Δt is the sampling

time. By applying inductive reasoning from equation (6.12), the dynamics of the BESS SoC at t^{th} sampling interval can be expressed in terms of its initial value $SoC(0)$ using the following equation [118]:

$$SoC(t) = SoC(0) \times (1 - d_b) + \left\{ \frac{\eta_C}{E_{Nom}} \sum_{\tau=0}^{t-1} [P_{chg}(\tau)] - \frac{1}{\eta_D \times E_{Nom}} \sum_{\tau=0}^{t-1} [P_{dis}(\tau)] \right\} \Delta t \tag{6.13}$$

where $SoC(0)$ is the initial SoC of the BESS. The following Equations (6.14) and (6.15) describe the charging and discharging power flow of the BESS, respectively.

$$P_2(t) + P_5(t) = P_{chg}(t) \tag{6.14}$$

$$P_7(t) = P_{dis}(t) \tag{6.15}$$

where $P_2(t)$ is the power flow from the PV system to the BESS, $P_4(t)$ is the power flow from the WT system to the BESS, $P_5(t)$ is the power flow from the BESS to the EV BSS, and $P_6(t)$ is the power flow from the BESS to the utility grid. In addition, at any given sampling interval, the BESS must adhere to specific constraints to ensure safe and reliable operation. These constraints stipulate that the BESS capacity must not fall below the minimum allowable capacity nor exceed the maximum permissible capacity, as defined in Equations (6.16), (6.17), and (6.18), respectively.

$$SoC^{min} \leq SoC(t) \leq SoC^{max} \tag{6.16}$$

$$0 \leq P_{chg}(t) \leq P_{chg}^{max}(t) \tag{6.17}$$

$$0 \leq P_{dis}(t) \leq P_{dis}^{max}(t) \tag{6.18}$$

where SoC^{min} and SoC^{max} are the minimum and maximum allowable states of charge, respectively, $P_{chg}^{max}(t)$ is the maximum allowable charging power to the BESS, and $P_{dis}^{max}(t)$ is the maximum allowable discharging power from the BESS. The SoC^{min} is related to the BESS depth of discharge (DoD) given by:

$$SoC^{min} = (1 - DoD)\ SoC^{max} \tag{6.19}$$

where DoD denotes the depth of discharge given in percentage.

6.2.5 Utility Grid

The power flow from the utility grid is modelled as an all-time available power source supplying the charging demands at the EV-BSS. The grid system in this setup not only supplies power for charging depleted EV batteries but also facilitates the selling of excess electricity back to the utility grid, providing an additional revenue stream. This bidirectional flow of energy allows for better integration of RES. The energy drawn from the utility grid ($E_g(t)$) is calculated based on the power demand of the depleted EV battery charging at any time t as follows:

$$E_g = \sum_{t=1}^{N} P_8(t)\ \Delta t \tag{6.20}$$

where P_8 is the power flow from the utility grid to supply the depleted EV batteries at the BSS, and Δt is the sampling time. Therefore, the energy cost that can be extracted from the utility grid is determined by the local electricity market policy and time of use (TOU) tariff. The cost of energy (C_{Eg}) that can be drawn from the utility grid when charging the depleted EV batteries can be calculated from

$$C_{Eg} = p_e(t) \sum_{t=1}^{N} P_8(t)\ \Delta t \tag{6.21}$$

where $P_e(t)$ is the TOU electricity price at the t-th sampling interval per kWh.

On the other hand, the energy sold back to the utility grid ($E_{g_{in}}(t)$) is expressed as follows:

$$E_{g_{in}} = [P_3(t) + P_6](t)\ \Delta t \tag{6.22}$$

where P_3 is the power flow from the PV generation to the utility grid at time t, P_6 is the power flow from the WT to the utility grid at time t. The revenue generated from selling electricity back to the utility grid (R) is as follows:

$$R = p_{r1}(t) \sum_{t=1}^{N} P_3(t)\ \Delta t + p_{r2}(t) \sum_{t=1}^{N} P_6(t)\ \Delta t \tag{6.23}$$

where $p_{r1}(t)$ is the feed-in tariff for the solar PV at time t, $p_{r2}(t)$ is the feed-in tariff for the WT at time t. This model helps optimize energy exchange with the utility grid, balancing costs and revenue to enhance the overall economic performance of the hybrid renewable power system. In addition, the power from the utility grid can be constrained to a limited range given by:

$$0 \leq P_8\,(t) \leq +\infty \tag{6.24}$$

6.2.6 Battery swapping station power demand

A BSS is a facility designed to allow EV drivers to quickly exchange depleted EV batteries for fully charged ones, addressing the challenges of traditional plug-in charging methods [91, 92]. A standard BSS

features multiple battery swapping units, allowing the simultaneous exchange of EV batteries for several EVs. The power demand is influenced by the charging and swapping processes and the characteristics of EV batteries, such as capacity, technology and initial SoC [93]. Accurate modelling of power demand is crucial, especially during the charging of depleted EV batteries, to meet the swapping demand when EVs arrive. The total charging and discharging power of depleted EV batteries at the BSS are represented by Equations (6.25) and (6.26), respectively:

$$P_{c,BSS}(t) = \sum_{EV,b=1}^{n} P_{c,(EV,b)}(t) \tag{6.25}$$

$$P_{d,BSS}(t) = \sum_{EV,b=1}^{n} P_{d,(EV,b)}(t) \tag{6.26}$$

where n is the total number of the depleted EV batteries, $P_{c,BSS}(t)$ is the total charging power of the depleted EV batteries, $P_{d,BSS}(t)$ is the total discharging power of the depleted EV batteries, $P_{c,(EV,b)}(t)$ is the charging power of one depleted EV battery, $P_{d,(EV,b)}(t)$ is the discharging power of one depleted EV battery. Each depleted EV battery undergoes charging and discharging processes akin to a conventional battery. The charging of these depleted EV batteries is determined by their SoC during specific time intervals, which quantifies the available capacity relative to the maximum capacity when fully charged. Taking into account these factors, the SoC of the EV battery at the t^{th} sampling interval can be generally expressed as [75, 94]:

$$SoC_{EV,b}(t) = SoC_{EV,b}(t-1) + \left(P_{c,(EV,b)}(t) - \frac{P_{d,(EV,b)}(t)}{\eta_{EV,b}} \right) \times I_{dur}(t) \tag{6.27}$$

where $I_{dur}(t)$ is the duration of time interval, $\eta_{EV,b}$ is the EV battery efficiency (%), calculated as:

$$\eta_{EV,b} = \frac{\sum_{t=1}^{N} P_{d,(EV,b)}(t) \times I_{dur}(t)}{\sum_{t=1}^{N} P_{c,(EV,b)}(t) \times I_{dur}(t)} \tag{6.28}$$

During the battery swapping process, the power and SoC of the EV battery are set to zero, as described by Equation (6.29).

$$\begin{cases} P_{c,(EV,b)}(t) = 0 \\ P_{d,(EV,b)}(t) = 0 \\ SoC_{EV,b}(t) = 0 \end{cases} \qquad \forall t = t_{swap} \tag{6.29}$$

Prior to the battery swapping, the depleted EV battery must be fully charged to prepare for the next swap. Consequently, the energy management system must ensure that an adequate number of fully charged EV batteries are available at each time interval to meet the demand for upcoming swaps. This requirement is formalized in Equation (6.30).

$$SoC_{EV,b}(t) = SoC_{EV,b}(t-1) \qquad \forall t = (t_{swap} - 1) \tag{6.30}$$

The total power demand at the BSS, which is based on the power capacity of the charging station, is determined by summing the discretized charging power requirements for each depleted EV battery. Consequently, the total expected power demand for all n depleted EV batteries charged at the BSS at time t can be estimated using Equation (6.31).

$$P_{Ld,BSS}(t) = \sum_{EV,b=1}^{n} \left(P_{c,(EV,b)}(t) - P_{d,(EV,b)}(t)\right) \tag{6.31}$$

where $P_{Ld,BSS}(t)$ is the total expected power demand of all depleted EV batteries charged at time (t).

6.2.7 Open loop optimal control model

The optimization framework aims to regulate power flow effectively, ensuring system efficiency while leveraging economic benefits. The grid power P_8 is modelled as a controllable variable power source with minimum and maximum output power. The output power from the WT and solar PV systems are also modelled as controllable variable power sources, with their output varying between zero and their maximum available capacity within the 24-hour control horizon. Additionally, the BESS is modelled as an energy storage unit with specified minimum and maximum capacity limits, allowing efficient energy management. To solve the optimization problem, the OPTI Toolbox SCIP algorithm in MATLAB is utilized. This approach ensures an effective balance between energy generation, storage, and grid interaction, thereby enhancing the overall performance and profitability of the hybrid renewable energy system. The multi-objective optimization function governing this model is mathematically expressed as follows:

$$\min J = \left(\xi_1 \sum_{t=1}^{N} p_e(t) P_8(t) + \xi_2 \sum_{t=1}^{N} [\phi(P_7(t) + 24a] - \xi_3 \sum_{t=1}^{N} [p_{r1}(t) P_3(t) - \xi_4 \sum_{t=1}^{N} p_{r2}(t) P_6(t)]\right) \Delta t \tag{6.32}$$

where $\xi_1, \xi_2, \xi_3, \xi_4$ are weighting factors, respectively, adjusted according to the BSS's preferred outcomes with $\xi_1 + \xi_2 + \xi_3 + \xi_4 = 1$, $p_e(t)$ is the electricity price under the TOU tariff, $p_{r1}(t)$ is the feed-in tariff for the solar PV, $p_{r2}(t)$ is the feed-in tariff for the WT, P_7 is the power flow from the utility grid to the EV BSS, P_5 is the power flow from the BESS to the EV BSS, P_6 is the power flows from the BESS to the utility grid, Δt is the sampling time, N is the sampling period number, ϕ is the wearing cost coefficient of the hybrid system, and a is the hourly wearing cost of other components. The TOU electricity tariff and the feed-in tariff are key parameters in the optimization process. In this multi-objective function represented by 6.32, the first term aims to minimize the cost of power drawn from the utility grid, the second term minimizes the wear cost of the hybrid system influenced by the frequent charging and discharging cycles of the BESS, which directly affects its operational lifespan, the third term maximizes the cost of power sale to the utility grid from the solar PV system, and lastly, the fourth term maximizes the cost of power sale to the utility grid from the WT. To achieve this, the multi-objective function is subject to the following

technical and operational constraints:

$$P_1(t) + P_4(t) + P_7(t) + P_8(t) = P_{Ld,BSS}(t) \tag{6.33}$$

$$0 \leq P_4(t) + P_5(t) + P_6(t) \leq P_{WT}(t) \tag{6.34}$$

$$0 \leq P_1(t) + P_2(t) + P_3(t) \leq P_{PV}(t) \tag{6.35}$$

$$SoC^{min}(t) \leq SoC(t) \leq SoC^{max}(t) \tag{6.36}$$

$$0 \leq P_i(t) \leq P_i^{max}(t), \tag{6.37}$$

where i = 1,2,3,..,7 is the index of power flows, $P_i^{max}(t)$ is the maximum limits for each decision variable $P_i(t)$ at the sampling time t.

6.2.8 MPC optimization problem

The optimal control strategy described above follows an open-loop approach, operating without feedback from system states. However, the absence of feedback may make the system susceptible to disturbances in charging demand, wind power, and solar PV generation. To address this limitation, this subsection introduces a closed-loop linear MPC framework. The proposed MPC ensures that charging demand is met at each sampling interval while minimizing operational costs. Additionally, it enhances the system's robustness against fluctuations and disturbances in charging demand and RES power output.

6.2.8.1 Discrete linear MPC model

MPC is a closed-loop control strategy designed to predict system outputs and optimize control actions accordingly. The fundamental principle of MPC is based on an open-loop optimization process that is solved iteratively within the control horizon at each sampling interval. At each step, the system state is re-evaluated, and the optimization process is updated based on newly acquired data. This iterative approach allows for continuous assessment and adjustment of the control strategy, ensuring that unforeseen variations, such as energy flow to the grid or energy discharge from the storage system to the charging demand, are effectively managed. This process is repeated at every sampling interval to enhance system performance and robustness [119]. The discrete linear MPC model for a given system is defined as:

$$x(k+1) = Ax(k) + Bu(k) \tag{6.38}$$

$$y(k) = Cx(k) \tag{6.39}$$

Where A is the system matrix with dimensions $n \times n$, B is the control matrix with dimensions $m \times n$, C is the output matrix with dimensions $n \times p$, $x(k)$ is a state matrix, $u(k)$ is the input matrix, and $y(k)$ is the output matrix. The objective function of the MPC, which aims to minimize the cost function, is given by the following equation:

$$J = \sum_{i=1}^{N_p} \left(y(k+i-1 \mid k) - r(k+i-1)\right)^2 = (Y-R)^T(Y-R) \tag{6.40}$$

subject to the following constraint:

$$Mu(k) \leq \gamma \tag{6.41}$$

where $Y(k) = [y^T(k), y^T(k+1|k), \ldots, y^T(k+N_p-1|k)]^T$, and $y(k+i|k)$ represents the predicted value of y at step i $(i = 1, \ldots, N_p)$ from the sampling time k, $R(k) = [r(k), r(k+1), r(k+2), \ldots, r(k+N_p-1)]$ represents the predicted reference value for Y, M and γ are matrices and vector with proper dimensions, respectively, and N_p represents the predicted horizon. In this chapter, the control horizon is chosen to be equal to the predicted horizon. The predicted states are as follows:

$$\begin{aligned}
x(k+1|k) &= Ax(k) + Bu(k), \quad y(k) = Cx(k), \\
x(k+2|k) &= Ax(k+1|k) + Bu(k+1|k) \\
&= A^2x(k) + ABu(k) + Bu(k+1|k), \\
&\vdots \\
x(k+N_p-1|k) &= \cdots = A^{N_p-1}x(k) + \sum_{i=1}^{N_p-1} A^{N_p-1-i}Bu(k+i-1|k),
\end{aligned}$$

and the predicted outputs are:

$$Y(k) = [C, C, \ldots, C]X(k) = Fx(k) + \Phi U \tag{6.42}$$

where $X(k) = [x^T(k), x^T(k+1|k), \ldots, x^T(k+N_p-1|k)]^T$, $U(k) = [u^T(k), u^T(k+1|k), \ldots, u^T(k+N_p-1|k)]^T$, and

$$F = \begin{bmatrix} CA \\ CA^2 \\ \vdots \\ CA^{N_p} \end{bmatrix}, \quad \Phi = \begin{bmatrix} CB & 0 & \cdots & 0 \\ CAB & CB & \cdots & 0 \\ \vdots & \vdots & \ddots & \vdots \\ CA^{N_p-1}B & CA^{N_p-2}B & \cdots & CA^{N_p-N_c}B \end{bmatrix}. \tag{6.43}$$

The predicted output, given by equation 6.42, can be substituted into equation 6.40. Therefore, it follows that minimizing 6.40 is equivalent to minimizing $\hat{J} = U^TEU + FU$, where

$$E = \Phi^T \Phi, \quad H = (Fx(k) - R(k))^T \Phi. \tag{6.44}$$

Numerical tools are required to solve the optimization problem presented below, taking into account the constraint specified in equation 6.41, as follows:

$$U = \arg\min_U U^T EU + FU, \quad \text{s.t.} \quad MU \leq \gamma \tag{6.45}$$

The receding control horizon forms the foundation of the MPC implementation. This is described as follows:

$$u(k) = [I, 0, \ldots, 0]U \tag{6.46}$$

where I represents the identity matrix with the appropriate dimensions.

The fundamental principle of MPC involves calculating the control sequence $U(k)$ at each time step k using an optimal control strategy. However, only the first element of $U(k)$, corresponding to the dimension of $u(k)$, is applied. Feedback is integrated into the system by optimizing a cost function. At the subsequent time step $k+1$, the closed-loop system's performance is evaluated, and the control sequence is recalculated and re-implemented using updated information. This approach allows the system to address unforeseen disturbances effectively.

6.2.8.2 Objective function

The primary objective of the MPC system is to reduce reliance on the utility grid by minimizing the cost of energy purchased from the utility grid and to promote the utilization of RESs by maximizing the sale of energy to the utility grid. To achieve these objectives, the cost function can be structured as a combination of two components:

1. **Minimization of grid usage**: The first component aims to minimize the cost of power output drawn from the utility grid, thereby reducing operational costs. This is expressed as:

$$\min J_1 = \min \sum_{t=k}^{k+N_p} p_e(t) P_8(t \mid k) = \min \sum_{t=k}^{k+N_p} (P_{Ld,BSS}(t \mid k) - y_m(k))^2 \tag{6.47}$$

   where $P_L Ld, BSS(t \mid k)$ represents the charging power demand and $y_m(k)$ denotes the power supplied by the utility grid.

2. **Promotion of RE usage**: The second component focuses on maximizing the use of RESs, such as solar PV and wind power. This is formulated as:

$$\max J_2 = \max \sum_{t=k}^{k+N_p} (p_{r1}(t) P_{PV}(t \mid k) + p_{r2}(t) P_{WT}(t \mid k) - y_a(k))^2 \tag{6.48}$$

where $P_{PV}(t \mid k)$ and $P_{WT}(t \mid k)$ are the total power outputs from solar PV and wind sources, respectively, and $y_a(k)$ is the actual power utilized from RESs.

Define the reference value $R(k) = [P_{Ld,BSS}(t|k), P_{PV}(t|k) + P_{WT}(t|k), P_{Ld,BSS}(t|k+1), P_{PV}(t|k+1) + P_{WT}(t|k+1), \ldots, P_{Ld,BSS}(t|k+N_p-1), P_{PV}(t|k+N_p-1) + P_{WT}(t|k+N_p-1)]^T$. The overall objective function is then given by

$$\min J = \min(J_1 - J_2) = \min(Y(k) - R(k))^T (Y(k) - R(k)). \tag{6.49}$$

By integrating these components, the MPC system effectively balances the need for reliable power supply with the objective of enhancing sustainability through increased RE adoption. The objective function is subject to the following technical and operational constraints:

$$P_1(t) + P_4(t) + P_7(t|k) + P_8(t|k) = P_{Ld,BSS}(t|k) - y_m(k) \tag{6.50}$$

$$0 \leq P_4(t) + P_5(t) + P_6(t|k) \leq P_{WT}(t) \tag{6.51}$$

$$0 \leq P_1(t) + P_2(t) + P_3(t|k) \leq P_{PV}(t) \tag{6.52}$$

$$SoC^{min}(t) \leq SoC(t) \leq SoC^{max}(t) \tag{6.53}$$

$$0 \leq P_i(t) \leq P_i^{max}(t), \tag{6.54}$$

where i = 1,2,3,..,7 is the index of power flows, $P_i^{max}(t)$ is the maximum limits for each decision variable $P_i(t)$ at the sampling time t.

6.2.9 MPC algorithm

The following steps outline the development of the model using MPC gains:

1. Define the state-space representation and establish the initial conditions for the solar PV system, wind power, BESS, and utility grid.
2. Compute the MPC gains to determine matrices E and H, as given by equation 6.44.
3. Solve the optimization problem by applying the objective function and its constraints, which are defined in equations 6.40 and 6.41, respectively.

4. Determine and implement the receding horizontal control, as described by equation 6.46.
5. Update the system information by incrementing k ($k = k + 1$) and applying the control input $u(k)$.
6. Repeat steps 1–5 until k reaches the predicted value.

6.3 Case study

The case study focuses on a heavy-duty truck battery swapping station (BSS) located at a central logistics hub in Shanghai Port, China. It examines the station's energy demand patterns and evaluates the effectiveness of the proposed energy management strategy under various operational scenarios.

6.3.1 EV BSS power demand load profile

The load profile of the EV BSS was developed using historical data from a heavy-duty truck-swapping facility located at a central logistics hub in Shanghai Port, China. Figures 6.2 depict a typical weekday's daily energy consumption patterns, respectively. The results highlight peak demand periods that align with increased traffic volumes and the station's operational hours, providing valuable insights for optimizing energy management strategies.

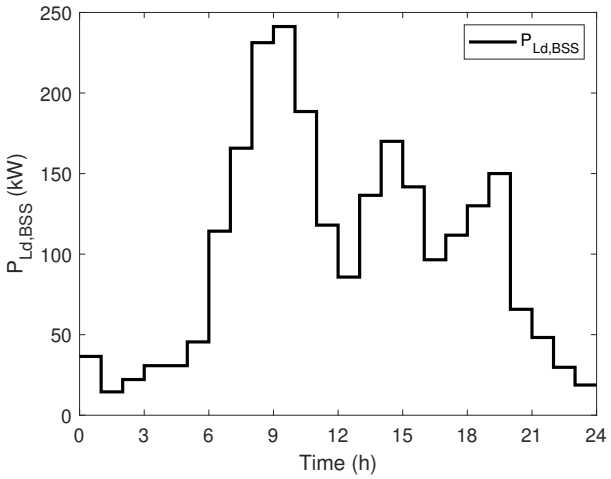


FIGURE 6.2: Charging patterns of the electric vehicle battery swapping station on a weekday.

6.3.2 Renewable energy power supply

The proposed hybrid renewable power generation system incorporates WT and solar PV panels as primary energy sources, supplemented by the power from the utility grid with a storage system to ensure a reliable supply. The input parameters for WT system power generation, such as the wind speed, and for solar PV power generation, such as the solar radiation and ambient temperature, are obtained from a typical day in

Cape Town, South Africa, as referenced in [112]. Figure 6.3 presents the hourly average wind speed at 10 m above the ground in high demand season, while Figure 6.4 presents the hourly average wind speed at 10 m above the ground. For more information, the average hourly wind speed over the year is presented in Figure 6.7. Additionally, the daily average for PV generation is depicted in Figure 6.5, indicating that the peak incident short-wave radiation for solar PV power generation reaching the ground's surface over a wide area is approximately 0.67 kW/m^2 around noon in high demand season, while Figure 6.6 indicating that the peak incident short-wave radiation for solar PV power generation reaching the ground's surface over a wide area is approximately 0.79 kW/m^2 between 1PM and 2PM in low demand season. For more information, The annual short-wave radiation for solar PV power generation reaching the surface of the ground over a wide area is presented in Figure 6.8, which gives significant seasonal variation with the peak brighter and lowest darker period of the year around December and June, respectively.

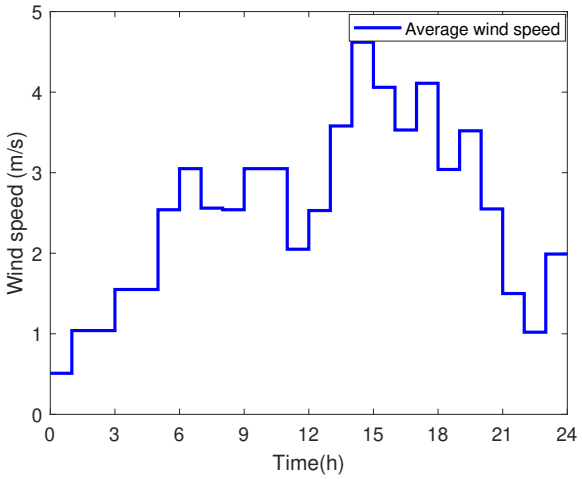


FIGURE 6.3: Average hourly wind speed HD.

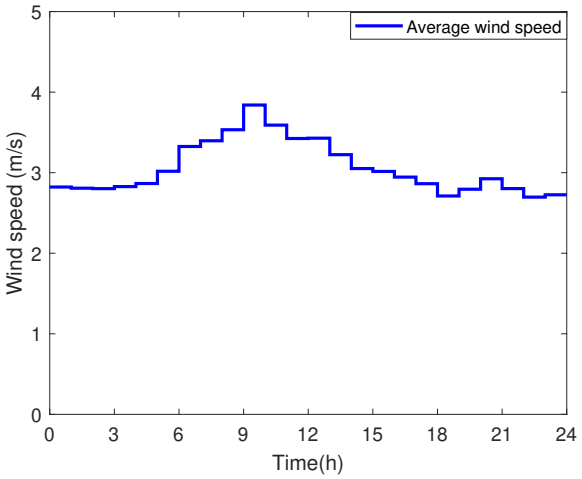


FIGURE 6.4: Average hourly wind speed LD.

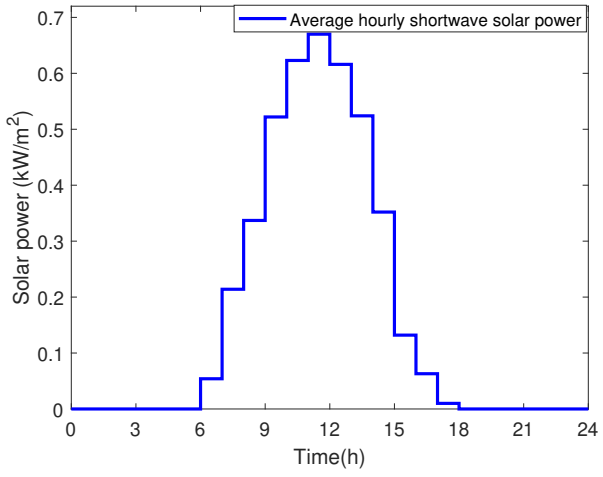


FIGURE 6.5: Daily average shortwave solar power HD.

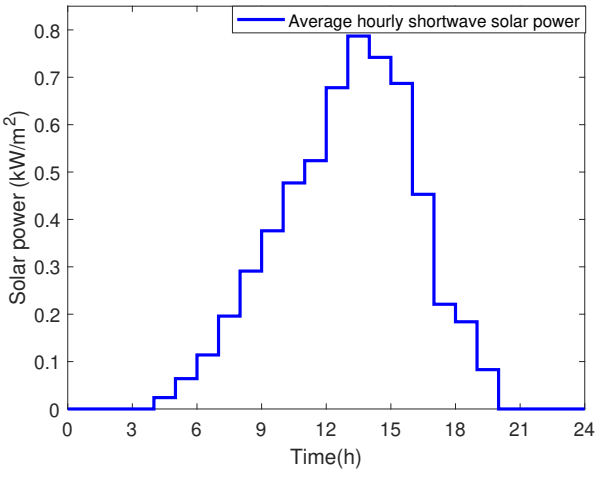


FIGURE 6.6: Daily average shortwave solar power LD.

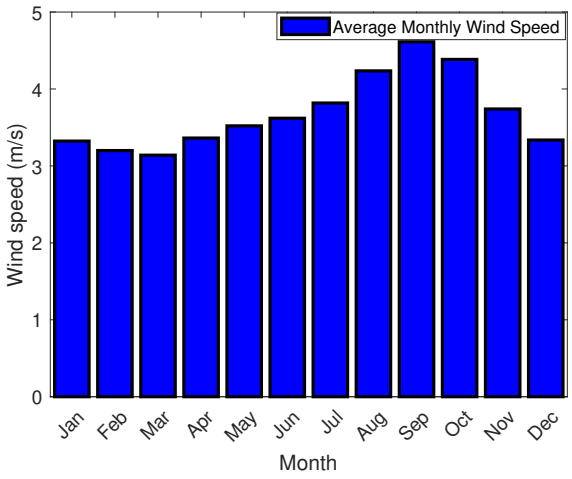


FIGURE 6.7: Monthly average wind speed.

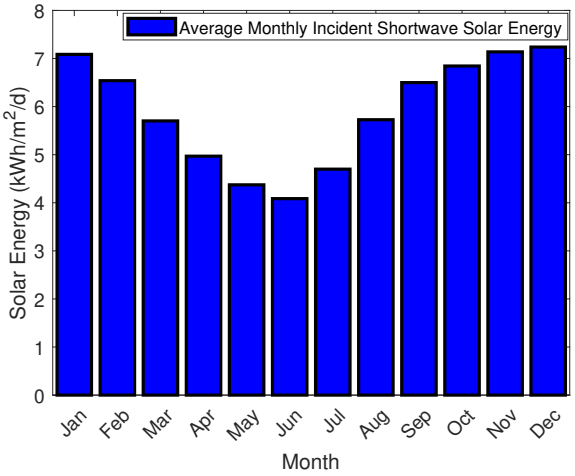


FIGURE 6.8: Monthly average shortwave PV power

6.3.3 Time-of-use electricity tariff

The South African power grid is managed by the national utility, "Eskom", with electricity tariffs regulated by the National Energy Regulator of South Africa (Nersa). Eskom's tariff structure typically includes both flat and dynamic TOU pricing systems. TOU pricing is a demand-side management strategy that reflects the varying costs of electricity production throughout the day and is divided into three periods: off-peak ($p_{e\ off}$), standard-peak ($p_{e\ std}$), and on-peak ($p_{e\ pk}$). These periods correspond to times when electricity demand and generation costs are low, moderate, and high, respectively, implementing in a seasonal price variation. In the seasonal pricing, the winter months of June to August are classified as high demand season and electricity prices per unit are higher, while the remaining months of the year, September to May are classified as low demand season with lower electricity prices. In the context of our optimization problem, the TOU electricity tariff significantly influences the energy efficiency of the EV BSS. The 2023/2024 Eskom Megaflex TOU tariff scheme, which applies to industrial consumers who both consume energy from the utility grid and generate energy at the same point of supply is considered for the case study for the high and low-demand season weekday and weekend is used as the basis for the TOU electricity tariff analysis given by (6.55) to (5.44), respectively [1]:

High demand season for weekdays and weekends:

$$p_{e(t)} = \begin{cases} p_{e\ off} = 1.0370\ ZAR/kWh\ ;\ \text{if}\ t \in [00:00, 06:00) \cup [22:00, 24:00)\ , \\ p_{e\ std} = 1.8991\ ZAR/kWh\ ;\ \text{if}\ t \in [09:00, 17:00) \cup [19:00, 22:00)\ , \\ p_{e\ pk} = 6.2421\ ZAR/kWh\ ;\ \text{if}\ t \in [06:00, 09:00) \cup [17:00, 19:00)\ . \end{cases} \tag{6.55}$$

Low demand season for weekdays and weekends:

[1] https://www.eskom.co.za/distribution/wp-content/uploads/2023/03/Schedule-of-standard-prices-2023_24-140323.pdf

$$p_{e(t)} = \begin{cases} p_{e\ off} = 0.8992\ ZAR/kWh\ ;\ \text{if}\ t \in [00:00, 06:00) \cup [22:00, 24:00)\ , \\ p_{e\ std} = 1.4104\ ZAR/kWh\ ;\ \text{if}\ t \in [06:00, 07:00) \cup [10:00, 18:00) \cup [20:00, 22:00)\ , \\ p_{e\ pk} = 2.0440\ ZAR/kWh\ ;\ \text{if}\ t \in [07:00, 10:00) \cup [18:00, 20:00)\ . \end{cases} \tag{6.56}$$

where ZAR is the South African currency (Rand), t represents the time of day in hours, and $p_{e(t)}$ represents the daily electricity price. One can notice that in both high and low demand seasons on the weekend (5.42) and (5.44), respectively, the TOU electricity pricing has only two periods, which are off-peak and standard-peak periods. There is no on-peak period. The utility grid can accommodate excess power generated by the wind and solar PV systems while supplementing renewable resources to meet the charging demand of the EV BSS. The feed-in tariff for distributed renewable energy sources (DREs) is regulated by the National Energy Regulator of South Africa (NERSA) [2], which oversees the establishment of feed-in tariffs for RE in the country. The current feed-in tariff is 1.12 ZAR/kWh for solar PV power generation and 1.0398 ZAR/kWh for WT power generation. The power is supplied to the utility grid to maximize sales when charging demand within the control horizon, which has been met at different times of the day. This strategy benefits the utility grid by enabling optimal network operation and reducing system losses.

6.4 Simulation results and discussion

This section presents and analyzes the simulation results obtained from the optimization model, focusing on the system's performance and efficiency. The impact of key input parameters, including the power capacity of WTs, solar PV panels, the utility grid, and TOU electricity tariffs, is examined to provide insights into optimal operational strategies for the grid-connected wind-solar hybrid power system with BESS supplying the EV BSS. The optimization problem is solved using the SCIP solver in MATLAB's OPTI Toolbox over a 24-hour horizon, with a sampling interval of $\Delta t = 1$h, starting at midnight. The initial values of $P_i(k)$ $(i = 1, 2, 3, ...8)$ are set to zeros. The initial values of the SoC are set to $x_m(1) = 0.6SoC^{max}$. Furthermore, two operational scenarios are considered: high-demand and low-demand seasons for every control approach.

6.4.1 Open-loop control simulation results

The open-loop control strategy governs the power distribution within the grid-connected wind-solar hybrid system with BESS, ensuring continuous operation of the EV BSS. Figure 6.9 illustrates the power flow dynamics, highlighting the contributions of solar PV, WT, BESS, and the utility grid during high demand season, while Figure 6.10 illustrates the BESS dynamic Soc. During off-peak hours (00:00–06:00 and 22:00–00:00), charging demand primarily relies on the grid due to low electricity prices and minimal renewable generation. As solar radiation increases after sunrise, PV power reduces grid dependence,

[2] https://www.nersa.org.za/

while wind power remains variable throughout the day. The BESS is utilized to store excess energy and support peak demand periods (06:00–09:00 and 17:00–19:00). During standard periods (09:00–17:00 and 19:00–22:00), the hybrid system alone meets the charging demand, minimizing grid reliance and enabling BESS charging.

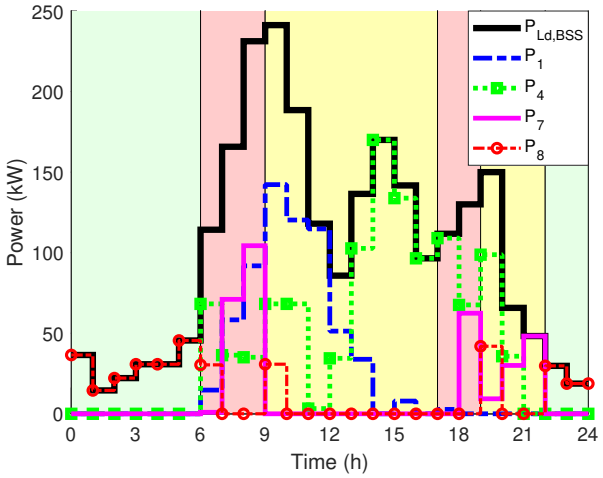


FIGURE 6.9: Simulation result of open loop control.

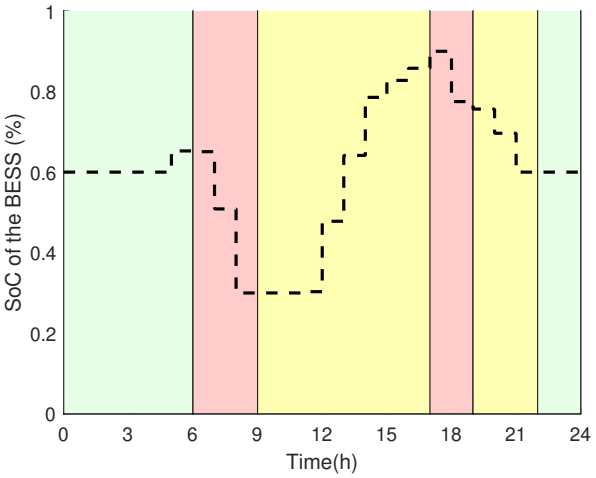


FIGURE 6.10: Simulation result of BESS dynamic SoC.

Figure 6.11 illustrates the power flow contributions from solar PV, wind turbines, BESS, and the utility grid. During off-peak hours (00:00–06:00 and 22:00–00:00), the system relies primarily on grid power due to low electricity prices and minimal renewable generation. As solar radiation increases after sunrise, PV power significantly reduces grid dependence, while wind power remains variable throughout the day. The BESS stores surplus energy and discharges it during peak periods (07:00–10:00 and 18:00–20:00) to balance supply and demand. During standard periods (06:00–07:00, 10:00–18:00, and 20:00–22:00), the hybrid system primarily meets charging needs, with the grid serving as backup, especially in the morning and evening. Figure 6.12 shows the BESS state of charge (SoC), which rises in the early morning due to wind generation and later between 11:00 and 14:00 due to high solar radiation, enabling energy storage. The SoC decreases during peak hours as stored energy is used to reduce grid dependence. Throughout the simulation, the SoC boundary and final-state constraints are maintained, ensuring optimal storage operation without overcharging or excessive discharge.

6.4.2 Model predictive control simulation results in high demand season

The simulation for the case study is conducted for a selected weekday during a high-demand season, implementing closed-loop control without disturbances in the proposed grid-connected wind-solar hybrid power supply with a storage system. Figures 6.13 and 6.14 present the simulation results of the closed-loop control strategy and the dynamic state of charge (SoC) of the BESS under these conditions. As shown in Figure 6.13, the closed-loop system effectively schedules power flows to meet the charging demand of depleted EV batteries. With the influence of MPC, the hybrid system prioritizes the use of PV (P_1) and

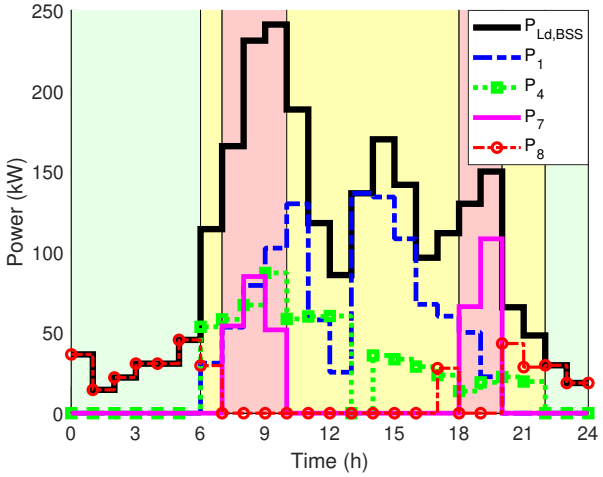


FIGURE 6.11: Simulation result of open loop system.

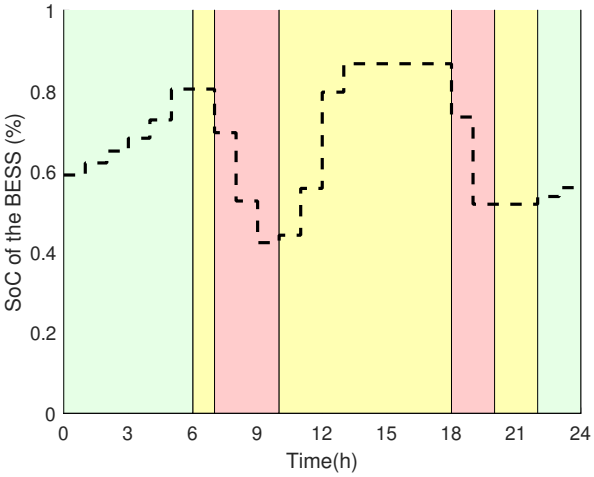


FIGURE 6.12: Simulation result of BESS dynamic SoC

WT (P_4) power when sufficient RE is available. Any surplus energy from PV and WT is either fed back to the utility grid or stored in the BESS. When RE is insufficient, the system prioritizes BESS discharge to meet charging demand, particularly during peak periods. The utility grid power flow (P_8) is used as a last resort during peak and standard periods, while during off-peak hours, grid power is utilized due to the lack of renewable generation. Figure 6.14 further illustrates the charging and discharging behavior of the BESS, highlighting its role in stabilizing power supply during standard and peak periods.

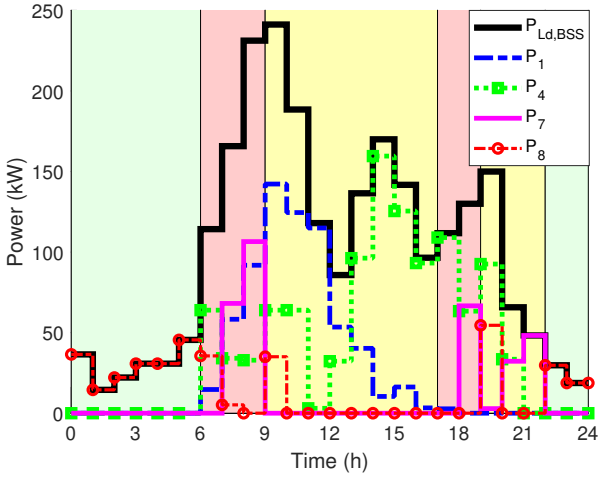


FIGURE 6.13: Simulation result of close loop system without disturbances.

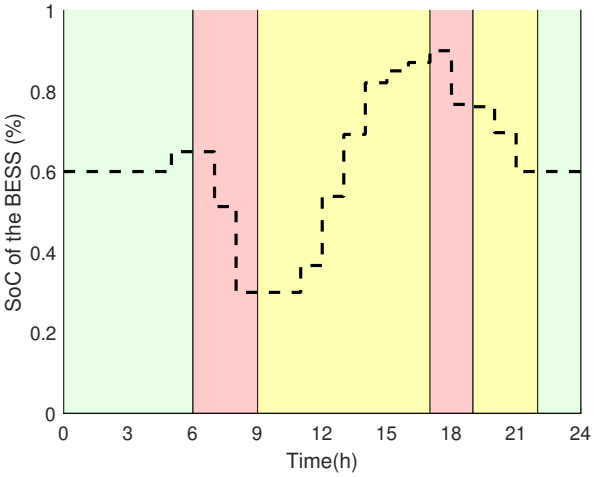


FIGURE 6.14: Simulation result of BESS Dynamic SoC without disturbances.

Figure 6.15 and Figure 6.16 present the simulation results of the closed-loop control and the dynamic SoC of the BESS under disturbances during a high-demand period. The charging demand and RE generation considered in the case study are based on prior expectations, but real-world conditions introduce uncertainties due to weather variations, disasters, and migration. In this scenario, the proposed grid-connected wind-solar hybrid system with energy storage encounters a particularly adverse condition where the actual

charging demand is 30% higher than expected, while the energy supplied by RE generation and the power grid is 30% lower than anticipated. As shown in Figure 6.15, the closed-loop system with disturbances demonstrates superior performance, highlighting its robustness compared to the open-loop system. This improvement is attributed to the predictive capability of MPC, which adjusts control actions based on real-time feedback and anticipated future states, even under disturbances. In contrast, open-loop control lacks adaptability to unexpected changes, relying solely on activating grid power when the charging demand exceeds expectations.

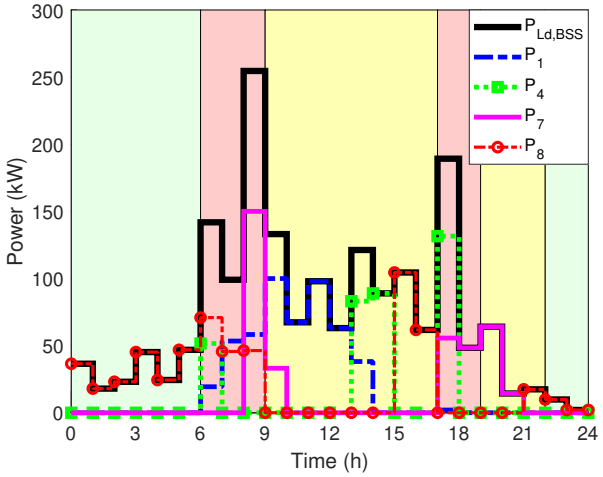


FIGURE 6.15: Simulation result of close loop system with disturbances.

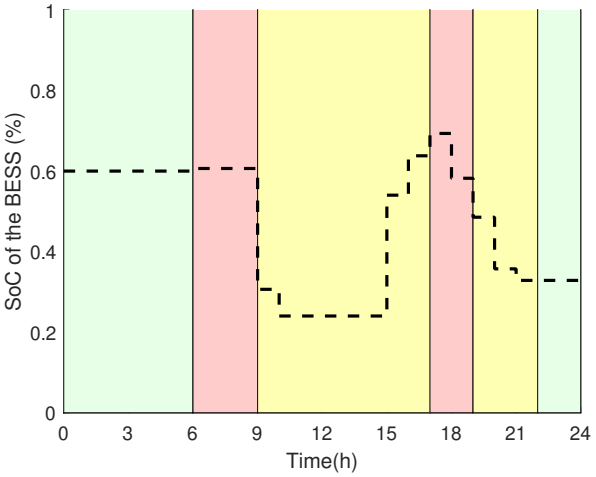


FIGURE 6.16: Simulation result of BESS Dynamic SoC with disturbances.

6.4.3 Model predictive control simulation results in low demand season

Figures 6.17 and 6.18 illustrate the simulation results of the MPC-based closed-loop control strategy and the dynamic SoC of the BESS during a low-demand season without any disturbances. As shown in Figure 6.17, the MPC effectively optimizes power flow to meet the charging demand of depleted EV batteries. The system prioritizes RES, utilizing PV (P_1) and WT (P_4) when sufficient generation is available. Any surplus energy is either stored in the BESS or exported to the utility grid. During periods of low RE generation, the BESS discharges to support charging demand, particularly during peak periods, while the utility grid serves as a last resort during standard and off-peak periods and is primarily used during off-peak periods when renewable generation is minimal. Figure 6.18 presents the SoC profile of the BESS over 24 hours. The SoC increases during high PV and WT generation, particularly around midday, allowing surplus energy to be stored. Conversely, it decreases during peak periods as stored energy is discharged to support charging demand, effectively minimizing reliance on the utility grid. The results confirm the effectiveness of the MPC strategy in ensuring optimal energy management, stabilizing power supply, and enhancing system efficiency without disturbances.

Figure 6.19 and Figure 6.20 present the simulation results of the closed-loop control and the dynamic SoC of the BESS under disturbances during a low-demand period. The load demand and RE generation considered

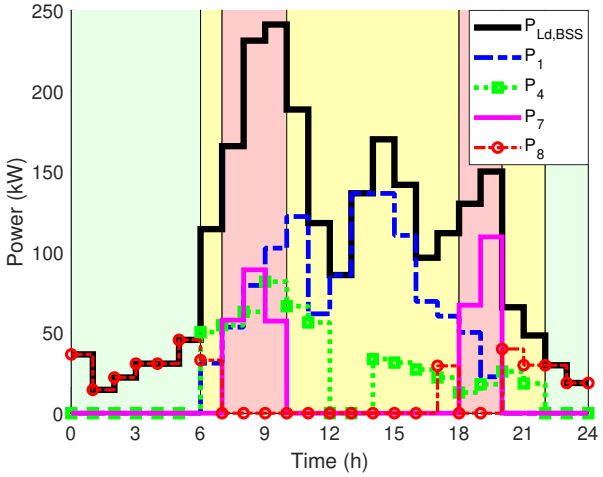


FIGURE 6.17: Simulation result of close loop system without disturbances.

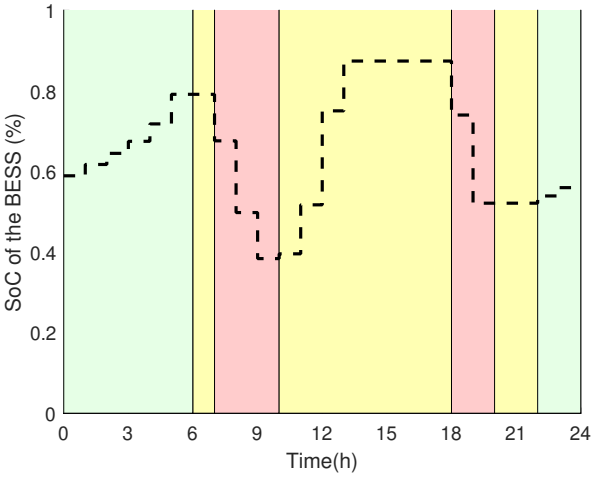


FIGURE 6.18: Simulation result of BESS Dynamic SoC without disturbances.

in this case study are based on prior expectations, but real-world conditions introduce uncertainties due to weather variations, and migration. In this scenario, the proposed grid-connected wind-solar hybrid system with energy storage encounters a particularly adverse condition where the actual charging demand is 30% higher than expected, while the energy supplied by RE generation is 30% lower than anticipated. As shown in Figure 6.19, the closed-loop system with disturbances demonstrates superior performance, highlighting its robustness compared to the open-loop and close-loop system with disturbance. This improvement is attributed to the predictive capability of MPC, which adjusts control actions based on real-time feedback and anticipated future states, even under disturbances. The MPC system effectively manages the power distribution among different generators, prioritizing RESs and utilizing the BESS and release as needed. In contrast, open-loop control lacks adaptability to unexpected changes, relying solely on activating the grid power when the charging demand exceeds expectations. Figure 6.20 illustrates the dynamic SoC of the BESS, showing how the BESS is charged during periods of surplus renewable generation and discharged to meet charging demand during deficits, thereby enhancing system resilience and efficiency.

A comparative analysis of the simulation results for the open-loop, closed-loop without disturbance, and closed-loop with disturbance control strategies highlights the significant advantages of Model Predictive Control (MPC) in optimizing the performance of the proposed system. The open-loop system, while functional, lacks adaptability to fluctuations in renewable energy generation and charging demand, resulting in inefficient energy utilization and increased reliance on the utility grid. In contrast, the closed-loop system without disturbance demonstrates superior performance by dynamically adjusting power distribution based on real-time conditions, effectively prioritizing renewable energy sources and battery storage while minimizing grid dependency. When disturbances are introduced, such as unexpected variations in energy supply and demand, the closed-loop system with MPC maintains a more stable and reliable operation compared to the open-loop approach. The ability of MPC to predict and compensate for disturbances enhances system robustness, ensuring efficient energy management even under uncertain conditions. These findings emphasize the importance of advanced control strategies in achieving a cost-effective and resilient energy

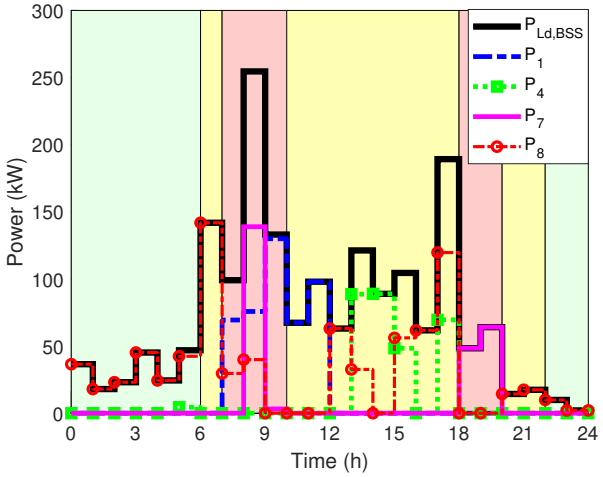


FIGURE 6.19: Simulation result of close loop system with disturbances.

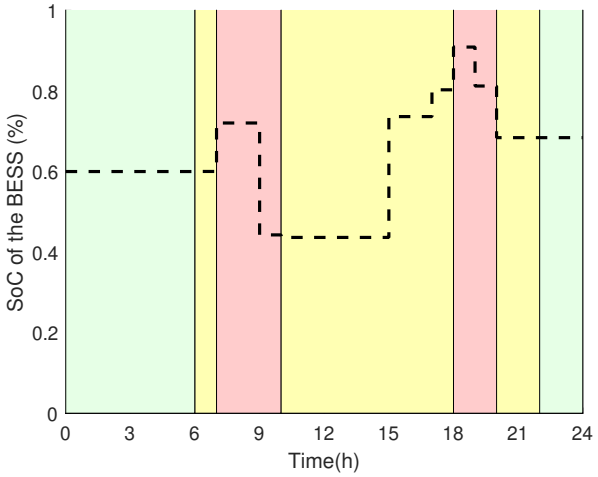


FIGURE 6.20: Simulation result of BESS Dynamic SoC with disturbances.

management framework for the grid-connected wind-solar hybrid system with energy storage. Table 6.1 summarizes the cost savings achieved under the scenarios discussed above.

TABLE 6.1: Daily energy consumption savings and hybrid feed-in.

	Open loop		**Close loop without dist.**		**Close loop with dist.**	
	hybrid feed-in (ZAR)	Cost saving (%)	hybrid feed-in (ZAR)	Cost saving (%)	hybrid feed-in (ZAR)	Cost saving (%)
Weekday HD	129.00	92.64	133.12	93.24	701.95	90.61
Weekday LD	322.78	91.69	364.51	88.87	1 018.13	62.34

6.5 Summary

This chapter has demonstrated the application of MPC for optimal operation management in a grid-connected wind-solar hybrid power system with energy storage for the BSS. A comparative analysis was conducted between open-loop and MPC-based closed-loop control models under varying conditions, including high-demand and low-demand seasons and scenarios with and without disturbances. The results indicate that the closed-loop system consistently outperforms the open-loop model, with the disturbance-free closed-loop approach demonstrating superior robustness and adaptability in handling uncertainties. The simulation results highlight MPC's effectiveness in optimizing the proposed system's operational costs by ensuring efficient power distribution, minimizing dependence on the utility grid, and maximizing the utilization of RESs. While the computational complexity of MPC may pose challenges, its benefits are particularly significant for industrial operations, where real-time optimization can enhance efficiency, reliability, and cost-effectiveness.

The next chapter will present the overall conclusions of this research study, summarizing key findings and outlining potential directions for future work.

Chapter 7

CONCLUSIONS AND FUTURE WORKS

This thesis presents a comprehensive approach to the optimal design and operation of electrical vehicle battery swapping stations (BSSs), integrating hybrid renewable energy sources and grid power systems. The primary objective is to address the challenges associated with electric vehicle (EV) charging infrastructure, focusing mainly on reducing charging times and enhancing energy efficiency through innovative solutions. The work is structured into three main categories: optimal design of BSSs, optimal operational control strategies, and model predictive control approach for real-time optimization in order to satisfy the charging demand of the depleted EV battery at the BSS.

The study has developed and evaluated three complementary models. Specific optimization cases considered for minimizing system operational costs illustrate the benefits of energy management and system reliability provided by RE-based grid-connected hybrid systems. This chapter includes a brief summary of each chapter and important conclusions.

7.1 Conclusions

The pursuit of sustainable transportation solutions is critical in addressing climate change and reducing dependence on fossil fuels. The transportation sector, being a significant contributor to air pollution and energy consumption, necessitates innovative approaches to enhance energy efficiency and reduce greenhouse gas emissions. Electric vehicles (EVs) have emerged as a promising solution, yet challenges such as long charging times and range anxiety persist. Battery swapping stations (BSSs) offer a viable alternative by enabling quick battery exchanges, thereby reducing downtime and enhancing EV adoption.

This research focuses on optimizing the design and operation of BSSs, leveraging renewable energy sources to minimize energy consumption and operational costs while improving charging performance. The following key approaches are presented:

- An optimization model is developed to minimize the overall life cycle cost and electricity costs for a grid-connected hybrid power supply system in Chapter 3. The model considers the integration of wind turbines and solar PV panels, providing a cost-effective and reliable power solution. The optimization problem is formulated using mixed integer linear programming (MILP) to determine key decision variables, such as the number of wind turbines and solar panels, and the power drawn from the utility grid. Simulation results demonstrate substantial energy cost savings and a feasible payback period, underscoring the economic benefits of the proposed system and robustness of the design.

- In Chapter 4, an advanced control strategy is designed to minimize total operation costs, including electricity purchases and wear costs of the hybrid system associated with battery energy storage systems (BESS) while maximizing the use of locally generated renewable energy by enforcing power feedback to the utility grid. Multiple scenarios, representing both high- and low-demand season conditions, have validated that the integration of renewable energy with energy storage not only enhances self-consumption but also facilitates revenue generation through surplus power feedback to the grid. Simulation results across various scenarios show significant energy and cost savings, along with additional revenue generation through surplus power sales.

- In chapter 5, the application of Model Predictive Control (MPC) for dynamic power flow optimization is presented, demonstrating its superiority over traditional open-loop models. By leveraging real-time data, MPC effectively manages system uncertainties, ensuring efficient power distribution while minimizing operational costs and maximizing renewable energy utilization. The results highlight MPC's ability to enhance reliability and adaptability under varying demand conditions and disturbances, continuously adjusting power dispatch to optimize overall performance. Despite its computational complexity, the closed-loop control strategy of MPC significantly reduces dependency on grid-supplied energy, reinforcing its effectiveness in achieving a more resilient and cost-efficient energy management system.

In summary, the research contributes significant insights into the design and operational strategies for EV BSSs. By bridging the gap between internal operational optimizations and the external challenges of integrating renewable energy with grid systems, this work not only advances academic understanding but also provides a practical framework for enhancing the efficiency and sustainability of urban transport infrastructures. The demonstrated cost-effectiveness and reliability of the proposed models support the broader transition toward cleaner energy sources in the transportation sector, thus aligning with global environmental goals.

7.2 Recommendations for Future Work

The strategies presented in this study demonstrate the potential for significant economic and environmental benefits through the integration of renewable energy sources into BSS. Although the objectives of this research have been met, however, further research and development are needed to enhance the impact of these interventions:

1. Integration of Vehicle-to-Grid (V2G) and Grid-to-Vehicle (G2V) strategies. BSS can serve as energy hubs, allowing electric vehicle (EV) batteries to supply power back to the grid during peak demand and recharge when electricity prices are low. Optimizing the scheduling of battery swapping operations based on energy prices, grid demand, and renewable energy availability can help improve grid stability while maximizing the financial benefits for both operators and users.

2. Implementing blockchain-based or peer-to-peer energy trading platforms can enable decentralized energy transactions, enhancing operational efficiency and reducing dependence on centralized grid infrastructure.

3. The application of real-time scheduling using machine learning (ML) is another promising research direction. Machine learning models can analyze historical data on user demand, grid conditions, and renewable energy generation to predict and optimize BSS operations. Reinforcement learning (RL) algorithms can be employed to dynamically adjust battery allocation, improving efficiency and minimizing waiting times for users while balancing energy supply and demand.

4. Further research can also explore hybrid renewable energy integration to enhance the sustainability of BSS. Integrating energy storage systems such as second-life EV batteries or hydrogen fuel cells can help store excess renewable energy and provide backup power when needed. Optimization models can be developed to manage the balance between solar, wind, grid power, and stored energy, ensuring continuous operation and reducing dependency on the traditional power grid.

5. Future research on economic and policy optimization is essential for large-scale BSS deployment. This involves analyzing different pricing models, government incentives, and carbon credit mechanisms to improve financial viability. Policymakers can develop regulatory frameworks that encourage investments in BSS while ensuring fair electricity pricing and sustainable energy management. Optimizing these economic and policy aspects will be crucial for accelerating the widespread adoption of BSS in smart city infrastructure.

Bibliography

[1] J. Rogelj, M. Den Elzen, N. Höhne, T. Fransen, H. Fekete, H. Winkler, R. Schaeffer, F. Sha, K. Riahi, and M. Meinshausen. "Paris Agreement climate proposals need a boost to keep warming well below 2 C." *Nature*, vol. 534, no. 7609, pp. 631–639, 2016.

[2] S. N. Seo. "Beyond the Paris Agreement: Climate change policy negotiations and future directions." *Regional Science Policy & Practice*, vol. 9, no. 2, pp. 121–140, 2017.

[3] G. Nhamo and S. Nhamo. "Paris (COP21) Agreement: Loss and damage, adaptation and climate finance issues." *International Journal of African Renaissance Studies-Multi-, Inter-and Transdisciplinarity*, vol. 11, no. 2, pp. 118–138, 2016.

[4] D. P. van Vuuren, M. van Sluisveld, and A. F. Hof. "Implications of long-term scenarios for medium-term targets (2050)." *PBL Netherlands Environmental Assessment Agency, The Hague*, 2015.

[5] H. Hao, Y. Geng, and J. Sarkis. "Carbon footprint of global passenger cars: Scenarios through 2050." *Energy*, vol. 101, pp. 121–131, 2016.

[6] H. S. Rao, H. Hettige, N. Singru, R. Lumain, and C. Roldan. "Reducing carbon emissions from transport projects." *Evaluation knowledge brief, H. Dalkmann (Editor)*, vol. 1, 2010.

[7] A. J. Krupnick, R. D. Rowe, and C. M. Lang. "Transportation and air pollution: the environmental damages." In *The Full Costs and Benefits of Transportation*, pp. 337–369. Springer, 1997.

[8] T. Lyons, J. Kenworthy, C. Moy, and F. Dos Santos. "An international urban air pollution model for the transportation sector." *Transportation Research Part D: Transport and Environment*, vol. 8, no. 3, pp. 159–167, 2003.

[9] B. Giles-Corti, A. Vernez-Moudon, R. Reis, G. Turrell, A. L. Dannenberg, H. Badland, S. Foster, M. Lowe, J. F. Sallis, M. Stevenson, et al. "City planning and population health: a global challenge." *The lancet*, vol. 388, no. 10062, pp. 2912–2924, 2016.

[10] P. Jittrapirom, V. Caiati, A.-M. Feneri, S. Ebrahimigharehbaghi, M. J. Alonso González, and J. Narayan. "Mobility as a service: A critical review of definitions, assessments of schemes, and key challenges." 2017.

[11] B. Merven, A. Stone, A. Hughes, and B. Cohen. "Quantifying the energy needs of the transport sector for South Africa: A bottom-up model." 2012.

[12] R. Colvile, E. Hutchinson, and R. Warren. "The transport sector as a source of air pollution." *Developments in Environmental Science*, vol. 1, pp. 187–239, 2002.

[13] P. Schmidt, W. Zittel, W. Weindorf, T. Rakasha, and D. Goericke. "Renewables in transport 2050–Empowering a sustainable mobility future with zero emission fuels." In *16. Internationales Stuttgarter Symposium*, pp. 185–199. Springer, 2016.

[14] B. G. Pollet, I. Staffell, and J. L. Shang. "Current status of hybrid, battery and fuel cell electric vehicles: From electrochemistry to market prospects." *Electrochimica Acta*, vol. 84, pp. 235–249, 2012.

[15] J. A. Manzolli, J. P. Trovão, and C. H. Antunes. "Scenario-Based Multi-criteria decision analysis for rapid transit systems implementation in an urban context." *ETransportation*, vol. 7, p. 100101, 2021.

[16] L. Ianniciello, P. H. Biwolé, and P. Achard. "Electric vehicles batteries thermal management systems employing phase change materials." *Journal of power sources*, vol. 378, pp. 383–403, 2018.

[17] M. E. Moeletsi. "Future Policy and Technological Advancement Recommendations for Enhanced Adoption of Electric Vehicles in South Africa: A Survey and Review." *Sustainability*, vol. 13, no. 22, p. 12535, 2021.

[18] I.E.A. *Global EV Outlook 2021*. International Energy Agency, Paris, November 2021. URL https://www.iea.org/reports/global-ev-outlook-2021.

[19] M. Alexander and L. Tonachel. "Projected Greenhouse Gas Emissions for Plug-in Electric Vehicles." *World Electric Vehicle Journal*, vol. 8, no. 4, pp. 987–995, 2016.

[20] N. Sujitha and S. Krithiga. "RES based EV battery charging system: A review." *Renewable and Sustainable Energy Reviews*, vol. 75, pp. 978–988, 2017.

[21] X. Tan, G. Qu, B. Sun, N. Li, and D. H. Tsang. "Optimal scheduling of battery charging station serving electric vehicles based on battery swapping." *IEEE Transactions on Smart Grid*, vol. 10, no. 2, pp. 1372–1384, 2017.

[22] F. Ahmad, M. Saad Alam, I. Saad Alsaidan, and S. M. Shariff. "Battery swapping station for electric vehicles: opportunities and challenges." *IET Smart Grid*, vol. 3, no. 3, pp. 280–286, 2020.

[23] H. Bian, Q. Ren, Z. Guo, and C. Zhou. "Optimal Scheduling of Integrated Energy System Considering Electric Vehicle Battery Swapping Station and Multiple Uncertainties." *World Electric Vehicle Journal*, vol. 15, no. 4, p. 170, 2024.

[24] A. R. Singh, P. Vishnuram, S. Alagarsamy, M. Bajaj, V. Blazek, I. Damaj, R. S. Rathore, F. N. Al-Wesabi, and K. M. Othman. "Electric vehicle charging technologies, infrastructure expansion, grid

integration strategies, and their role in promoting sustainable e-mobility." *Alexandria Engineering Journal*, vol. 105, pp. 300–330, 2024.

[25] M. Kumar, K. P. Panda, R. T. Naayagi, R. Thakur, and G. Panda. "Comprehensive review of electric vehicle technology and its impacts: Detailed investigation of charging infrastructure, power management, and control techniques." *Applied Sciences*, vol. 13, no. 15, p. 8919, 2023.

[26] L. T. Nyamayoka, L. M. Masisi, D. G. Dorrell, and S. Wang. "Optimisation Design of On-Grid Hybrid Power Supply System for Electric Vehicle Battery Swapping Station." In *2023 IEEE International Future Energy Electronics Conference (IFEEC)*, pp. 296–299. IEEE, 2023.

[27] M. Amir, R. G. Deshmukh, H. M. Khalid, Z. Said, A. Raza, S. Muyeen, A.-S. Nizami, R. M. Elavarasan, R. Saidur, and K. Sopian. "Energy storage technologies: An integrated survey of developments, global economical/environmental effects, optimal scheduling model, and sustainable adaption policies." *Journal of Energy Storage*, vol. 72, p. 108694, 2023.

[28] G. Barone, A. Buonomano, F. Calise, C. Forzano, and A. Palombo. "Building to vehicle to building concept toward a novel zero energy paradigm: Modelling and case studies." *Renewable and Sustainable Energy Reviews*, vol. 101, pp. 625–648, 2019.

[29] M. Amer, J. Masri, U. Sajjad, K. Hamid, et al. "Electric vehicles: Battery technologies, charging standards, AI communications, challenges, and future directions." *Energy Conversion and Management: X*, p. 100751, 2024.

[30] G. Zhao, X. Wang, and M. Negnevitsky. "Connecting battery technologies for electric vehicles from battery materials to management." *Iscience*, vol. 25, no. 2, 2022.

[31] T. H. Wu, G. K. Pang, K. Choy, and H. Lam. "An optimization model for a battery swapping station in Hong Kong." In *2015 IEEE Transportation Electrification Conference and Expo (ITEC)*, pp. 1–6. IEEE, 2015.

[32] H. Wu, G. K.-H. Pang, K. L. Choy, and H. Y. Lam. "A charging-scheme decision model for electric vehicle battery swapping station using varied population evolutionary algorithms." *Applied Soft Computing*, vol. 61, pp. 905–920, 2017.

[33] M. Schücking, P. Jochem, W. Fichtner, O. Wollersheim, and K. Stella. "Charging strategies for economic operations of electric vehicles in commercial applications." *Transportation Research Part D: Transport and Environment*, vol. 51, pp. 173–189, 2017.

[34] I. Pavić, H. Pandžić, and T. Capuder. "Electric vehicle based smart e-mobility system–Definition and comparison to the existing concept." *Applied Energy*, vol. 272, p. 115153, 2020.

[35] Y. Feng and X. Lu. "Construction Planning and Operation of Battery Swapping Stations for Electric Vehicles: A Literature Review." *Energies*, vol. 14, no. 24, p. 8202, 2021.

[36] M. R. Sarker, H. Pandžić, and M. A. Ortega-Vazquez. "Optimal operation and services scheduling for an electric vehicle battery swapping station." *IEEE transactions on power systems*, vol. 30, no. 2, pp. 901–910, 2014.

[37] M. VikramGoud, P. K. Biswas, C. Sain, T. S. Babu, and P. K. Balachandran. "Advancement of electric vehicle technologies, classification of charging methodologies, and optimization strategies for sustainable development-a comprehensive review." *Heliyon*, 2024.

[38] F. Amoroso. "Managing charging of electric vehicles in electricity transmission and distribution networks." In *Eco-Friendly Innovation in Electricity Transmission and Distribution Networks*, pp. 363–376. Elsevier, 2015.

[39] T. Arunkumari and V. Indragandhi. "An overview of high voltage conversion ratio DC-DC converter configurations used in DC micro-grid architectures." *Renewable and Sustainable Energy Reviews*, vol. 77, pp. 670–687, 2017.

[40] G. Benysek and M. Jarnut. "Electric vehicle charging infrastructure in Poland." *Renewable and Sustainable Energy Reviews*, vol. 16, no. 1, pp. 320–328, 2012.

[41] H. Fathabadi. "Novel grid-connected solar/wind powered electric vehicle charging station with vehicle-to-grid technology." *Energy*, vol. 132, pp. 1–11, 2017.

[42] C. Ghenai, A. Merabet, T. Salameh, and E. C. Pigem. "Grid-tied and stand-alone hybrid solar power system for desalination plant." *Desalination*, vol. 435, pp. 172–180, 2018.

[43] H. Wu. "A survey of battery swapping stations for electric vehicles: Operation modes and decision scenarios." *IEEE Transactions on Intelligent Transportation Systems*, vol. 23, no. 8, pp. 10163–10185, 2021.

[44] R. Fachrizal, M. Shepero, M. Åberg, and J. Munkhammar. "Optimal PV-EV sizing at solar powered workplace charging stations with smart charging schemes considering self-consumption and self-sufficiency balance." *Applied Energy*, vol. 307, p. 118139, 2022.

[45] A. R. Bhatti, M. Tamoor, R. Liaqat, A. Rasool, Z. Salam, A. Ali, and A. Sherefa. "Electric vehicle charging stations and the employed energy management schemes: a classification based comparative survey." *Discover Applied Sciences*, vol. 6, no. 10, p. 503, 2024.

[46] L. Zhong and M. Pei. "Optimal design for a shared swap charging system considering the electric vehicle battery charging rate." *Energies*, vol. 13, no. 5, p. 1213, 2020.

[47] S. R. Revankar and V. N. Kalkhambkar. "Grid integration of battery swapping station: A review." *Journal of Energy Storage*, vol. 41, p. 102937, 2021.

[48] D. Cui, Z. Wang, P. Liu, S. Wang, D. G. Dorrell, X. Li, and W. Zhan. "Operation optimization approaches of electric vehicle battery swapping and charging station: A literature review." *Energy*, vol. 263, p. 126095, 2023.

[49] A. Kavousi-Fard and A. Khodaei. "Efficient integration of plug-in electric vehicles via reconfigurable microgrids." *Energy*, vol. 111, pp. 653–663, 2016.

[50] F. Schneider, U. W. Thonemann, and D. Klabjan. "Optimization of battery charging and purchasing at electric vehicle battery swap stations." *Transportation Science*, vol. 52, no. 5, pp. 1211–1234, 2018.

[51] M. Longo, F. Foiadelli, and W. Yaïci. "Electric vehicles integrated with renewable energy sources for sustainable mobility." *New trends in electrical vehicle powertrains*, vol. 10, pp. 203–223, 2018.

[52] B. Anthony Jnr. "Integrating electric vehicles to achieve sustainable energy as a service business model in smart cities." *Frontiers in Sustainable Cities*, vol. 3, p. 685716, 2021.

[53] B. Avci, K. Girotra, and S. Netessine. "Electric vehicles with a battery switching station: Adoption and environmental impact." *Management Science*, vol. 61, no. 4, pp. 772–794, 2015.

[54] M. Ban, Z. Zhang, C. Li, Z. Li, and Y. Liu. "Optimal scheduling for electric vehicle battery swapping-charging system based on nanogrids." *International Journal of Electrical Power & Energy Systems*, vol. 130, p. 106967, 2021.

[55] S. Bhattacharjee and C. Nandi. "Design of an industrial internet of things-enabled energy management system of a grid-connected solar–wind hybrid system-based battery swapping charging station for electric vehicle." In *Applications of Internet of Things: Proceedings of ICCCIOT 2020*, pp. 1–14. Springer, 2021.

[56] J. Yan, M. Menghwar, E. Asghar, M. K. Panjwani, and Y. Liu. "Real-time energy management for a smart-community microgrid with battery swapping and renewables." *Applied energy*, vol. 238, pp. 180–194, 2019.

[57] M. S. Mastoi, S. Zhuang, H. M. Munir, M. Haris, M. Hassan, M. Usman, S. S. H. Bukhari, and J.-S. Ro. "An in-depth analysis of electric vehicle charging station infrastructure, policy implications, and future trends." *Energy Reports*, vol. 8, pp. 11504–11529, 2022.

[58] S. J. Shern, M. T. Sarker, M. H. S. M. Haram, G. Ramasamy, S. P. Thiagarajah, and F. Al Farid. "Artificial Intelligence Optimization for User Prediction and Efficient Energy Distribution in Electric Vehicle Smart Charging Systems." *Energies*, vol. 17, no. 22, p. 5772, 2024.

[59] M. Rashid, T. Elfouly, and N. Chen. "A comprehensive survey of electric vehicle charging demand forecasting techniques." *IEEE Open Journal of Vehicular Technology*, 2024.

[60] Q. Sui, F. Li, C. Wu, Z. Feng, X. Lin, F. Wei, and Z. Li. "Optimal scheduling of battery charging–swapping systems for distribution network resilience enhancement." *Energy Reports*, vol. 8, pp. 6161–6170, 2022.

[61] J. Sarda, N. Patel, H. Patel, R. Vaghela, B. Brahma, A. K. Bhoi, and P. Barsocchi. "A review of the electric vehicle charging technology, impact on grid integration, policy consequences, challenges and future trends." *Energy Reports*, vol. 12, pp. 5671–5692, 2024.

[62] A. Chandwani, S. Dey, and A. Mallik. "Cybersecurity of onboard charging systems for electric vehicles—Review, challenges and countermeasures." *IEEE access*, vol. 8, pp. 226982–226998, 2020.

[63] D. Sperling. *Three revolutions: Steering automated, shared, and electric vehicles to a better future*. Island Press, 2018.

[64] S. S. A. Salam, V. Raj, M. I. Petra, A. K. Azad, S. Mathew, and S. M. Sulthan. "Charge scheduling optimization of electric vehicles: a comprehensive review of essentiality, perspectives, techniques and security." *IEEE Access*, 2024.

[65] M.-D. Lin, P.-Y. Liu, M.-D. Yang, and Y.-H. Lin. "Optimized allocation of scooter battery swapping station under demand uncertainty." *Sustainable Cities and Society*, vol. 71, p. 102963, 2021.

[66] Nio. "The Current State of EV Battery Swapping." https://www.nio.com/blog/current-state-ev-battery-swapping. Online access: 15 November 2024.

[67] M. C. Kocer, A. Onen, J. Jung, H. Gultekin, and S. Albayrak. "Optimal location and sizing of electric bus battery swapping station in microgrid systems by considering revenue maximization." *IEEE Access*, vol. 11, pp. 41084–41095, 2023.

[68] R. Bouhedir, A. Mellit, M. Benghanem, and B. Hassan. "Optimal energy management strategy for electric vehicle charging station based on tied photovoltaic system." *Computers and Electrical Engineering*, vol. 121, p. 109875, 2025.

[69] Z. Wang, S. Hou, and W. Guo. "Inventory management of battery swapping and charging stations considering uncertainty." *International Journal of Electrical Power & Energy Systems*, vol. 155, p. 109528, 2024.

[70] W. K. M. Al-Zaidi and A. Inan. "Optimal Planning of Battery Swapping Stations Incorporating Dynamic Network Reconfiguration Considering Technical Aspects of the Power Grid." *Applied Sciences*, vol. 14, no. 9, p. 3795, 2024.

[71] X. Zhao, Q. Xu, Y. Yang, and G. Zhou. "Distributed distributionally robust optimization of distribution network incorporating novel battery charging and swapping station." *International Journal of Electrical Power & Energy Systems*, vol. 155, p. 109643, 2024.

[72] Y. Zhang, L. Yao, L. Hu, J. Yang, X. Zhou, W. Deng, and B. Chen. "Operation optimization of battery swapping stations with photovoltaics and battery energy storage stations supplied by transformer spare capacity." *IET Generation, Transmission & Distribution*, vol. 17, no. 17, pp. 3872–3882, 2023.

[73] M. S. Gull, M. Khalid, and N. Arshad. "Multi-objective optimization of battery swapping station to power up mobile and stationary loads." *Applied Energy*, vol. 374, p. 124064, 2024.

[74] Y. Li, Y. Cai, T. Zhao, Y. Liu, J. Wang, L. Wu, and Y. Zhao. "Multi-objective optimal operation of centralized battery swap charging system with photovoltaic." *Journal of Modern Power Systems and Clean Energy*, vol. 10, no. 1, pp. 149–162, 2021.

[75] M. Mahoor, Z. S. Hosseini, and A. Khodaei. "Least-cost operation of a battery swapping station with random customer requests." *Energy*, vol. 172, pp. 913–921, 2019.

[76] M. A. Jirdehi and V. S. Tabar. "Risk-aware energy management of a microgrid integrated with battery charging and swapping stations in the presence of renewable resources high penetration, crypto-currency miners and responsive loads." *Energy*, vol. 263, p. 125719, 2023.

[77] Z. Li, W. Zhu, and G. Wang. "Charging Dispatching Strategy for Islanded Microgrid Battery-Swapping Stations." *Electronics*, vol. 13, no. 1, p. 49, 2023.

[78] X. Yang, R. Du, Z. Ji, Q. Wang, M. Qu, and W. Gao. "A Management Framework and Optimization Scheduling for Electric Vehicles Participating in a Regional Power Grid Demand Response under Battery Swapping Mode." *Electronics*, vol. 13, no. 20, p. 3987, 2024.

[79] Y. Guo, X. Lei, and Q. Wang. "Capacity coordination planning of isolated microgrid and battery swapping station based on the quantum behavior particle swarm optimization algorithm." *International Transactions on Electrical Energy Systems*, vol. 31, no. 3, p. e12804, 2021.

[80] L. T.-E. Nyamayoka, L. Masisi, D. Dorrell, and S. Wang. "Techno-Economic Feasibility and Optimal Design Approach of Grid-Connected Hybrid Power Generation Systems for Electric Vehicle Battery Swapping Station." *Energies*, vol. 18, no. 5, p. 1208, 2025. URL https://www.mdpi.com/1996-1073/18/5/1208.

[81] D. Banks and J. Schäffler. *The potential contribution of renewable energy in South Africa*. Sustainable Energy & Climate Change Project (SECCP), 2005.

[82] S. Diaf, M. Belhamel, M. Haddadi, and A. Louche. "Technical and economic assessment of hybrid photovoltaic/wind system with battery storage in Corsica island." *Energy policy*, vol. 36, no. 2, pp. 743–754, 2008.

[83] S. Diaf, D. Diaf, M. Belhamel, M. Haddadi, and A. Louche. "A methodology for optimal sizing of autonomous hybrid PV/wind system." *Energy policy*, vol. 35, no. 11, pp. 5708–5718, 2007.

[84] A. Belkaid, I. Colak, and O. Isik. "Photovoltaic maximum power point tracking under fast varying of solar radiation." *Applied energy*, vol. 179, pp. 523–530, 2016.

[85] D. Abbes, A. Martinez, and G. Champenois. "Life cycle cost, embodied energy and loss of power supply probability for the optimal design of hybrid power systems." *Mathematics and Computers in Simulation*, vol. 98, pp. 46–62, 2014.

[86] H. A. Kazem and T. Khatib. "Techno-economical assessment of grid connected photovoltaic power systems productivity in Sohar, Oman." *Sustainable Energy Technologies and Assessments*, vol. 3, pp. 61–65, 2013.

[87] M. A. Ramli, A. Hiendro, and S. Twaha. "Economic analysis of PV/diesel hybrid system with flywheel energy storage." *Renewable Energy*, vol. 78, pp. 398–405, 2015.

[88] L. Bokopane, K. Kanzumba, and H. Vermaak. "Is the South African Electrical Infrastructure Ready for Electric Vehicles?" In *2019 Open Innovations (OI)*, pp. 127–131. IEEE, 2019.

[89] A. Dane, D. Wright, and G. Montmasson-Clair. "Exploring the Policy Impacts of a Transition To Electric Vehicles in South Africa." *Pretoria: Trade & Industrial Policy Strategies*, 2019.

[90] N. Sooknanan Pillay, A. C. Brent, J. K. Musango, and F. van Geems. "Using a System Dynamics Modelling Process to Determine the Impact of eCar, eBus and eTruck Market Penetration on Carbon Emissions in South Africa." *Energies*, vol. 13, no. 3, p. 575, 2020.

[91] X. Chen, K. Xing, F. Ni, Y. Wu, and Y. Xia. "An electric vehicle battery-swapping system: Concept, architectures, and implementations." *IEEE Intelligent Transportation Systems Magazine*, vol. 14, no. 5, pp. 175–194, 2021.

[92] B. Lebrouhi, Y. Khattari, B. Lamrani, M. Maaroufi, Y. Zeraouli, and T. Kousksou. "Key challenges for a large-scale development of battery electric vehicles: A comprehensive review." *Journal of Energy Storage*, vol. 44, p. 103273, 2021.

[93] M. Brenna, F. Foiadelli, C. Leone, and M. Longo. "Electric vehicles charging technology review and optimal size estimation." *Journal of Electrical Engineering & Technology*, vol. 15, no. 6, pp. 2539–2552, 2020.

[94] R. Hemmati. *Chapter 3—Integration of electric vehicles and charging stations. In Energy Management in Homes and Residential Microgrids: Short-Term Scheduling and Long-Term Planning*. Elsevier, 2024.

[95] A. Evans, V. Strezov, and T. J. Evans. "Assessment of sustainability indicators for renewable energy technologies." *Renewable and Sustainable Energy Reviews*, vol. 13, no. 5, pp. 1082–1088, 2009.

[96] T. Adefarati, R. Bansal, T. Shongwe, R. Naidoo, M. Bettayeb, and A. Onaolapo. "Optimal energy management, technical, economic, social, political and environmental benefit analysis of a grid-connected PV/WT/FC hybrid energy system." *Energy Conversion and Management*, vol. 292, p. 117390, 2023.

[97] G. Al-Sharrah, A. Elkamel, and A. Almanssoor. "Sustainability indicators for decision-making and optimisation in the process industry: The case of the petrochemical industry." *Chemical Engineering Science*, vol. 65, no. 4, pp. 1452–1461, 2010.

[98] M. Bilal, J. O. Oladigbolu, A. Mujeeb, and Y. A. Al-Turki. "Cost-effective optimization of on-grid electric vehicle charging systems with integrated renewable energy and energy storage: An economic and reliability analysis." *Journal of Energy Storage*, vol. 100, p. 113170, 2024.

[99] M. M. Sediqi, M. Furukakoi, M. E. Lotfy, A. Yona, and T. Senjyu. "Optimal economical sizing of grid-connected hybrid renewable energy system." *Journal of Energy and Power Engineering*, vol. 11, no. 4, pp. 244–53, 2017.

[100] W. Zhang, A. Maleki, M. A. Rosen, and J. Liu. "Optimization with a simulated annealing algorithm of a hybrid system for renewable energy including battery and hydrogen storage." *Energy*, vol. 163, pp. 191–207, 2018.

[101] A. Kaabeche, M. Belhamel, and R. Ibtiouen. "Sizing optimization of grid-independent hybrid photovoltaic/wind power generation system." *Energy*, vol. 36, no. 2, pp. 1214–1222, 2011.

[102] A. Kamjoo, A. Maheri, A. M. Dizqah, and G. A. Putrus. "Multi-objective design under uncertainties of hybrid renewable energy system using NSGA-II and chance constrained programming." *International journal of electrical power & energy systems*, vol. 74, pp. 187–194, 2016.

[103] J. A. Duffie, W. A. Beckman, and N. Blair. *Solar engineering of thermal processes, photovoltaics and wind*. John Wiley & Sons, 2020.

[104] A. M. Eltamaly and M. A. Mohamed. "Optimal sizing and designing of hybrid renewable energy systems in smart grid applications." In *Advances in renewable energies and power technologies*, pp. 231–313. Elsevier, 2018.

[105] A. Askarzadeh and L. dos Santos Coelho. "A novel framework for optimization of a grid independent hybrid renewable energy system: A case study of Iran." *Solar Energy*, vol. 112, pp. 383–396, 2015.

[106] A. Maleki, F. Pourfayaz, and M. A. Rosen. "A novel framework for optimal design of hybrid renewable energy-based autonomous energy systems: a case study for Namin, Iran." *Energy*, vol. 98, pp. 168–180, 2016.

[107] K. Anoune, M. Ghazi, M. Bouya, A. Laknizi, M. Ghazouani, A. B. Abdellah, and A. Astito. "Optimization and techno-economic analysis of photovoltaic-wind-battery based hybrid system." *Journal of Energy Storage*, vol. 32, p. 101878, 2020.

[108] R. Lamedica, E. Santini, A. Ruvio, L. Palagi, and I. Rossetta. "A MILP methodology to optimize sizing of PV-Wind renewable energy systems." *Energy*, vol. 165, pp. 385–398, 2018.

[109] M. Bénichou, J.-M. Gauthier, P. Girodet, G. Hentges, G. Ribière, and O. Vincent. "Experiments in mixed-integer linear programming." *Mathematical programming*, vol. 1, pp. 76–94, 1971.

[110] O. Penangsang and P. Sulistijono. "Suyanto," Optimal power flow using multi-objective genetic algorithm to minimize generation emission and operational cost in micro-grid,"." *International Journal of Smart Grid and Clean Energy*, vol. 3, no. 4, pp. 410–416, 2014.

[111] N. Gunantara. "A review of multi-objective optimization: Methods and its applications." *Cogent Engineering*, vol. 5, no. 1, p. 1502242, 2018.

[112] WeatherSpark. "Average Weather in Cape Town, Western Cape, South Africa, Year-Round." https://weatherspark.com/y/82961/Average-Weather-in-Cape-Town-Western-Cape-South-Africa-Year-Round. Online access: 25 November 2023.

[113] DMRE. "DMRE, South Africa. Integrated Resource Plan (IRP, 2023). 2023." https://www.gov.za/sites/default/files/gcis_document/202401/49974gon4238.pdf. Online access: 15 January 2024.

[114] J. Hoppmann, J. Volland, T. S. Schmidt, and V. H. Hoffmann. "The economic viability of battery storage for residential solar photovoltaic systems–A review and a simulation model." *Renewable and Sustainable Energy Reviews*, vol. 39, pp. 1101–1118, 2014.

[115] G. Liu. "Development of a general sustainability indicator for renewable energy systems: A review." *Renewable and Sustainable Energy Reviews*, vol. 31, pp. 611–621, 2014.

[116] S. Sichilalu, T. Mathaba, and X. Xia. "Optimal control of a wind–PV-hybrid powered heat pump water heater." *Applied energy*, vol. 185, pp. 1173–1184, 2017.

[117] L. T.-E. Nyamayoka, L. Masisi, and D. G. Dorrell. "Optimal power dispatch of solar PV-battery storage system for electric vehicle battery swapping stations under grid scheduled load-shedding." In *2025 33rd Southern African Universities Power Engineering Conference (SAUPEC)*, pp. 1–6. IEEE, 2025.

[118] Z. Wu, H. Tazvinga, and X. Xia. "Demand side management of photovoltaic-battery hybrid system." *Applied Energy*, vol. 148, pp. 294–304, 2015.

[119] X. Xia, J. Zhang, and A. Elaiw. "An application of model predictive control to the dynamic economic dispatch of power generation." *Control Engineering Practice*, vol. 19, no. 6, pp. 638–648, 2011.